

CYCLE-TO-CYCLE VARIATIONS
IN
SPARK-IGNITION ENGINES.

By

ANIL KAPIL

B.Eng., Walchand College Of Engineering, India, 1981.

A THESIS SUBMITTED IN PARTIAL FULFILLMENT OF
THE REQUIREMENTS FOR THE DEGREE OF
MASTERS IN APPLIED SCIENCE.

in
THE FACULTY OF GRADUATE STUDIES
Department of Mechanical Engineering

We accept the thesis as conforming
to the required standard

THE UNIVERSITY OF BRITISH COLUMBIA

May, 1988

© Anil Kapil, 1988

In presenting this thesis in partial fulfilment of the requirements for an advanced degree at the University of British Columbia, I agree that the Library shall make it freely available for reference and study. I further agree that permission for extensive copying of this thesis for scholarly purposes may be granted by the head of my department or by his or her representatives. It is understood that copying or publication of this thesis for financial gain shall not be allowed without my written permission.

Department of Mechanical Engineering.

The University of British Columbia
Vancouver, Canada

Date 11.10.88

ABSTRACT

Pressure data measurements have been made in a single-cylinder, spark-ignition engine over 100 consecutive cycles. The engine was operated on natural gas at a wide range of engine speed and equivalence ratios. The effects of spark electrode geometry, combustion chamber geometry, spark gap and throttling have also been examined. From these pressure measurements standard deviations in burning times in mass-fraction-burned values were determined. Because of the existing evidence that the origin of cyclic variations is in the early combustion period, the standard deviations of cyclic variation in time required for a small (almost zero) mass-fraction-burned is estimated by extrapolation. These extrapolated values of standard deviation are compared with the implication of a hypothesis that cyclic variations in combustion in spark-ignition engines originate in the small-scale structure of turbulence (after ignition).

The nature of turbulence structure during combustion is deduced from existing knowledge of mixture motion within the combustion chamber of the engine. This research determines the turbulent parameters, such as turbulence intensity, turbulent length scales and laminar burning velocity. The standard deviation in burning times in the early stages of combustion is estimated, within experimental uncertainty, by the parameter $\lambda/4u_{\ell}$ where λ is the Taylor microscale and u_{ℓ} is the laminar burning velocity of the unburned mixture. This parameter is the consequence of the Tennekes model of small-scale structure of turbulence and Chomiak's explanation of the high flame propagation rate in regions of concentrated vorticity and the assumption that the

ignition behaves as though it were from a point source.

The general conclusion reached is that the standard deviation in the burning time for small mass-fraction-burned is associated with the early stages of burning-predictable from the knowledge of the Taylor microscale and the laminar burning velocity.

TABLE OF CONTENTS

Page:

Abstract.....	ii
Table of Contents.....	iv
List of Tables	viii
List of Figures	ix
Nomenclature.....	xii
Acknowledgements.....	xv
1. INTRODUCTION.....	1
2. LITERATURE REVIEW.....	6
2.1 Introduction.....	6
2.2 Effect of Air-Fuel Mixture Composition.....	7
Equivalence Ratio.....	7
Fuel Type.....	9
Charge Dilution.....	10
2.3 Effect of Ignition Variables.....	12
Ignition Systems.....	12
Spark Electrode Geometry.....	13
Spark Jitter.....	13
2.4 Engine Speed and Compression Ratio.....	14
2.5 Effect of Combustion Chamber Geometry.....	15
Chamber Shape and Spark Location.....	16
Spark Timing.....	17
Valve Shrouding.....	17
2.6 Comments.....	20
3. APPARATUS AND INSTRUMENTATION.....	21
3.1 Introduction.....	21
3.2 Apparatus.....	21
Engine.....	21
Air Inlet System.....	21
Fuel Intake System.....	22
Coolant System.....	22
Oil System.....	23
Dynamometer.....	23
Ignition System.....	24
3.3 Instrumentation.....	24
Pressure Measurement.....	24
Volume Assignment.....	25
Air Flow Measurement.....	26
Gas Flow Measurement.....	26
Fuel-Air Ratio.....	27
Speed Measurement.....	27

<u>TABLE OF CONTENTS (Continued)</u>		<u>Page</u>
	Torque Measurement.....	27
	Data Acquisition System.....	28
3.4	Operational Control.....	29
	Control Console.....	29
	Starting Procedure.....	30
3.5	Data Acquisition and Transfer.....	31
	Data Acquisition.....	31
	Data Transfer.....	32
4.	MEASUREMENTS WITH MOTORED ENGINE.....	33
4.1	Introduction.....	33
4.2	Phasing of Pressure-Volume Data.....	33
4.3	Polytropic Exponents.....	37
4.4	Volumetric Efficiency.....	40
4.5	Peak Pressure.....	41
5.	FIRED DATA ANALYSIS.....	42
5.1	Introduction.....	42
5.2	Scaling of Pressure.....	42
5.3	Volume Calculation.....	43
5.4	Mass-Burned-Fraction Calculation.....	43
	Initial Conditions.....	44
	Compression Stroke.....	45
	Combustion Process.....	48
	Dissociation Calculation.....	51
	Stanjan.....	51
5.5	Statistical Analysis.....	52
6.	FIRED ENGINE MEASUREMENTS AND RESULTS.....	54
6.1	Introduction.....	54
6.2	Cyclic Variations in Pressure.....	55
6.3	Cyclic Variations in Burning Time.....	57
6.4	Effect of Spark Plug Geometry.....	63
6.5	Effect of Spark Gap Width.....	63

<u>TABLE OF CONTENTS (Continued)</u>	<u>Page</u>
6.6 Effect of Part Throttle.....	64
6.7 Disk Combustion Chamber.....	65
6.8 Summary.....	68
7. TURBULENCE AND IGNITION IN ENGINES.....	70
7.1 Introduction.....	70
7.2 Homogeneity and Isotropy In Engine Turbulence.....	70
7.3 Turbulence Measurements in Engines.....	72
Mean Velocity.....	72
Turbulence Intensity.....	73
7.4 Turbulent Scales.....	74
7.5 Small Scale Structure of Turbulence.....	78
7.6 Initial Flame Propagation.....	80
7.7 Laminar Burning Velocity.....	84
7.8 Summary.....	85
8.0 COMPARISON OF MEASUREMENTS AND THEORETICAL ESTIMATES OF STANDARD DEVIATION.....	86
8.1 Introduction.....	86
8.2 Mean Random Time Delay.....	86
8.3 Comparison of Data.....	90
8.4 Summary.....	91
9.0 CONCLUSIONS.....	92
10. RECOMMENDATIONS.....	95
REFERENCES.....	96
APPENDICES	
A: CALIBRATION CURVES.....	100
B: COMBUSTION-VOLUME PHASING.....	102
C: LAMINAR BURNING VELOCITY.....	105

TABLE OF CONTENTS (Continued)

Page

D: PROPERTIES OF B.C.NATURAL GAS.....109

E: SENSITIVITY ANALYSIS.....110

LIST OF TABLES

Page

Table 1.	Engine Specifications.....	112
Table 2.	Sensitivity of IMEP and P MEP to 1° Change in Phasing Motored Engine.....	35
Table 3.	Polytropic Exponents of Compression and Expansion in a Motored Engine.....	39
Table 4.	Typical Length and Velocity Scales For Engine Turbulence at 3000 RPM.....	89
Table A.1	Pressure and Voltage values for Calibration of Piezo-Electric Pressure Transducer.....	101
Table B.1	Peak Pressure and its Crank-Angle Occurance for Changes in Phasing.....	103

LIST OF FIGURES

Page

Fig 1.	Cyclic Pressure Variations in a Spark Ignition Engine.....	113
Fig 2.	Engine, Dynamometer and Control Systems Layout.....	114
Fig 3.	Ricardo Hydra Engine Cross-Sectional Views.....	115
Fig 4.	Combustion Chamber Shapes a) Bath-Tub Chamber. b) Disc Chamber.....	116
Fig 5.	Instrumentation Layout.....	117
Fig 6.	Hardware Arrangement.....	118
Fig 7.	Ensemble-Averaged Pressure [Motored Engine].....	119
Fig 8.	Indicator Diagram on Logarithmic Scale [Motored Engine]....	120
Fig 9.	Indicator Diagram on Logarithmic Scale.....	121
Fig 10.	Indicator Diagram on Logarithmic Scale	122
Fig 11.	Volumetric Efficiency in a Motored Engine.....	123
Fig 12.	Ensemble-Averaged Peak Pressure in a Motored Engine.....	124
Fig 13.	Typical Pressure Variations and Frequency Histogram for Peak Pressure. Speed = 3000 RPM, $\phi = 1.015$	125
Fig 14.	Typical Pressure Variations and Frequency Histogram for Peak Pressure. Speed = 3000 RPM, $\phi = 0.674$	126
Fig 15.	Ensemble-Averaged Peak Pressure Variation with Speed And Equivalence Ratio.....	127
Fig 16.	Coefficient of Variation for Different Speeds and Equivalence Ratios.....	128
Fig 17.	Typical Mass-Fraction-Burned Variation with Time, From Ignition. N=3000 RPM. $\phi = 1.25$	129
Fig 18.	Typical Frequency Histogram for Burning Times (X=0.10, N = 3000, $\phi = 1.105$.).....	130
Fig 19.	Typical Frequency Histogram for Burning Times (X=0.30, N = 3000 RPM. $\phi = 1.05$.).....	131
Fig 20.	Typical Frequency Histogram for Burning Times (X=0.50, N = 3000 RPM. $\phi = 1.05$.).....	132

List of Figures (Continued)

Page

Fig 21. Typical Frequency Histogram for Burning Times
($X=0.10$, $N = 3000$ RPM. $\phi = 1.22$.).....133

Fig 22. Typical Frequency Histogram for Burning Times
($X=0.10$, $N = 3000$ RPM. $\phi = 1.38$.).....134

Fig 23. Standard Deviation in Burning Time. $N = 2400$ RPM.
(Bath Tub Chamber).....135

Fig 24. Standard Deviation in Burning Time. $N = 2400$ RPM.
(Bath Tub Chamber).....136

Fig 25. Standard Deviation in Burning Time. $N = 3000$ RPM.
(Bath Tub Chamber).....137

Fig 26. Standard Deviation in Burning Time. $N = 3000$ RPM.
(Bath Tub Chamber).....138

Fig 27. Standard Deviation in Burning Time. $N = 3600$ RPM.
(Bath Tub Chamber).....139

Fig 28. Standard Deviation in Burning Time. $N = 3600$ RPM.
(Bath Tub Chamber).....140

Fig 29. Standard Deviation in Burning Time. $N = 4200$ RPM.
(Bath Tub Chamber).....141

Fig 30. Extrapolated Standard Deviation in Early Burning Time.....142

Fig 31. Extrapolated Standard Deviation in Early Burning
Crank Angle Interval.....143

Fig 32. Cross Correlation Coefficient Of Standard Deviation
In Burning Time.....144

Fig 33. Modified Spark Plug With Fine Point Electrodes.....145

Fig 34. Standard Deviation in Burning Time. $N = 3000$ RPM.
(Needle Point Electrode Geometry).....146

Fig 35. Standard Deviation in Burning Time. $N = 3000$ RPM.
(Needle Point Electrode Geometry).....147

Fig 36. Extrapolated Standard Deviation in Early Burning Time.
Different Electrode Geometries $N = 3000$ RPM.....148

Fig 37. Modified Spark Plug With Wide Gap Electrodes.....149

Fig 38. Standard Deviation in Burning Time. $N = 3000$ RPM.
(Spark Plug Gap = 2.3 mm).....150

List of Figures (Continued)

Page

Fig 39.	Standard Deviation in Burning Time. N = 3000 RPM. (Spark Plug Gap = 2.3 mm).....	151
Fig 40.	Extrapolated Standard Deviation in Early Burning Time. Different Spark Gaps N = 3000 RPM.	152
Fig 41.	Standard Deviation in Burning Time. N = 3000 RPM. (Half Open Throttle).....	153
Fig 42.	Standard Deviation in Burning Time. N = 3000 RPM. (Half Open Throttle).....	154
Fig 43.	Extrapolated Standard Deviation in Early Burning Time. Different Throttle Settings N = 3000 RPM.	155
Fig 44.	Standard Deviation in Burning Time. N = 2400 RPM. (Disc Chamber).....	156
Fig 45.	Standard Deviation in Burning Time. N = 3000 RPM. (Disc Chamber).....	157
Fig 46.	Standard Deviation in Burning Time. N = 3600 RPM. (Disc Chamber).....	158
Fig 47.	Standard Deviation in Burning Time. N = 4200 RPM. (Disc Chamber).....	159
Fig 48.	Standard Deviation in Burning Time. N = 3000 RPM. (Disc Chamber- Fine Point Electrode Geometry).....	160
Fig 49.	Standard Deviation in Burning Time. N = 3000 RPM. (Disc Chamber- Spark Plug Gap = 1.5 mm).....	161
Fig 50.	Standard Deviation in Burning Time. N = 3000 RPM. (Disc Chamber- Half Open Throttle).....	162
Fig 51.	Extrapolated Standard Deviation in Early Burning Time. (Disk Chamber).....	163
Fig 52.	Extrapolated Standard Deviation in Early Burning Time. (Disk Chamber) Different Electrode Geometries N = 3000 RPM..	164
Fig 53.	Extrapolated Standard Deviation in Early Burning Time. (Disk Chamber) Different Spark Gaps N = 3000 RPM.....	165
Fig 54.	Extrapolated Standard Deviation in Early Burning Time. (Disk Chamber). Different Throttle Settings N = 3000 RPM..	166

Fig 55. Effect of Different Combustion Chambers on Standard Deviation. N=2400 RPM.....	167
Fig 56. Effect of Different Combustion Chambers on Standard Deviation. N=3000 RPM.....	168
Fig 57. Effect of Different Combustion Chambers on Standard Deviation. N=3600 RPM.....	169
Fig 58. Effect of Different Combustion Chambers on Standard Deviation. N=4200 RPM.....	170
Fig 59. Effect of Different Combustion Chambers on Standard Deviation Different Spark Gaps.....	171
Fig 60. Effect of Different Combustion Chambers on Standard Deviation. Fine Point Electrodes.....	172
Fig 61. Effect of Different Combustion Chambers on Standard Deviation. Partly Opened Throttle.....	173
Fig 62. Model of Concentrated Vorticity Region as Proposed by Tennekes.....	174
Fig 63. Effect of Equivalence Ratio on Mean Random Time Delay.....	175
Fig 64. Comparison of Extrapolated Standard Deviation and Mean Random Time Delay with Equivalence Ratio. - 2400 RPM. (Bath-Tub Chamber).....	176
Fig 65. Comparison of Extrapolated Standard Deviation and Mean Random Time Delay with Equivalence Ratio. - 3000 RPM. (Bath-Tub Chamber).....	177
Fig 66. Comparison of Extrapolated Standard Deviation and Mean Random Time Delay with Equivalence Ratio. - 3600 RPM. (Bath-Tub Chamber).....	178
Fig 67. Comparison of Extrapolated Standard Deviation and Mean Random Time Delay with Equivalence Ratio. - 4200 RPM. (Bath-Tub Chamber).....	179
Fig 68. Relationship Between Mean Random Time Delay and Extrapolated Standard Deviation in Burning Time Within a Bath-Tub Chamber.....	180
Fig 69. Relationship Between Mean Random Time Delay and Extrapolated Standard Deviation in Burning Time Within a Disc Chamber.....	181

<u>List of Figures (Continued)</u>	<u>Page</u>
Fig 70. Calibration Curve For Laminar Flow Element (Natural Gas)..	182
Fig 71. Calibration Curve For Laminar Flow Element (Air).....	183
Fig 72. Calibration Curve For Kistler Pressure Transducer.....	184
Fig 73. Combustion Time at 10% Mass-Fraction-Burned on Probability Paper.....	185
Fig 74. Combustion And Motored Pressure At Different Crank Angle Intervals - 3000 RPM.(For Sensitivity Analysis).....	186
Fig 75. Combustion Pressure Less Motored Pressure at Different Crank Angle Intervals- 3000 RPM (Sensitivity Analysis)....	187
Fig 76. Mass-Fraction-Burned and Time Sensitivity at Different Crank Angles (Sensitivity Analysis).....	188

NOMENCLATURE

A	Area (m^2)
BDC	Bottom Dead Centre
Cov	Normalized Covariance
COV	Coefficient Of Variation
C_p	Constant pressure specific heat (kJ/kg-K)
C_v	Constant volume specific heat (kJ/kg-K)
E	Total energy (kJ)
EVC	Exhaust Valve Closing
EVO	Exhaust Valve Opening
e	Specific energy (kJ/kg)
h_f^o	Enthalpy of formation (kJ/kmol)
\bar{h}	Specific enthalpy (kJ/kmol)
H	Clearance height (mm)
H	Total Enthalpy (kJ)
IMEP	Indicated mean effective pressure (kPa)
IVC	Inlet Valve Closing
IVO	Inlet Valve Opening
k	Isentropic Exponent
L	Connecting rod length (mm)
L, l	Integral length scale
MBT	Minimum for best torque
MW	Molecular weight(kg/kmol)
N	Number of Engine Cycles
P	Pressure (kPa)
PMEP	Pumping Mean Effective Pressure (kPa)
Q	Heat added or lost to the cylinder walls (kJ)

Q_{air}	Total Volume Of Air Inhaled By the Engine in m^3/min
R	Crank radius.
R, r	Radius (mm)
Re_L	Reynolds number based on the integral length scale
Re_λ	Reynolds number based on the Taylor micro scale
RPM	Engine speed (Revolutions per minute)
\bar{R}	Universal gas constant (kJ/kmol-K)
St	Turbulent Burning Velocity.
T	Temperature (k)
TDC	Top dead centre
U	Velocity (m/s)
$U(t)$	Instantaneous velocity (m/s)
$\bar{U}(t)$	Turbulent mean velocity (m/s)
U_ℓ	Laminar burning velocity (m/s)
$u(t)$	Fluctuating component of the instantaneous velocity (m/s)
u'	Turbulent intensity, RMS of velocity fluctuations (m/s)
V	Volume (m^3)
v	Specific volume (m^3/kg)
WOT	Wide open throttle
X, x	Mass-burned-fraction
\bar{x}	Mean of Sample Data
ϕ	Equivalence ratio
λ	Taylor microscale of turbulence (mm)
λ	Normalised Air fuel ratio
ν	Kinematic viscosity (m^2/s)
η	Kolmogorov scale of turbulence (mm)
η_v	Volumetric efficiency

θ	Instantaneous Value of Crank Position
σ	Standard Deviation of Sample Data.
σ_0	Extrapolated Standard Deviation in Burning time for small mass-fraction-burned.
δ_q	Quenching Distance (mm)
δ_c	Width Of The Flame Kernel (mm)

Subscripts

amb	Ambient conditions
b	Burned mixture
intake	Conditions in the intake manifold
0	Reference condition at 273°K
u	Unburned mixture
tot	Total cylinder conditions
1	Initial crank angle step in the calculations
2	Final crank angle step in the calculations

ACKNOWLEDGEMENTS

I would like to acknowledge the guidance and support of Professor P.G. Hill during the course of my program towards a masters degree in mechanical engineering. I am extremely grateful to him for his untiring support, stimulating discussions and the opportunities he presented to me. I am thankful to him for his confidence in me. I would also like to acknowledge other members of the faculty who provided their assistance and support to me. Special thanks to the Technical support staff viz: Shu Oshika, John Richards and Len Drake and my colleagues for helping me in various forms towards the completion of the program. I also appreciate the support provided by Ragini during the course of my research.

1. INTRODUCTION

Cycle to cycle variations in combustion process are characteristic of all spark ignition engines and are observed at all operating conditions.

The combustion process in a spark ignition engine is controlled such that the chemical energy of the air-fuel mixture is released into useful mechanical work near the top-dead-centre (TDC) of the engine. The mechanical work is the result of the gas pressure acting on the face of the piston at the time of the release of chemical energy in the chamber. Cylinder pressure is thus a direct indicator of the combustion process within the engine.

Typical physical evidence of cyclic variations is illustrated in Fig 1. This diagram shows sample pressure data versus crank angle for 10 consecutive engine cycles at 3000 rpm, wide open throttle (WOT) and stoichiometric equivalence ratio. The engine was a four stroke cycle; hence two revolutions of the engine or 720 degrees of crank angle constitutes one cycle. In Fig 1 '0' corresponds to the bottom dead centre (BDC) at the beginning of the exhaust stroke, '180' corresponds to the top dead centre (TDC) at the beginning of the intake stroke, '360' corresponds to the BDC at the beginning of the compression stroke and '540' represents TDC at the beginning of the expansion stroke. The plot has no misfiring cycles since all the pressure traces in the sample lie above the motored pressure values. The plot displays wide variations in the maximum pressure development from one cycle to another

with steady operating conditions of speed, throttle and spark timing. Variations in the pressure-time plots are due to variation in combustion from cycle-to-cycle. These variations between the pressure-crank angle plots, for the same set of operating conditions, between cycles is termed cycle to cycle variations in a spark ignited engine.

Consistency in cycle-to-cycle pressure development would mean an increase in the mean peak pressure, thereby increasing the power output, improving the fuel economy and the reliability. These improvements are especially useful at leaner fuel-air mixtures because at this fuel-air mixture strength we also have improved efficiency and reduced exhaust gas emissions. Thus, to achieve the benefits of the improvements due to decrease in cyclic variations of pressure the combustion variations should be minimized.

Cyclic variations in combustion have been of interest for the past 30-35 years. Initially, the research was aimed at determining the influence of engine and operating variables on cyclic combustion variations. The major parameters explored were equivalence ratio, fuel type, residuals, ignition systems including spark energy, combustion chambers, speed, compression ratio and intake valve modifications. The consensus conclusions that emerged from the initial studies were that:

- a) although engine operating variables significantly affect the combustion variation of an spark ignition engine they do not seem to cause them; and
- b) in-cylinder velocity variations that exist near the spark plug at the time of ignition affect the cyclic combustion variations.

Later studies based on the previous experimental findings concentrated mainly on those design parameters which modify the in-cylinder flows near the spark plug at the time of ignition. Young, [1] in a review paper, has shown that such modifications are effective in reducing cyclic variations.

Pressure is the most common parameter in studying cyclic variations because of the ease and accuracy with which it can be measured and because it is directly proportional to the amount of charge burned in the combustion chamber. Pressure as a parameter is, in itself, ineffective in studying the initial stages of combustion which is the important area of interest in studying the sources of cyclic variations.

Pressure change is a direct consequence of the mass-fraction-burned; the mass-fraction-burned values at different crank angle positions can be obtained from the experimental pressure data.

Though the design modifications that affect the initial flame period have been shown to decrease the combustion variations, the causes of these cyclic variations have still not been determined.

The objective of this research is to study the origin of these cyclic variations whose explanation has eluded researchers for over three decades. The work consists of three stages:

- a) analysis of experimental pressure data collected from engine tests.
- b) identification of the nature of turbulence at spark from recent trends in research in this area.

c) comparison of experimental results with the reported values of turbulence parameters in accordance with the hypothesis that "Cyclic variations in combustion in spark ignition engines are mainly due to (and predictable from) the small scale structure of turbulence and can be correlated with the Taylor microscale and the laminar burning velocity".

where the Taylor microscale is a characteristic length scale of turbulence described in detail later, and the laminar burning velocity is the burning velocity of the fuel-air mixture in the engine.

Experiments were conducted on an engine (described in chapter 3) at different operating conditions of speeds, equivalence ratios and geometries. Firstly, the experimental pressure data is processed to obtain the values of mass-fraction-burned at every crank angle position for all the cycles within the sample data at a given set of operating conditions. Secondly, the standard deviation in burning times is determined at the different values of mass-fraction-burned within the sample data. The values of the standard deviation in burning times at higher mass-fraction-burned values are used to extrapolate the values of standard deviation in burning time in the initial burning period i.e. for zero mass-fraction-burned. This initial period following spark is the main area of interest. This randomness in the initial stages of combustion is the extrapolated standard deviation in burning time.

Research in the area of the nature of turbulence structure in a spark ignition engine provides quantitative information on the structure of turbulence, the turbulence parameters such as turbulence intensity,

and the length scale. Most of these studies aimed at understanding turbulence within the engine have been conducted in a motored engine (without combustion) wherein the spark plug is replaced by a hot wire and measurements taken using a Constant Temperature Anemometer (CTA). More recent studies in the same area of in-cylinder flows within the engine are conducted using Laser Doppler Anemometry (LDA). Results using either of the two methods in an engine show comparable results for the region near the spark plug at TDC during combustion. Inferences from experiments within the wind tunnel also help to obtain the nature of turbulence within the engines. The turbulent flow in the cylinder at the TDC is random and is dependent on the engine operating conditions. The turbulence can be characterised by determining the nature, the length scales and the turbulence intensity of the flow. This characterization, along with the idea that the spark is almost a point source, shows a random behaviour of the initial flame-kernel propagation with time, called the mean random time delay.

The comparison between the value of the extrapolated standard deviation in burning time and the mean random time delay in burning time shows a linearly increasing relationship between the extrapolated standard deviation in burning time from the experimental data with the data on turbulence as inferred from the trends of recent research.

The following chapters expand on the information provided here and then discuss the results obtained using the above mentioned hypothesis.

2. LITERATURE REVIEW

2.1 Introduction

This chapter reviews the available literature on cyclic variations in spark ignition engines in combustion and pressure development. Most of the experiments described herein were carried out by systematically changing one variable at a time and observing its effect on a parameter chosen to characterize cyclic variations. The various parameters used by researchers in the study of cyclic variations are:

- a) Peak Pressure: the maximum cylinder pressure within each combustion cycle.
- b) Maximum rate of pressure rise
- c) Crank angle at which peak pressure occurs
- d) Flame arrival times: the time for the flame front to travel across the chamber or between flame detectors at specified points.
- e) Burning times: the time duration from ignition to specified mass-burned-fraction or complete combustion.
- f) Indicated mean effective pressure: the work per cycle divided by the displacement volume.

The first five parameters described above are directly related to the combustion process and help in quantifying the cyclic variations. The sixth parameter is an integral parameter which is more useful in determining the effects of combustion variations on engine speed or vehicle motion. The ease and accuracy of measuring the pressure in the combustion chamber using piezo-electric transducers has made the peak pressure or rate of pressure rise the most commonly used parameter in

studying cyclic variations in engines.

The initial burning period in an engine (following spark) is of particular interest in this research due to the evidence (which will be discussed later) that cyclic variations have been found to originate early in the combustion period. The time to burn the first 5% of the fuel may, therefore, be more significant than the cyclic variations in peak pressures in any discussion of the causes of cyclic variations.

The cyclic variations, which are the subject of this review, are not those which are associated with engine misfiring or lack of homogeneity in the fuel-air mixture or malfunctioning of the ignition system. They are those present in a well designed, well tuned engine operating on fully mixed high quality fuels.

2.2 Effect of Air-Fuel Mixture Composition

The principal characteristics of the inflammable air-fuel mixture in the engine are the equivalence ratio, fuel type, and the degree of charge dilution by residual gas from the previous cycle.

Equivalence Ratio

Warren and Hinkamp [44] studied the effects of change in equivalence ratio on cyclic variations in a single cylinder modified CFR engine using well mixed iso-octane fuel at a compression ratio of 9.5:1, WOT, and MBT spark timing at 1200 rpm. Using ionization gaps to detect the flame arrival times at 73mm from the spark plug, they observed minimum variations in flame arrival times at 1.15 equivalence ratio. As a fraction of mean arrival times, the minimum spread was reported to be 0.38. The spread in flame arrival times increased with both richer and leaner mixtures. They also showed that this minimum variation in flame

arrival times occurred at the mixture strength corresponding to the maximum power. In this study, it was found that minimum variations in flame arrival times occurred when the mean arrival times were a minimum i.e., mean flame speeds were the highest.

Using a single cylinder Renault engine and iso-octane as the fuel Karim [11] observed minimum coefficient of variations in the range of 1.25 to 1.35 equivalence ratio for speeds of 3500 and 2500 rpm at 8.5:1 compression ratio. In addition, Karim noted that the value of the mean coefficient of variation a) approached the weaker mixture strength as the speed was increased; b) increased as the equivalence ratio was changed from the optimum value; and c) the value was never less than 5% even under the most steady operating conditions.

Soltau [10] used a similar, but petrol fuelled, engine and observed minimum variation in the peak pressure at 1.06 ϕ to 1.23 ϕ at 9:1 compression ratio at 3500 rpm and 500 rpm respectively.

Both Soltau and Karim observed best-power values at the equivalence ratio corresponding to the minimum variations in the measuring parameter.

Thus, the equivalence ratio was found to be an important factor influencing cyclic variations in combustion and subsequent pressure development in the engine. Minimum cyclic variations in combustion were found to occur at the equivalence ratio corresponding to the mixture strength for maximum power typically in the range of 1.06 to 1.35, depending on the speed, fuel and the compression ratio. At these mixture-strengths the combustion duration was the shortest and the values of peak pressure were the highest.

The effect of measuring parameter such as peak pressure, COV and flame arrival times being such that variations in flame arrival times increase slowly away from the minimum point at both rich and lean equivalence ratios and variations in peak pressure increase rapidly from the minimum point.

Fuel Type

Fuels with faster flame speeds can release a larger part of their energy near TDC where the volume change due to piston movement is minimum. Pressure variations, therefore, are mainly due to the combustion variations. With slower burning velocity, substantial energy is released late in the cycle, past TDC, when the volume is changing faster due to the increasing piston velocity. The variations in pressure due to the combustion variations then include the effect of the changing pressure due to rapidly varying cylinder volume during this part of the cycle motion. A numerical calculation undertaken in appendix B shows the effect of this combustion volume phasing on the magnitude of the pressure.

Starkman, Strange and Dahm [54] performed experiments in a single cylinder CFR engine in which ionization gaps were placed in the path of the flame travel and were used to monitor flame arrival times of the reaction front for many cycles. They found that for each fuel studied there existed a minimum reaction front propagation rate which was a function of equivalence ratio. For the nitroparaffin family, the peak reaction front propagation rate was approximately near $\phi = 1.0$ and for iso-octane and methanol the peaks were at $\phi = 1.15$ and 1.45 respectively. Thus, the equivalence ratio at which minimum cyclic

variations occurred depended greatly on the fuel used. Starkman et al. also showed that the maximum flame speeds for different fuels had different magnitudes. Methanol had the highest normal rate of reaction front propagation of 180 ft/sec. The different rates of pressure rise is thus related to the fuel used in the study and better combustion-volume phasing of the fuels with faster flame speeds will show less pressure variations compared to the slower burning fuels.

To study the effects of different fuels, both liquid and gaseous, on the flame development in a combustion chamber using a Renault engine, Soltau [10] noted that for a certain equivalence ratio the mean variation in pressure was not identical for all the fuels and some pressure variation was observed with each and every fuel fed to the engine. He also found that a pre-mixed charge obtained with gaseous fuels such as methane, towngas and butane did not display less pressure fluctuations than a well-mixed liquid petrol fuel-air mixture carburetted or sprayed into the intake manifold.

Thus, the magnitude of the propagation flame speed and the mixture strength at which it occurs are the two important fuel related characteristics that influence cyclic variations in pressure development. It can also be deduced that the faster the fuel burns, the less the cycle is troubled with peak pressure fluctuation from one cycle to another.

Charge Dilution

Karim performed tests in which the level of the residuals in the chamber was increased by partly closing the throttle. From these tests he found the minimum coefficient of variation increased from 0.08 at WOT

to 0.10 at 1/4 throttle and 0.25 at 1/8 open throttle. He concluded that increased residuals resulted in higher cyclic pressure variability. Karim found that increased dilution of the fresh charge with either nitrogen or carbon dioxide resulted in increased variations in peak pressure. The difference in the variation of peak pressure using added carbon dioxide or nitrogen was relatively small, which showed that the effect of the residual concentration on the pressure variability did not depend on the major constituent of the residual gases.

To eliminate residuals, Soltau operated his engine by "skip" firing every fourth cycle. From the P-V diagrams generated, he observed that almost complete purging of residual gases resulted in steadier operation although some variation still occurred. This steady operation, he noted, was due to the fast burning that occurred in the absence of residuals. The parameter (IMEP) used to study cyclic variations in this case were qualitative and the numerical results were not presented by the author.

Patterson [40] investigated the influence of residuals by "skip" firing every fourth, second and every cycle on a CFR engine fueled with indolene at about 0.8 ϕ , MBT spark timing and 1600 RPM. He observed that results of the cyclic variations in maximum rate of pressure rise for all the cases tested showed no significant changes. This results contradicts Soltau's or Karim's results and can be explained by noting that the results reflect the combined effects of residuals and MBT spark timing on cyclic variations.

Thus, an increase in dilution whether with exhaust residuals or with other inert gases, was generally found to result in increased cyclic

variations in pressure development. This pressure development could have been due to decreased flame speeds in the presence of residuals.

2.3 Effect of Ignition Variables

The effects of the ignition variables on cyclic combustion variations reviewed are- ignition system, electrode geometry and spark jitter.

Ignition System

Soltau used two different ignition systems to investigate the influence of the spark energy on the burning process. The first one was a standard suppressed coil ignition system. The other system was modified with a rheostat in the primary winding to reduce the primary coil current and thus the spark energy. Both systems initiated a single spark at the plug electrode. He noted that at any load or speed the energy content of the spark had no influence on the repeatability of the cycles as long as no misfiring occurred. However, at the fringe of air-fuel ignitability, if the energy was reduced, then misfiring did occur. He also found that with a wide-open throttle, the air fuel ratio at which the engine started misfiring was virtually the same for all practical amounts of spark energy, as long as the gap length was greater than the quenching distance. Soltau found that pressure records taken under identical conditions of load and speed but with spark energy varying from 0.20 to 200 mJ showed no difference in peak pressure variation.

Patterson [40] studied the contribution of the ignition system to the combustion variations by using a high energy fast-rise-time (40 μ sec) capacitive discharge system and an inductive system (120 μ sec) and

observed no difference in the mean torque at the dynamometer.

Therefore, there is little evidence of the influence of the type of ignition system on the cyclic variation in the absence of misfiring.

Spark Electrode Geometry

Soltau [10] used different types of electrode shape on the spark plug in a Renault engine and observed no difference in the peak pressure variations and I.M.E.P. He used non standard forms of electrodes such as sharp points, special discharge surfaces and large mass plug points.

The shape of the spark plug was thus insignificant in studying cyclic variations (i.e. electrode shape was found to have no effect on cyclic variations of pressure).

Spark Jitter

Spark Jitter is defined as the variation in the spark timing from cycle-to-cycle. This jitter could be due to the vibration of the drive or distributor mechanism so that it does not occur at the same crank angle for each cycle within the sample.

Soltau [10], from his experiments using a standard type of distributor and Renault research engine, noted that the point of ignition was repeatable. He used a quartz-window engine and high speed photography to find that the point of ignition did not vary by more than 2° crank angle due to the vibration in the distribution. Assuming that in each combustion cycle the heat release diagram is similar, Soltau calculated that it would require variations in spark timing of over 15° at 2500 rpm to produce the observed differences in peak pressure.

Careful examination of the ignition setting by Karim [11] revealed that spark at a point setting is consistent to within 1.5° crank angle.

Albrecht et al [53] studied the development of the spark discharge, as well as the initiation of chemical reaction experimentally using high frequency measuring techniques in an inflammable mixture. They noted that the activation radicals could be detected at an early stage (about 10 nanoseconds) and the starting point for combustion was determined to exist between 10 to 20 microseconds. This led them to conclude that the spark process is highly repeatable and does not contribute to the cyclic variations.

Thus, Soltau and Karim noted that spark jitter was too small to account for the observed cyclic variations.

Summarizing the effects of ignition variables on cyclic variations, previous research has shown that a) the improvement in combustion using different ignition systems is insignificant; b) the shape of the electrode geometry does not affect cyclic variations; and c) the spark initiation process is highly repeatable.

Thus, cyclic variations in combustion are affected little if at all by changes in the type of ignition system, quantity of spark energy, presence of spark jitter and the shape of the electrodes.

2.4 Engine Speed and Compression Ratio

Karim [11] found that the influence of speed on combustion variation is related to the equivalence ratio. He observed that for the lean range of mixtures an increase in speed reduces the COV. At best power mixture strengths, the speed had no visible effect and at rich equivalence ratios, an increase in speed resulted in a deterioration of COV.

Soltau [10] found that the average peak pressure deviation from the

mean increased from 7.24 at compression ratio of 6:1 to 12.9 at a compression ratio of 9:1 and showed steadier influence at a large compression ratio when it decreased from 12.9 to 9.8 at 12:1 compression ratio at 2000rpm and best-power equivalence ratio in a Renault engine.

Winsor and Patterson [20] found an increase in peak pressure variation as engine speed was increased. They conducted tests at an equivalence ratio of 1.06, at 8.5:1 compression ratio and spark advance of 35° before TDC.

To study the effects of compression ratio and speed Barton et al [14] increased the compression ratio from 7:1 to 16:1 and speed from 900 to 1800 rpm. Barton et al observed a) increase in pressure variations with increase in speed and compression ratio b) increase in flame speeds and variations in flame speed with increase in speed and compression ratio.

Young [1], in his review paper, reported that increasing engine speed usually results in larger cyclic combustion variation and pressure variations. He stated that increases in flame speed has been attributed to increase in engine turbulence with engine speed and this higher turbulence also probably causes an increase in flame speed variations. The increase in compression ratio slightly decreases the cyclic variations because of the lower residuals and higher temperatures.

Nevertheless, the values reported on the effect of engine speed and compression ratio on cyclic variations indicate that the relationship is weak.

2.5 Effect of Combustion Chamber Geometry

The design variables considered in this section are relatively

rigid such as chamber shape, spark timing and valve shrouding. They are rigid in the sense that they cannot be changed in the course of experiments.

Chamber Shape and Spark Location

Young (1) made a comprehensive study of three different combustion chambers and noted that the best chamber shape from the cyclic dispersion point of view is the one that allows the greatest amount of cylinder volume to be engulfed per unit of travel of an assumed spherical flame front propagating from the spark plug. This efficient chamber with the efficient location of the spark plug would have the shortest combustion duration period of all possible locations of the spark plug and hence the lowest cyclic variations of the engine.

Soltau [10] observed decreased peak pressure variations when the charge was ignited by moving the spark plug near or to the center of the combustion chamber rather than placing it at the near wall location.

Hirao and Kim [41], in their experiment, moved the spark plug location from directly above the piston to the more open volume near the valves in an L head engine. They observed lower cyclic variations and noted that any change which decreased the maximum flame travel distance or increased the rate of mass burning and thus decreased flame travel times resulted in lowered cyclic variations.

Thus, the best chamber and spark plug combination would have the shortest combustion duration. A short combustion duration implies a fast burning cycle since the fast burning cycle releases most of its energy at or near TDC where there exists a good volume-pressure phasing. This phasing results in lower values of cyclic variability in combustion

duration.

Spark Timing

Karim [11] found that the effect of spark timing on the relative peak pressure variations was dependent on the mixture strength. From tests at the rich mixture of 1.15ϕ , using iso-octane as the fuel, Karim found that the effect of spark timing on the relative peak pressure variations were constant for a spark timing range of 30° to 70° BTDC and increased with retard in spark less than 30° BTDC. As the equivalence ratio was made leaner, spark timing had an increasingly stronger effect on the relative peak pressure variations. For all the cases considered Karim found that minimum cyclic pressure variations occurred at MBT spark timing.

Warren and Hinkamp [44], using ionization gaps along the flame path, observed minimum variations in flame arrival time near MBT spark timing. At this minimum the spread was about 35% of the total travel duration. The ionization gap was located 73mm from the spark plug so the total travel duration included both the ignition delay and the actual propagation rate.

There is a general consensus regarding the views presented above that minimum variations occur at the MBT spark timing and that the effect of spark timing is influenced by the mixture strength and spark plug location.

Valve Shrouding

Patterson [40] investigated the effect of turbulence and mixture motion on cyclic variations by observing the effect of shrouded intake valve. He observed a decrease in the pressure rate variation from about

55% with the normal unshrouded valve to about 30% with a shrouded intake valve. The shrouded intake valve induced swirl in a propane fuelled, CFR engine at 1600 rpm and WOT condition. The experiment showed that the absolute spread in pressure rates remained essentially unchanged, while the mean rate was nearly doubled. Patterson postulated that swirl produced by this shrouded valve affects early flame kernel development by smearing the kernel and increasing its surface area. As swirl increased the combustion rates, Patterson postulated that cyclic variations in mixture motion would lead to cyclic variations in pressure or any other parameter used in the study of cyclic variations.

Broeze [42] used three different types of intake valves on a CFR research engine: a standard unshrouded intake valve, a shrouded valve and a castellated valve, to examine the effect of the change in intake valve geometry on the delay period and the main combustion period. Broeze defined the delay period as the period without appreciable pressure rise on the fired engine pressure curve from the motored engine pressure curve under the same operating conditions. The shrouded intake valve was filed progressively such that all the three valves gave the same volumetric efficiency. Broeze found that the standard non-shrouded valve had the longest burning period for both the initial and the main stage period. The castellated valve shortened the initial and the main stage burning period, possibly due to the increased turbulence. The shrouded intake valve results showed that the initial burning period was shortened more than with the castellated valve and the main burning stage was the same as with the castellated valve.

Broeze [42] also found that the ignition delay period was strongly

affected by the mixture strength for all the intake valves considered and the main combustion duration was nearly constant with change in mixture strength.

The shrouded valve produced enhanced turbulence as well as swirl. Broeze thus postulated that both swirl and turbulence decreased the boundary layer thickness and allowed the developing flame kernel to interact with the turbulent mainstream earlier. Furthermore, since swirl could persist longer than the compression stroke, it was thought to be more effective than turbulence in decreasing the initial delay period.

Thus, though Broeze did not consider cyclic variations, his experimental results using different intake valves show that the shrouded intake valve and a castellated valve have a strong effect of decreasing the initial delay period.

Young [1], in his review paper, noted that mixture motions and turbulence are mostly responsible for cyclic variations in combustion and subsequent pressure development. He also stated that due to the difficulty of measuring in-cylinder flows, the role of turbulence and mixture motion in cyclic variations has been largely inferred from the physical changes made to the engine.

Karim [11], in his study of cyclic variations stated that "by far the greatest variable element in engine operation is that of charge motion inside the cylinder both in quantity and direction."

Summarizing the effects of the different design variables, it can be seen that valve shrouding and turbulence are the two factors that can improve cyclic variations. The effect of swirl induced by the shrouded

valve is more than that of turbulence alone produced by the castellated valve. Valve shrouding has been shown to influence the initial burning period although there still exists randomness of the flow within the engine at the time of the spark. The main conclusion from this particular design variable is that if the initial burning period can be affected, then the cyclic variations can be reduced.

2.6 Comments

The importance of the initial burning period has also been shown by various other researchers.

Soltau [10] used coal dust for flow visualization in a modified Renault engine using a quartz-window with no squish or swirl. He observed no conformity to any pattern within the engine from the high speed-movies collected by him from this simple chamber. He then postulated that this randomness in flow contributes to the randomness in cyclic variations in engines.

Peters and Borman [12] have reported that cycles with varied burning rates in the initial burning period continue to have lower burning rates even when combustion is well under way.

Belmont, Hancock and Birmingham [36], from viewing a succession of indicator diagrams from successive cycles, noted that the future of the combustion appeared to be defined at a very early stage in the cycle.

Young's review paper summarized the findings by stating that "cycle-to-cycle variations in combustion originate early in the combustion process. Although hard evidence is still lacking, it is thought that a main cause of these variations is the cycle-to-cycle variations of velocity in the vicinity of the spark plug at the time of ignition, which affects the developing flame kernel."

3. APPARATUS AND INSTRUMENTATION

3.1 Introduction

This chapter provides an overview of the experimental setup to study cyclic variations in the engine. Fig 2 shows gives a brief idea of the experimental setup. First a brief description of the apparatus is given. Second, the instrumentation used to evaluate the cyclic variations quantitatively is described. Third, the controls are described, as well as the starting procedure. Finally, an overview of the data acquisition and data transfer techniques is presented.

3.2 Apparatus

The apparatus consists of the engine and the dynamometer, air and fuel intake systems, oil and cooling systems and the ignition system.

Engine

The engine used throughout the investigation is a Ricardo research engine. A cross-sectional view of the engine is shown in Fig 3. It is a four-stroke, single-cylinder, water cooled, spark-ignition engine, having an 80.2mm bore and 88.2mm stroke and compression ratio of approximately 8.9:1. The engine is fitted with the "bath-tub" combustion chamber shown in Fig 4 and has vertical overhead valves actuated from an overhead camshaft driven by a belt through the crankshaft. The specifications of the engine are given in Table 1. The combustion chamber forms the heart of the apparatus. The related components that form the whole assembly are now briefly described.

Air Inlet System

The air-inlet system consists of an air filter, aluminum alloy heater chamber with a 1 kW heater, throttle body assembly with servo

motor controlled throttle, and inlet manifold. The position of the throttle butterfly is remotely controlled from the control console. Signals for the temperature indicator are provided by a duplex thermocouple installed in the inlet manifold. A laminar flow element (Cussons VFAM-120C) is mounted just ahead of the air filter to enable accurate metering of the air flow. The pressure drop across the laminar flow element is sensed by a differential manometer in the control room.

Fuel Intake System

The fuel-intake system consists of a 1.5" Meriam laminar flow element, piping and a flow control valve which is used to vary the air-fuel ratio. The fuel (natural gas) from the mains passes through the regulator before it goes through the laminar flow element. A Celesco P7D differential pressure transducer measures the pressure drop across the laminar flow element. This signal from the differential pressure transducer is then amplified by the Celesco low cost carrier demodulator, and made compatible with the data acquisition system. The pressure drop across the laminar flow element is also sensed by a differential manometer in the control room.

Coolant System

The coolant system circuit is closed and pressurized. The coolant, consisting of water and commercial antifreeze/inhibitor, is drawn from the bottom of the header tank and pumped through the a heat exchanger before passing through to the engine block and cylinder head. The header tank contains low coolant level sensor and two thermocouples one trips the system if overheated and the other provides temperature data to the control console. The temperature of the cooling water can be

controlled by the limit switches on the cooling tank on the engine. Temperatures in the range of 60 to 75°C were observed on the console in the course of these experiments and the temperature was set to trip at 100°C due to the overheating of the coolant.

Oil System

The lubricating oil which is contained in the engine sump is pressure fed to the crankshaft and the big end bearings and camshaft bearings. The oil pressure is limited to 4 bar by a relief valve in the engine. A pressure switch on the engine trips the engine in case of oil pressure failure. A thermocouple trips the system if overheated, and another thermocouple provides oil temperature data to the console.

Dynamometer

The dynamometer is a D.C machine mounted on trunnion bearings supported by pedestals. Load is measured by means of a torque arm mounted from the frame of the dynamometer. The arm carries a strain gauge load cell whose output provides a continuous display of the torque at the control console. A pedestal houses a calibration weight equivalent of 20 Nm for static checking of the torque measuring system. The dynamometer is operated through a KTK thyristor converter unit. The dynamometer can act as a d.c. motor to drive the engine during starting and motoring operations or as a d.c. generator when the engine is in firing mode. A tachometer mounted on the dynamometer shaft provides a speed signal to the closed loop speed control system. The engine is coupled to a D.C dynamometer and utilizes regenerative load absorption which facilitates motoring over variable speed range and assessment of the frictional losses when required. The dynamometer unit is capable

of absorbing up to 44 kW of engine power at up to 5500 rpm.

Ignition System

The engine ignition system is a conventional coil and spark plug arrangement with the primary coil circuit operated by a "Lumenition" electronic ignition unit. The principle of the Lumenition unit is that signal pickups of speed and TDC reference from the flywheel on the crankshaft are processed by the electronic system along with the desired remotely set signal of the ignition timing from the control console. The lumenition system then provides the ignition trigger signal at the correct spark advance. This electronic ignition system model PHY 623 eliminates spark jitter due to mechanical cams or distributors.

3.3 Instrumentation

The instrumentation on the research engine which aids in monitoring the engine as well as obtaining quantitative data is now described and is as shown in Fig 5. The pressure transducer, optical pickup unit, air and gas flow metering units, lambda sensor, speed and torque measuring sensors constitute the instrumentation described below. The data acquisition systems used are also described.

Pressure Measurement

The engine is equipped with a Kistler 6121 piezo-electric pressure transducer mounted in an extension sleeve into the outer sleeve located in the cylinder head of the engine. For the piezo-electric transducer no water jacket or cooling water is necessary since it is self cooling. The charge output from the transducer was integrated by the Kistler model 5004 charge amplifier to yield a voltage proportional to the

cylinder pressure. Thus the signal from the transducer yielded the cylinder pressure and rate of pressure rise. The display of the pressure signal was monitored using a Tektronix oscilloscope. One hundred consecutive cycles of pressure data were digitized at a rate of 1 sample/degree for each set of operating condition.

The combination of the piezo-electric pressure transducer and charge amplifier was calibrated with a dead weight tester in the laboratory prior to performing any tests. The calibration curve for the transducer is provided in appendix A.

Volume Assignment

The accuracy of the pressure measurement was complemented by an accurate measurement of the crank angle position using an AVL optical-pickup-unit. An optical crank angle pickup unit model 360c/600 was mounted on the engine crank shaft. This sensor generated pulses every crank angle degree which were used to trigger the data acquisition system. A single pulse from the BDC is used to synchronize the data with the position of the crank shaft. The volume at any instant of the piston motion is then deduced from the physical dimensions of the engine and the crank position. The physical dimensions can be determined quite accurately hence the accuracy of the total volume calculation is limited by the accuracy of both the clearance volume measurement and the determination of crank angle. The synchronization of the pressure-volume data is further verified by analyzing the motored engine data in chapter 4.

The data obtained using an engine driven optical pulse generator synchronizes digital scanning of pressure signal with crank angle . A

BDC marker pulse on one channel of the pulse generator was used to initiate scanning. The second channel provides 600 pulses which are further resolved to 1800 pulses through the pulse multiplier and depending on the number of pressure points to be scanned they are further divided by the pulse divider. In this particular case 360 pulses per revolution at one crank angle degree interval determines the actual scanning points. As the location of each scanning pulse was fixed in relation to the marker pulse (BDC pulse) the locations of the other scanning pulses were determined by determining the crank angle at which the marker pulse of BDC occurred.

Air flow Measurement

The metering of the air inducted into the engine is done by reading the differential pressure across the laminar flow element in inches of water gauge on an inclined differential manometer situated in the control room. The laminar flow element is an accurate measuring instrument which is calibrated by the manufacturer. The calibration constant at standard normal conditions is provided with the instrument. These calibration constants are used to translate the pressure into the volume flowrate. The calibration curve for the laminar flow element is provided in appendix A.

Gas flow Measurement

The metering of the fuel inducted into the engine is done by using the differential pressure across the laminar flow element in inches of water gauge on an inclined differential manometer situated in the control room. The laminar flow element is an accurate measuring instrument which is calibrated by the manufacturer and the calibration

constant at standard normal conditions are provided with the instrument. These calibration constant are used to translate the pressure into the volume flowrate of the gas into the engine. The calibration curve for the laminar flow element is provided in appendix A.

Fuel-Air Ratio

The normalized air-fuel ratio is the ratio of the actual air-fuel ratio to the theoretical air-fuel ratio. Control of the air-fuel ratio was assisted by the use of a zirconium dioxide oxygen sensor in the exhaust pipe. The output of the sensor was fed to a digital voltmeter to indicate whether the engine was running rich (approx 0.8 volts), stoichiometric (approx 0.1 to 0.5 volts), or lean (less than 0.1v). However, this is a rough indicator of the range of operation, and is more useful in assisting with the stoichiometric air-fuel ratio. The actual values of fuel-air ratio are shown on the PC monitor screen using the software.

Speed Measurement

Speed measurement is made by the tachometer attached to the dynamometer shaft. Speed is set by a set-speed potentiometer on the control console. A closed loop control system for the speed compares the actual and proposed speeds by the comparator. The error signal is then sent to maintain a constant speed irrespective of throttle setting changes, fuel-air ratio change or spark advance. The engine speed range is 1200-5500 rpm. Actual speed values on the console are steady to within $\pm 0.2\%$.

Torque measurement

The strain gage load cells mounted on the torque arm which is

mounted on the frame of the dynamometer provides the torque values as they are seen on the control console. A test was conducted to examine the variation in the torque meter at 2000 rpm in a motored engine. The static calibration of the engine using 20 Nm weight both before and after running the engine for about 10 minutes showed a variation in the torque meter of about 0.60 Nm. The torque values from the dynamometer as seen on the console show a variation in the results that are collected from the torque meter at every measuring point of engine data collection.

Data Acquisition System

Two data acquisition systems have been employed on this project to allow real time data to be collected for processing as shown in Fig 6.

The analogue signals from the instrumentation on the engine viz: ignition advance, airflow, fuel flow, speed and torque terminate near the first data acquisition system in a mil-spec connector, which plugs into the circuit box in control room. The circuit box contains screen terminal boards which connect to the data translation DT2801A data acquisition board installed inside the PC. Another circuit board provides trigger and clock pulses to the ISAAC 2000 where pressure data and BDC pulses are being recorded. Signals from the mil-spec connector entering the terminal boards are optically isolated and ion-pass filtered at 60 Hz before passing into the A/D converter inside the PC via the ribbon connector.

The second system consists entirely of an ISAAC 2000, which is a fast data acquisition unit and has 64K of buffer memory, off line block transfer of data and highly flexible sample control system. It uses

Labsoft II software and is compatible with the IBM PC used for this experimental setup. Sampling rates of 200 kHz are available at 16 channels.

3.4 Operational Control

The apparatus and procedure for engine control are now presented. The control console in the control room is first described followed by the starting procedure of the engine.

Control-Console

The control console in the control room shows the digital torque in the range of 0-50 Nm and digital speed in the range of 0-120 rev/sec and ignition advance +70 to -20 degrees analogue and running hours 0-999 digital. It also shows an 8 channel digital temperature indicator for inlet air, fuel, water (engine coolant) and oil temperature, exhaust gas temperature. Three channels are left open.

The controls of the engine room on the console are:

- a) dynamometer motor mode of start/auto/absorb mode depending on the testing conditions.
- b) set speed potentiometer to set the required speed on the engine.
- c) emergency stop button to stop the engine in case of emergency
- d) throttle position to control the volumetric efficiency, and
- e) ignition timing to set the spark timing.

The safety monitoring system on the console consists of the dynamometer temperature, oil pressure-low indicator, emergency stop switch, water level indicator and water and oil temperature indicators.

Starting Procedure

After preliminary checking of all apparatus and instruments a standard routine as described below is carried out before any actual firing or non-firing data is collected.

A check on the oil level in the crank case is carried out followed by a minimum of two hand crank rotations on the engine to check for any seizing of the piston or to avoid any other seizing problem. The mains are then turned on along with the water for the dynamometer. The engine lubricating oil and water pump are started, and the charge amplifier is left on for about an hour in a reset mode. The charge amplifier range adjustments should be set to give the longest system time constant without encountering signal drift. The time constant of the piezo-electric system is not a measure of the time it takes the system to respond to an input but rather a measure of the time required for a given pressure signal to decay. The lubricating oil temperature is heated to approximately 40°C before the engine is started. The engine is first set to partly open throttle and then started to rapidly reach a speed of about 1200rpm to avoid running at the natural frequency of vibration of the engine. This procedure described so far is common to both firing and non-firing engine studies.

For the motored case the design speed is set and the throttle opened wide to obtain WOT condition and the engine is all set to acquire the motored engine data.

For the fired engine case the ignition switch is turned on and the fuel supply is started until the engine starts stable firing. To reach the desired operating condition the speed and the throttle are slowly

coordinated and increased to reach the desired design state from the initial condition. The engine is then run in firing mode until conditions stabilize. The power output, efficiency and torque values are then monitored such that the setting of the minimum spark advance will give the best values of torque and power.

In both firing and non firing engine conditions the data collection program is simultaneously loaded and run to collect the data of 100 consecutive cycles at different operating conditions. This program scans the channels on the data acquisition board DT 2801A to read in the data coming from the various transducers attached to the engine. A total of 100 values are read in from each channel and averaged over a 5 second period. The values of voltages through appropriate signal conditioning systems and by integration with software from the PC are updated on the monitor screen of the PC every 5 seconds. For fired engine testing MBT (Minimum spark advance for Best Torque) timing of the ignition system is the value of spark advance at the required throttle setting which shows optimum values of brake power and thermal efficiency. After desired operating conditions on the engine are reached the data collection program is loaded on the computer.

3.5 Data Acquisition and Transfer

A discussion of the satisfactory set up of the apparatus and the instrumentation is followed by the procedure for data acquisition and subsequently the transfer of data for processing.

Data Acquisition

The pressure signals from the charge amplifier and the signals from the AVL optical pick up sensor are fed to the circuit-box to condition

the signals and then to the ISAAC 2000 data acquisition system for collection of data.

The software used for data acquisition is flexible and is an interactive program which asks for input such as the number of cycles for which data has to be collected, the number of channels to be read and the operating speed. This input is later used by the IBM PC computer to communicate with the ISAAC 2000 to acquire cylinder pressure at the appropriate intervals following the trigger from the BDC pulses. The operating conditions set, a trigger from the DT2801A board sent to ISAAC 2000 starts acquiring 100 consecutive cycles of data after the expansion stroke. This data is stored in the ISAAC 2000 fast data acquisition system. This stored data in the ISAAC is then transferred to the IBM PC onto a diskette. While the data is being collected by the ISAAC relevant information from the console at that particular operating conditions such as speed, air flow, fuel flow, temperatures, and the performance results is noted.

Data Transfer

The data collected on the PC, are then transferred to the mini computer VAX 11/750 by using a communication package. The data on VAX 11/750 is now prepared for detailed analysis by reducing it using a program called ISAC2VAX. This program ISAC2VAX concatenates the data into one single file of 100 consecutive cycles. It strips the first seven characters that are transferred with the binary data sent over to VAX, leaving behind the Pressure and BDC pulse data points which are bundled up into one large file for further statistical analysis.

4. MEASUREMENTS WITH MOTORED ENGINE

4.1 Introduction

Preliminary checks of the motored engine (non-firing) performance are undertaken before fired engine data is recorded, to validate the digital pressure and crank angle data.

Pressure data collected from the motored engine shows little cycle-to-cycle variability but can yield considerable information about the accuracy and reliability of the recording procedures. In a motored engine inhomogenieties, high heat transfer rates and combustion introduced quantities are largely absent. Hence it is worthwhile to critically analyze the motored pressure data before firing test data is recorded.

The monitored tests in a motored engine were carried out at 2400, 3000, 3600 and 4200 rpm, with wide-open throttle. While the pressure data are taken from an engine, other pertinent data from the console such as air flow rates, speed, temperature and atmospheric pressure are noted concurrently.

The pressure data is analyzed to ascertain: a) Proper phasing of pressure-volume data b) Polytopic exponents of compression and expansion c) Volumetric efficiency, and d) Peak pressures.

4.2 Phasing of Pressure-Volume Data

The initial check on the data is to observe the occurrence of peak pressure on the ensemble-averaged pressure data of 100 cycles, with respect to the volume by observing the phasing of pressure vs crank angle plot from Fig 7. The occurrence of peak pressure occurs slightly before TDC (in the range of TDC to 2° crank angle before TDC) serves as

an approximate check of pressure-crank angle phasing.

The ensemble-averaged peak pressure does not occur at the same crank angle before TDC for all the speed ranges considered in this research, but lies within the TDC to -2° before TDC range.

The indicator (P-V) diagram, as shown in Fig 8, serves as a qualitative check of the pumping loop (exhaust and intake stroke) pressure trace. The majority of the exhaust stroke pressure trace is above the mean exhaust manifold pressure. Similarly, during the intake stroke the cylinder pressure falls below the mean intake manifold pressure. The spikes in the pressure trace during the intake stroke may be due to the high instantaneous gas flow rate due to the changing valve movement during intake.

The effect of phasing of the pressure volume data is magnified in the IMEP values of the motored engine. The indicated mean effective pressure (IMEP) is the theoretical pressure at which a constant pressure expansion from minimum cylinder volume to maximum cylinder volume would produce an amount of work equal to the quantity being considered. The IMEP and PMEP (Pumping Mean Effective Pressure) values for the test cases considered are shown in Table 2. Table 2 also shows that deliberately retarding or advancing the phasing, the sensitivity of IMEP to the phasing is as high as 40% per degree crank angle, whereas the PMEP is relatively insensitive to changes in phasing.

TABLE 2: Sensitivity of IMEP and PMEP to 1° change in phasing-Motored Engine.

SPEED	NORMAL		1° ADVANCED		1° RETARDED	
	IMEP	PMEP	IMEP	PMEP	IMEP	PMEP
2400	-39.3	-24.2	-57.5	-24.1	-21.1	-24.3
3000	-38.5	-39.5	-57.5	-39.6	-19.6	-39.3
3600	-32.9	-55.8	-52.3	-56.3	-13.4	-55.3
4200	-28.9	-86.9	-48.2	-87.7	-09.6	-86.0

Phasing is, thus, an important check on motored pressure data as it confirms the compatibility of the pressure transducer and the crank angle pick up unit.

Figure 8 is a logarithmic P-V diagram of motored pressure data. It contains information about the scaling, phasing and the transducer performance.

The compression curve from the IVC to near TDC can be approximated by a polytropic process $PV^n = \text{constant}$. This function plots as a straight line on the logarithmic diagram with slope = $-n$. The deviation from a straight line of this function $PV^n = \text{constant}$ with slope equal to $-n$ can be caused by several factors viz:

- a) Improper Reference Pressure: If the reference pressure is improperly assigned at BDC (the transducer used is piezo-electric) then a small curvature is noticeable during the first part of the compression stroke after IVC. Fig 9 shows this effect of an

incorrect reference pressure allocated to the piezo-electric transducer. Since this is a simple scaling problem, it can be easily corrected.

b) Improper Clearance Volume: If the wrong clearance volume is assigned to the engine similar distortion of the curve is observed at the top end of compression stroke towards TDC. The central portion of the compression curves remains relatively unaffected by wrongful assignment of the values of Reference pressure and/or clearance volume. Deviations from the straight line in the central region is an indication that the pressure data and/or pressure transducer maybe faulty.

c) Improper Phasing: Improper phasing of the pressure-volume data distorts the logarithmic P-V plot. If the pressure data is retarded w.r.t the volume then the pressure data at the TDC during expansion are greater than compression pressure data. Figure 10 shows the effect of phasing when the pressure was intentionally retarded w.r.t volume. The higher values of pressure during expansion overlap the compression pressure data. A similar plot could also result for a faulty transducer.

Finally, the time constant setting on the charge amplifier also could give faulty results by showing distortion on the logarithmic P-V plot.

The log plots of the motored data collected for this experiment did not show any of the above distortions and hence the scaling, and calibration of the transducer assembly was shown to be acceptable for further engine data collection.

4.3 Polytropic Exponents

The compression and expansion curve from the IVC (Inlet Valve Closing) to nearly TDC, and from TDC to EVO (exhaust valve opening) respectively, can be approximated by a polytropic process $PV^n =$ constant. Figure 8 shows how the motored pressure data for the four stroke cycle plots as a straight line on a natural log plot. The slope of the plots for the compression and expansion gives the compression and expansion coefficients.

The slope of the compression and the expansion line represented as a polytropic process is another indicator of the quality of motored data. The range of the polytropic exponents is different for different engine geometries. The expansion exponents are higher than the compression exponents as discussed below.

From the first law of thermodynamics for the system per unit mass

$$dq = du + dw \dots \dots \dots (4.1)$$

$$dw = Pdv \quad \text{(constant pressure)}$$

from the definition of enthalpy

$$h = u + Pv \dots \dots \dots (4.2)$$

differentiating (4.2) we have

$$dh = du + Pdv + vdP \dots \dots \dots (4.3)$$

rearranging we have

$$du + Pdv = dh - vdP \dots \dots \dots (4.4)$$

$$dq = Tds \quad \dots \dots \dots (4.5)$$

$$dh = C_p dT \quad \dots \dots \dots (4.6)$$

$$C_p = \frac{k}{k-1} R \quad \dots \dots \dots (4.7)$$

using the relationship (4.2-4.7) we can write the first law from eq 1 as

$$Tds = dh - vdP \dots \dots \dots (4.8)$$

$$Tds = C_p dT - vdP \dots \dots \dots (4.9)$$

$$Tds = \frac{k}{k-1} R dT - vdP \dots \dots \dots (4.10)$$

dividing throughout by R T we have

$$\frac{ds}{R} = \frac{k}{k-1} \frac{dT}{T} - \frac{dP}{P} \dots \dots \dots (4.11)$$

from the polytropic equation $Pv^n = \text{constant}$ we have

$$\ln(P) + n \ln(v) = \ln(\text{const}) \dots \dots \dots (4.12)$$

integrating above we have

$$\frac{dP}{P} + n \frac{dv}{v} = 0 \dots \dots \dots (4.13)$$

from the equation of state we have $Pv = RT$

differentiating the above and rearranging we get

$$\frac{dP}{P} + \frac{dv}{v} = \frac{dT}{T} \dots \dots \dots (4.14)$$

from the above we get

$$\frac{ds}{R} = \frac{k}{k-1} \left[\frac{dP}{P} + \frac{dv}{v} \right] - \frac{dP}{P} \dots \dots \dots (4.15)$$

$$\frac{ds}{R} = \frac{1}{k-1} \left[\frac{dP}{P} \right] + \frac{k}{k-1} \left[\frac{dv}{v} \right] \dots \dots \dots (4.16)$$

$$(k-1) \frac{ds}{R} = \left[\frac{dP}{P} \right] + k \left[\frac{dv}{v} \right] \dots \dots \dots (4.17)$$

for an isentropic process

$$0 = \left[\frac{dP}{P} \right] + n \left[\frac{dv}{v} \right] \dots \dots \dots (4.18)$$

where n is the isentropic exponent.

subtracting the above we get

$$(k-1) \frac{ds}{R} = (k-n) \left[\frac{dv}{v} \right] \dots\dots\dots (4.19)$$

ds is negative due to the heat loss to the walls and any other irreversibility.

The term $\frac{dv}{v}$ is negative during compression and positive during expansion so that

k > n during compression

k < n during expansion.

Sample calculations for the engine at the compression ratio of 8.93 and inlet temperature of 293°K showed that the isentropic exponent value (for both compression and expansion) is approximately 1.365. The values of the compression and expansion exponents for the test cases in a motored engine are shown in Table 3. The results reported show a pattern similar to the one discussed above.

TABLE 3: Polytropic Compression and Expansion Exponents- Motored Engine.

Polytropic Index n

SPEED	COMPRESSION	EXPANSION
2400	1.35	1.385
3000	1.352	1.385
3600	1.351	1.380
4200	1.352	1.380

For the Engine operating conditions of

$$\text{inlet air temperature} = 294^{\circ}\text{K}$$

$$\text{pressure at BDC} = 101 \text{ kPa}$$

$$\text{compression ratio } \left(\frac{V_{\text{BDC}}}{V_{\text{TDC}}} \right) = 8.93$$

we can calculate the temperature at TDC using isentropic relations

$$\text{i.e. } T_{\text{TDC}} = T_{\text{BDC}} \left(\frac{V_{\text{BDC}}}{V_{\text{TDC}}} \right)^{k-1}$$

The above equation gives the temperature of air at TDC to be about 720°K at this temperature the value of the isentropic exponent from the air tables is about 1.365.

Assuming the temperature variation at TDC to be about 50°C then the variation in the value of k is $+ 0.003$

4.4 Volumetric Efficiency

Volumetric efficiency is the percentage of theoretical charge inside the engine. The plot of the volumetric efficiency for different speeds is shown in Fig 11. From this Figure it can be observed that there is a loss of volumetric efficiency with increase in speed of the engine. This loss in volumetric efficiency is responsible for the loss of power in engines at high speeds.

The volumetric efficiency η_v for a four stroke engine may be defined as:

$$\eta_v = \frac{2 Q_{\text{air}}}{V_s \text{ RPM}} \quad (4.20)$$

where Q_{air} is the total amount of air in m^3/min inhaled by the engine, V_s is the stroke volume in litres/min and RPM represents the speed of the engine in revolutions per minute.

4.5 Peak Pressure

The ensemble-averaged peak pressures in the motored engine at different speeds are shown in Fig 12. The difference in the values of the peak pressures for the same compression ratio but different speeds is due to the loss of the volumetric efficiency.

In summary, The piezo-electric transducer is a relative pressure measuring instrument which can be calibrated using a static dead weight tester in the laboratory for a small range of pressures. A detailed analysis of the motored engine data using the piezo-electric transducer is thus helpful in confirming the calibration of the transducer. The phasing of the indicator diagram confirms the compatibility of the crank angle pick up unit and the piezo-electric transducer. Other checks like the logarithmic plots of the data and the slopes of the polytropic exponents of compression and expansion further confirm the compatibility of the crank-angle unit and the transducer.

5. FIRED DATA ANALYSIS

5.1 Introduction

Digital data processing was used to quantitatively analyze cyclic variations in a spark ignition engine. The data processing included the scaling of the analog pressure transducer output data at each crank angle point, calculation of the volume at every crank angle position, calculation of mass-burned-fraction from the pressure data and finally the statistical analysis of the computed mass-fraction-burned data.

5.2 Scaling of Pressure

The data from the data acquisition system exists in an integer form. Two steps are taken to relate these integers to absolute cylinder pressure.

a) The integer output data from the data acquisition system ranges of 0 to 4096 of the charge amplifier are first converted to the relative pressure values using the relationship

$$\text{Pressure} = \left[\frac{\text{Integer}}{204.8} - 10 \right] * 10 \quad \dots\dots\dots (5.1)$$

the integer value of 0 to 4096 corresponds to -10 volts to +10 volts output. The scaling factor of the charge amplifier which gives the voltage to mechanical units conversion is then used to give the value of the relative pressure corresponding to the integer value.

b) The piezo-electric transducer provides relative pressures. Hence it is necessary to have a means of determining the absolute pressure at some point in the cycle and then all the data are scaled from this value of the reference pressure. We assume that the cylinder pressure at BDC after the intake stroke is given by

$$P_{\text{BDC}} = P_{\text{AMB}} \eta_v \frac{T_{\text{intake}}}{T_{\text{ambient}}} \quad \dots\dots\dots (5.2)$$

where P represents the pressure at BDC and ambient condition, η_v is the volumetric efficiency and T represents the temperature at intake and the ambient conditions. This value of pressure at BDC is used as a reference pressure in all the cases considered. The relative pressures are shifted by a constant value to obtain absolute cylinder pressures.

All the data are thus scaled using this value of reference pressure to give the pressure values for the whole cycle of intake, compression, expansion and exhaust stroke.

5.3 Volume Calculation

The absolute volume is calculated at any crankshaft position for the engine geometry and the clearance volume of the combustion chamber using the following relationship.

$$V = \text{Area} \left[H + R \left[1 + \frac{L}{R} \cos \theta - \left\{ \left(\frac{L}{R} \right)^2 - \sin^2 \theta \right\}^{1/2} \right] \right] \quad \dots (5.3)$$

where V is the instantaneous volume, H is the clearance height, Area is the cross-sectional area of the combustion chamber, R is the crank radius, L is the connecting rod length and θ is the instantaneous value of crank position ($\theta=0$ at TDC).

Minimum volume is assigned at TDC and it increases to a maximum at BDC.

5.4 Mass-Burned-Fraction Calculation

This section describes the program XPRESS used to calculate the mass-fraction-burned values from the experimentally obtained pressure data from the engine. Only the data for the compression stroke from BDC till the occurrence of spark and the combustion process thereafter are

used.

The initial conditions of pressure, temperature, and the energy of the initial charge prior to the compression are calculated from the constants of the engine geometry and the thermodynamic properties of the various species in the charge.

The thermodynamic properties during the compression process are calculated using the first law of thermodynamics, perfect gas law and the conservation of energy equations.

The actual pressure data is then read to calculate the mass-fraction-burned values using the conservation of energy and mass.

The efficiency of this program has been greatly enhanced by incorporating the application package "STANJAN". STANJAN calculates the thermodynamic properties of the hydrocarbon fuel and the values generated by this package are placed in tables which are read by XPRESS.

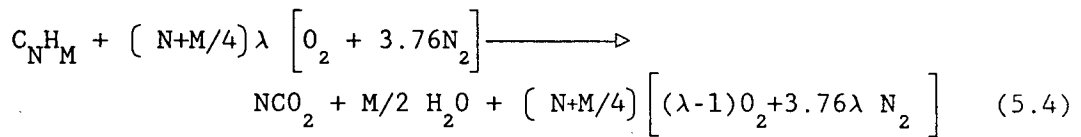
A full listing of the program is given in the appendix F.

Initial conditions

The initial conditions of the mass and the energy of the charge in the cylinder at the BDC are deduced from engine test data. The air and natural gas (fuel) flow rates, the intake manifold temperature, and the ambient pressure are entered before calculating the composition of the cylinder contents (charge) prior to the compression stroke at BDC.

The chemical equation for the combustion of a hydrocarbon fuel in air at a given relative fuel-air ratio gives the mole fraction of all the species present in the charge.

The chemical equation for the combustion of a hydrocarbon fuel in the air at a specific air-fuel ratio is:



where C,H,O,N,CO₂,H₂O represents carbon, hydrogen, oxygen, nitrogen, carbon dioxide and water, respectively, λ is the relative air-fuel ratio and subscripts N,M are the atoms of carbon and hydrogen in the fuel.

The total number of kmols of charge present in the cylinder at BDC is obtained from the ideal gas law,

$$N_{Tot} = \frac{P_{BDC} V_{BDC}}{R_{MOL} T_{BDC}} \quad (5.5)$$

The total mass of the charge in the cylinder is then calculated using the molecular weight of the charge. The molecular weight is calculated from the weight of its constituents.

The energy of the mixture is calculated using the relationship

$$E = (H-PV) = (H-RT) \quad (5.6)$$

$$\text{Energy} = \sum N_i \left(\bar{h}_{fi}^{\circ} + \bar{\Delta}h_i - \bar{R}T_1 \right) \quad (5.7)$$

where N_i is the number of kmols of constituent 'i', \bar{h}_{fi}° is the enthalpy of formation 'i' in kJ/kmol at 298°K and 1 bar, $\bar{\Delta}h_i$ is the difference in enthalpy of the constituent 'i' between temperature T_1 and 298°K obtained from Van Wylen and Sonntag [43], \bar{R} is the universal gas constant in kJ/kmol°K and T_1 is the inlet temperature of the mixture.

Knowing the mass composition and energy of the charge at BDC before compression, the mass-burned-fraction compression process can now be calculated.

Compression Stroke

The compression values of pressure, temperature, and total energy

are calculated at every crank angle degree increment from BDC until the occurrence of spark. In calculations, for every crank angle degree increment state 1 represents the initial state and state 2 represents the final state at the end of the step. To calculate the value of the pressure, temperature and the total energy at the state 2 initial values at state 1 are used as the starting condition. These calculation are accomplished by solving three equations simultaneously for every crank angle degree using the Newton-Raphson technique. The three equations are:

a) The equation of state:

$$P_2 = P_1 (V_1/V_2) (T_2/T_1) \quad (5.8)$$

b) The first law of thermodynamics:

$$E_2 = E_1 - (P_1 + P_2)(V_2-V_1)/2 + DQ \quad (5.9)$$

c) Conservation of energy:

$$E_2 = (M/MW)*Spec.Energy(T_2) \quad (5.10)$$

where P, V, E, T represents pressure, volume, energy and temperature respectively, DQ represents the heat loss from the engine MW represents the molecular weight of the cylinder contents, Spec.Energy represents the molar specific energy of cylinder content, M is the total mass in the cylinder and subscripts 1 and 2 represents the state 1 and 2.

These three equations are reduced to a single equation in 1 unknown the temperature T₂ as follows:

$$F(T_2) = C_1 + C_2 + C_3.Spec.Energy(T_2) = 0 \quad (5.11)$$

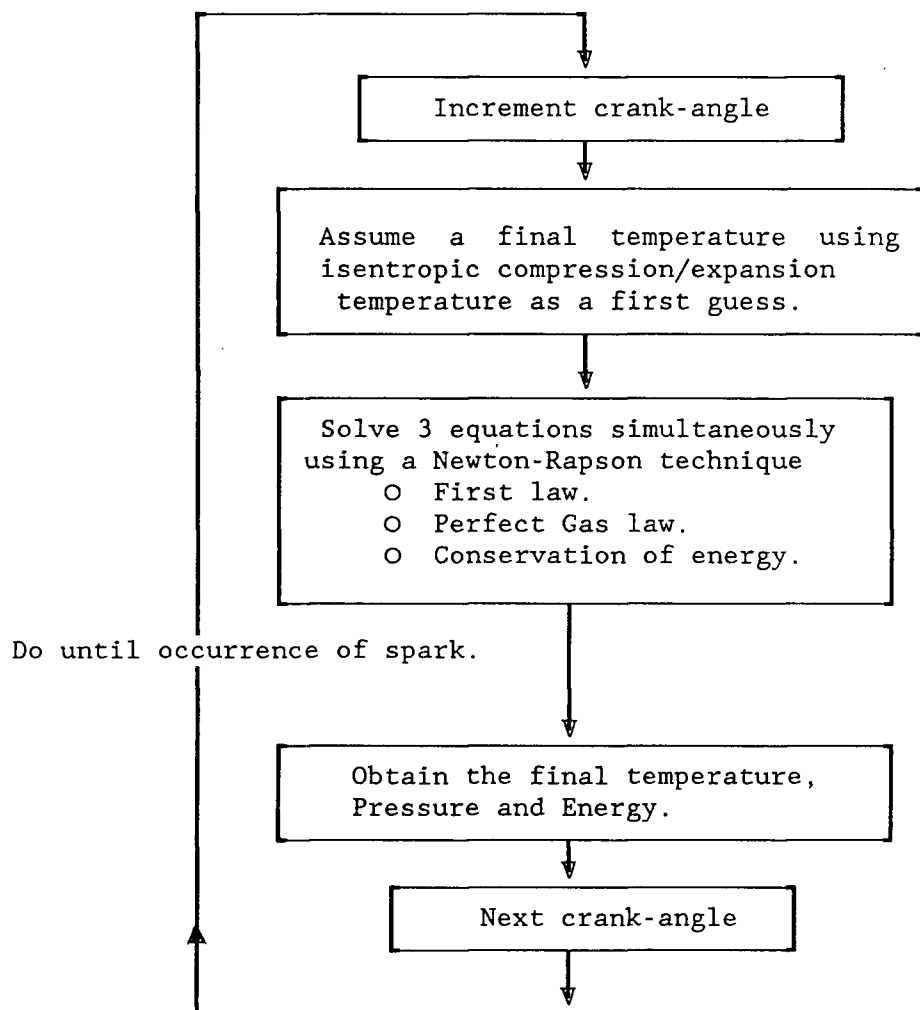
where $C_1 = E_1 - P_1(V_2-V_1)/2 + DQ$

$$C_2 = -P_1V_1.(V_2-V_1)/2. V_2.T_1 \quad (5.12)$$

$$C_3 = -M/MW \quad (5.13)$$

This equation in one unknown is solved iteratively to get the temperature T_2 . Then, corresponding to that temperature the pressure, the energy and the mass-burned-fraction are calculated.

The flow chart for this part of the program is as shown below:



Flow chart for compression until Spark

These calculations at every crank angle step are done till the occurrence of spark.

Combustion Process

The calculation procedure of the mass-fraction-burned values in the engine following spark is now shown:

The major assumptions made in this subroutine on progressive burning are:

- 1) The combustion chamber is divided into two zones by a thin, spherically expanding flame front separating the burned gas fraction (X) from the unburned gas fraction (1-X).
- 2) Both the burned and unburned gases have varying specific heats and obey the ideal gas law.
- 3) The unburned gas is isentropically compressed by the expanding burned gases.
- 4) The pressure is uniform throughout the combustion chamber.

Calculations based on these assumptions are performed at every crank angle degree from spark until the end of combustion.

The experimental pressure data is now read by the program to calculate the mass-burned-fraction values using the conservation of mass and energy equations as shown below.

From the conservation of Mass and Energy:

$$\frac{V}{M} = X \vartheta_b + (1-X) \vartheta_u \quad (5.14)$$

$$\frac{E}{M} = X e_b + (1-X) e_u \quad (5.15)$$

where V is the volume of the combustion chamber, E is the total energy in the cylinder, M is the molecular weight, X is the mass-fraction burned, ϑ is the specific volume, e is the specific energy and the subscript b and u, represents the burned gas properties and the

unburned gas properties respectively.

At each step of the combustion process the values of energy , temperature and volume are known for both the burned and unburned gases at the previous calculation step, state 1, and these are used as the starting values for calculating values for the current step, state 2.

The unknowns in the equations 1, and 2 above are determined as shown below.

a) The unknowns in the unburned gases are calculated using isentropic compression from the initial values of temperature, specific volume and the initial and final pressure (experimental data) to give the final temperature and specific volume.

From the assumption of isentropic compression of the unburned gases

$$v_{u2} = v_{u1} (P_1 / P_2)^{1/k} \quad (5.16)$$

Assuming ideal gas behaviour

$$T_u = P_2 v_{u2} / M_u \bar{R} \quad (5.17)$$

which allows the specific energy of the unburned gas to be calculated

$$e_{u2} = \frac{\sum N_i \left[\bar{h}_{fi}^{\circ} + \left\{ \bar{h}_{i(Tu)}^{\circ} - \bar{h}_{i(To)}^{\circ} \right\} - \bar{R}T_u \right]}{N_u MW_u} \quad (5.18)$$

where the values of $\bar{h}_{i(Tu)}$ are obtained from formulae representing curvefits to the published enthalpy data for each constituent (Van Wylen and Sontag [43]) \bar{h}_{fi}° is the heat of formation for the 'i'th species and $\bar{h}_{i(To)}$ is the enthalpy of the species at the base

conditions.

b) The new combustion chamber volume is obtained from the volume-crank angle relationship for the engine using all the appropriate constants from the engine geometry.

c) The unknown total energy of the control mass E_1 , contained in the combustion chamber is given by the first law

$$E_2 = E_1 - P.(V_2-V_1) + dq \quad (5.19)$$

The $P(V_2-V_1)$ term is approximated by $(P_1+P_2)/2 (V_2-V_1)$

d) The values of X_2 , V_{b2} and E_{b2} are unknown at this point, however

$$V_{b2} = f(T_{b2}, P_2) \quad \text{and} \quad (5.20)$$

$$e_{b2} = f(T_{b2}, P_2) \quad (5.21)$$

according to the following relationship

$$V_{b2} = M_{b2} \bar{R} T_{b2} / P_2 \quad (5.22)$$

$$e_{b2} = \frac{\sum N_j \left[\bar{h}_{fj}^\circ + \left\{ \bar{h}_{j(T_{b2})}^\circ - \bar{h}_{j(T_0)}^\circ \right\} - \bar{R} T_{ub2} \right]}{N_b MW_b} \quad (5.23)$$

To calculate the values of X_2 , V_{b2} and E_{b2} we proceed as follows:

Knowing the pressure and iterative temperature T_{b2} we can read the values of the dissociated species from the table created by STANJAN and thus calculate the values of V_{b2} and E_{b2} .

The program proceeds by iterating the burned gas temperature T_{b2} until the values of e_{b2} and v_{b2} calculated by equations 5.22 and 5.23 satisfy equations 5.14 and 5.15. At this point X_2 , the mass-burned-fraction is obtained.

The above procedure is repeated at each crank angle degree until

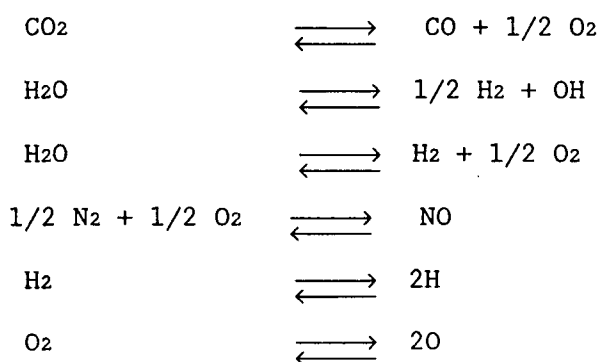
the mass fraction burned reaches a maximum value.

In practice the values of x computed for adiabatic combustion rise to a maximum of approximately 0.8 and stay constant thereafter. Assuming that all of the fuel is burned as x reaches a plateau, correction for the heat transfer effect is made by dividing each value of x by the maximum value of x for that particular cycle.

e) The laminar burning velocity was calculated using the expression presented by Guilder for methane from his experiments in constant volume bomb experiments. Laminar burning velocity is discussed in appendix C.

Dissociation Calculations

The dissociation calculations were performed by using the application package STANJAN. This package calculates the values of the species and places them in the form of a table which is then read by the program XPRESS. The dissociations considered in this model are



STANJAN

The application package STANJAN is briefly described in this section. This is a general-purpose interactive program that can be used to solve chemical equilibrium problems. The basic data in this program

is taken from the JANNAF tables. The user selects the species to be included in each phase of the system, sets the atomic populations and state parameter and then solves for the equilibrium state using the method of element potentials. The user-specified state parameters may be temperature and pressure or pressure and entropy or other options available. The results include the composition of each phase such as the dissociated species and the products, and the thermodynamic properties of the system such as the internal energy, enthalpy and entropy. This value of the dissociated species in the table eliminates the need for iterative calculations of dissociated products at high temperature and pressure thus saving a lot of time.

In this case a series of calculations were made over a matrix of T and P values. These tabulated results for each fuel-air ratio are stored in a file for later processing using user specified format.

5.5 Statistical Analysis

The statistical analysis used to determine the extent of cycle-by-cycle variations in engines from the mass-burned-fraction values was done using Fortran programs. The statistics calculated from the mass-burned-fraction values were the mean, standard deviation, and cross-correlation coefficient.

The mass-burned-fraction values at each crank angle calculated by XPRESS are used to calculate the values of the mass-burned-fraction in terms of time after the occurrence of the spark using the relationship.

$$\text{Burning time for } x \text{ crank angle after spark} = \frac{x}{6 * \text{RPM}} \quad (5.24)$$

Statistical analysis is then performed on the calculated values of the time taken for a specific discrete value of mass-fraction-burned for

100 cycles in one set of sample data. The mass-burned-fraction values at each crank angle showed a continuous set of data values. This data was first arranged such that burning times at 2, 3, 4, 5, 7, 10, 20, 30, 40, and 50 percent mass-fraction-burned were calculated using equation 24 above and the statistical analysis carried out to calculate the mean, standard deviation and cross correlation coefficient.

An initial test conducted with different sample sizes of consecutive cycles at 3000 RPM, WOT and 1.25 equivalence ratio showed that increasing the number of cycles increased the reliability of results. A sample case of 50 and 100 cycles showed that the value of standard deviation was 4% lower with 50 cycles. A sample size of 100 consecutive cycles is selected as an economical sample size as large number of tests can be easily conducted using the available computer size.

The mean of the time for the same mass fraction burned is calculated using the relationship

$$\bar{x} = \frac{1}{N} \sum_{i=1}^N x_i \quad (5.25)$$

where x_i is the i^{th} value and N is the number of measurements.

The standard deviation is calculated using the relationship

$$\sigma = \left[\frac{1}{N-1} \sum_{j=1}^N (x_j - \bar{x})^2 \right]^{1/2} \quad (5.26)$$

The normalized covariances (Cov) are calculated using the relationship

$$\text{Cov} = \frac{\sum_{i=1}^N (x_{1(i)} - \bar{x}_1) * (x_{2(i)} - \bar{x}_2)}{(\sigma_1) * (\sigma_2) * (N-1)} \quad (5.27)$$

The raw data collected from the engine in the form of integers is thus processed through various stages to a form that can be evaluated to study cyclic variations in the engines.

6. FIRED ENGINE MEASUREMENTS AND RESULTS.

6.1 Introduction.

This chapter discusses the results obtained from the experiments conducted on the Ricardo research engine. The calculating procedures are as described in chapter 5. Cylinder pressure measurements were made with different configuration setups as described below. A variety of equivalence ratios on either side of the stoichimetric air fuel ratio were considered, the range being approximately $0.70 < \phi < 1.15$. All the measurements were made at MBT spark timing. The variables in this experimental study are:

- a) speed: measurements were made at 2400, 3000, 3600 and 4200 rpm at WOT using a standard spark plug with an electrode diameter of 3mm and a spark gap of 0.7mm.
- b) spark plug geometry: In addition to the standard spark plug the effects on combustion of a modified spark plug with 1.3mm electrode diameter having pointed ends and 0.7mm spark gap at WOT and 3000 rpm were also studied.
- c) spark gap width: In addition to the standard spark plug the effects on combustion of another modified spark plug at WOT and 3000 rpm were also studied. The modified spark plug had spark gap width of 2.3mm for the bathtub chamber and about 1.5mm for the disc shaped combustion chamber.
- d) part throttle : measurements were made at partly opened throttle at 3000 rpm. Part-opened-throttle is described in terms of volumetric efficiency. The volumetric efficiency at 3000 rpm for fully opened throttle and partly-opened throttle are 85% and 64% respectively.

e) chamber geometry : pressure measurements were made at all the configurations described above with two different combustion chamber geometries the "bathtub" chamber and the "disc" chamber.

Section 6.3 to 6.6 discusses the results from the "bath-tub" chamber and section 6.7 discusses the results from the "disc" shaped chamber.

6.2 CYCLIC VARIATIONS IN PRESSURE

The ease and accuracy with which pressure in the combustion chamber can be measured using a piezo-electric transducer has made pressure the most common parameter for quantifying cyclic variations.

Fig 13 is a sample plot of the peak pressure distribution for a sample of 100 consecutive cycles at 3000 rpm WOT, and ϕ of 1.015. This plot shows the maximum and the minimum pressure curve within the sample for the compression and expansion phase of the cycle. Also shown is the ensemble-averaged mean of the 100 cycles for the same sample data. The spread of peak pressures within a sample of 100 consecutive cycles is shown on the histogram at the left hand side of the plot. The standard deviation in the peak pressure for this sample data is 325.7 kPa and the coefficient of variation is 0.0675.

Fig 14 is a similar plot for a sample data of 100 consecutive cycles at 3000 rpm, WOT and an equivalence ratio of 0.674 i.e a very lean operating condition. This sample has 8 misfiring cycles as shown by the peak pressure being less than the motored pressure. This misfiring in the engine increases the spread in the peak pressure variation. The standard deviation in peak pressures is about 450 kPa and the coefficient of variation is about 0.188. This example of an extreme

case is for illustration only; in none of the cases discussed hereafter is there any evidence of misfiring.

This combined plot for a particular sample data presents the character of the cyclic variations in engine pressure at that particular operating condition. The pressure curve shows the range in the absolute values of pressure within the sample and the histogram shows the distribution of the peak pressure within the sample data collected.

Fig 15 shows the ensemble-averaged peak pressure for samples of 100 cycles at different speeds and equivalence ratios. Ensemble-averaged peak pressure increases with speed from 2400 rpm to 3600 and thereafter shows a tendency to decrease with increase in speed. The lower values of peak-pressure at lower speed is associated with the lower level of turbulence at lower speeds. This lower turbulence causes the flame to travel slower which affects the phasing and thereby magnifies the effect of pressure due to increasing piston speed (This concept is discussed in detail in appendix B). This phenomenon of loss of peak pressure at high speeds is associated with reduced volumetric efficiency with increase in speed. The maximum value of the ensemble-averaged peak pressure occurs near the stoichiometric fuel-air ratio. The value of peak pressure decreases for both rich and lean mixtures away from the maximum value of the peak pressure. This decrease in peak pressure is associated with excess air in case of lean mixtures and incomplete combustion in case of rich mixtures; these decrease the temperature and hence the peak pressure in the combustion chamber. The effect of equivalence ratio on the peak pressure is significant and follows a steady pattern at all speeds, where as the peak pressure increases with speed from 2400 rpm to

3600 rpm but decreases with speed with increase from 3600 to 4200 rpm.

The standard deviation in the ensemble-averaged peak pressure (within the sample data of 100 cycles) normalized by the ensemble-averaged mean of peak pressure for the sample is termed the coefficient of variation (COV) [11]. The values of the coefficient of variation for the engine data at different speeds and equivalence ratio at WOT and MBT spark timing is shown in Fig 16. This plot of coefficient of variation against equivalence ratio shows that the minimum value of coefficient of variation occurs near the stoichiometric air-fuel ratio for all the speeds considered. The coefficient of variation increases more rapidly with departure from $\phi = 1$, i.e. as the equivalence ratio is made lean or rich, this increase being more rapid on the rich side than on the lean side. The coefficient of variation appears not to have a clear dependence with speed.

Thus, the influence of equivalence ratio on coefficient of variation is quite significant while the effect of engine speed is comparatively small.

6.3 CYCLIC VARIATIONS IN BURNING TIME

Peak pressure is directly influenced by the combustion in the engine but its occurrence is detached from the initial burning period. Most researchers have concluded that combustion variations originate in the early part of the burning period following spark. Young for example in his review paper [1] concluded that "cycle-to-cycle variations in combustion originate early in the combustion process. Although hard evidence is still lacking it is thought that a main cause of these variations is the cycle-to-cycle variations of velocity in the vicinity

of the spark plug at the time of ignition which affects the developing flame kernel".

The main area of interest in this research is concentrated on the early stages of combustion following spark. By calculating mass-fraction-burned values from the pressure data we can make inferences about cyclic variations in burning time early in the combustion period.

The pressure data collected from the engine is not smoothed in any way except for the pressure at the time of spark. The high energy at spark sometimes seems to interfere with the pressure output signal, giving an erratic value of pressure at spark. This drawback is rectified by calculating an average value for the compression exponent over the range from IVC to just before spark and then using this exponent 'n' calculate the value of the pressure at spark for every cycle using the simple relationship $P_1V_1^n = P_2V_2^n$. State 1 represents the conditions of pressure and volume at 5 degrees before spark and condition 2 represents the conditions at spark.

The mass-fraction-burned values are calculated from the pressure data collected using the energy and mass conservation equations. The details of these calculations are described in the chapter 5.

Fig 17 is a sample plot of mass-fraction-burned values plotted against time. Three of the fastest and three of the slowest mass-fraction-burned curves are shown in addition to the ensemble averaged mean curve from a sample of 100 consecutive cycles. The curve shows mass-fraction-burned value x ranging from 0 to 1. In practice the values of x computed for adiabatic combustion rise to a maximum of

approximately 0.8 and stay constant thereafter. Assuming that all of the fuel is burned as x reaches a plateau, correction for the heat transfer effect is made by dividing each value of x by the maximum value of x for that particular cycle.

Figure 17 shows typical difference in burning times between the fastest and the slowest burning cases. It may be noted that the shapes of the burned curves are similar. At $x = 0.5$ all the curves seem to have about the same slope, however they appear to be shifted in time. It seems that variation in the initial burning period sets up the trend for later combustion, which then proceeds in a similar manner for all cycles. The dispersion in burning time increases as x increases. However, as will be shown, the value of initial spread is not negligible in the early combustion region. This denotes that there is substantial randomness associated with the early stages of combustion following the spark.

The values of the standard deviation in burning time for each set of operating conditions at the appropriate x values can then be determined from statistical analysis. We now examine this value of standard deviation in burning time at different air-fuel ratio and x .

Fig 18 shows the frequency histogram of burning time for 10% mass-fraction-burned at 3000 rpm and an air-fuel ratio of 1.05. The standard deviation for this case is 0.08334 ms.

Fig 19 shows the frequency histogram of burning time for 30% mass-fraction-burned at 3000 rpm and an air-fuel ratio of 1.05. The standard deviation for this case is 0.1122 ms.

Fig 20 shows the frequency histogram of burning time for 50%

mass-fraction-burned at 3000 rpm and an air-fuel ratio of 1.05. The standard deviation for this case is 0.1247 ms.

Fig 18, 21 and 22 shows the frequency histograms and the values of the standard deviation of 10% mass-fraction-burned at air-fuel ratio of 1.05, 1.22 and 1.38 respectively. The standard deviation in burning times are 0.08334, 0.1137 and 0.2300 ms respectively.

Thus Figs. 18-22 show that the standard deviation in burning times increases

- a) as the mass-fraction-burned increases.
- b) as the equivalence ratio changes (all other conditions remaining constant).

The dependence of the standard deviation in burning time on x values and equivalence ratio is seen in Figs 23-29 which show the effects of speed and equivalence ratio for MBT spark timing. These plots show that there is an almost linear relationship between the standard deviation σ in burning time and x , with an almost linear increase in σ with x .

The increase in the value of standard deviation in burning times with increasing values of x may be due to the combined effect of random flame development and the wall interaction with the developing flame; the larger the flame size, i.e. the larger the value of x , the greater the contribution which might be expected from this source of randomness. However this effect should be negligible as x approaches zero.

As equivalence ratio is varied from the optimum, the flame temperature and the burning velocity decline, and the combustion period

increases. An explanation for the increase in cyclic variation with decline in laminar burning velocity will be proposed later in chapter 8.

Extrapolating the values of standard deviation to the initial stages of combustion (i.e. for $x \rightarrow 0$ and disregarding the highly uncertain determinations for x less than 0.03 or 0.04) we obtain the extrapolated standard deviation σ_0 . The extrapolated standard deviation in burning time σ_0 represents the standard deviation in burning time for zero mass-fraction-burned. The calculated values of x less than 0.04 show very high values of standard deviation. The extrapolation in these cases is carried out from values of x greater than 5%. In theory, the value of σ_0 has to be determined at very small values of x i.e. just as the developing flame kernel following spark hits the faster burning vortex tubes in the turbulent structure. This average distance that has to be covered by the flame is approximately 0.22mm. In practice, exact determination of the value of x from the pressure data in the early stages following spark is very difficult, as when the outer flame radius is of the order of 10mm, the value of x is well below 1% (i.e. within the uncertain region.) Hence, for all practical purposes the value of σ_0 is obtained by extrapolation from higher values of x . This value of standard deviation for very small values, almost zero, of x is termed the standard deviation in burning time at zero mass fraction burned.

Appendix E shows the effect of the small uncertainty in the pressure data on the calculated burning time for small values of x . The pressure is deliberately modified by a small amount equal to the uncertainty in the pressure acquisition equipment.

Appendix E shows that this pressure uncertainty prevents the determination of σ_0 for values of x less than about 0.03 (3%).

The facts that the extrapolated standard deviation values are not negligible, and that the initial spark process is highly repeatable, suggests that the behaviour of the flame in the initial stages is important in locating the origin of cyclic variations. It is consistent with the idea that the burning curves appear to be the same except for a variable shift in the time for flame initiation. We proceed to examine this dependence on x for different equivalence ratios and speeds.

Fig 30 shows the behavior of the extrapolated standard deviation σ_0 at different speeds and equivalence ratios. This plot shows that the σ_0 values increase systematically on both sides of the minimum; the minimum occurs near the stoichiometric value. The slight tendency for the values of σ_0 to decrease with speed can be due to higher turbulence levels at high speeds. The change in σ_0 with speed at different equivalence ratios shows a similar behaviour as the change of coefficient of variation (COV) under similar operating conditions. This similarity between σ_0 (in the initial stages) and COV (for peak pressures) appears consistent with the view that the variations in the initial stages sets the stage for further pressure development and that the pressure is directly related to combustion variation in the engine.

The value of σ_0 plotted in terms of crank angle values instead of time in milliseconds exhibit somewhat less variation in standard deviation with speed, as seen in Fig 31. They tend to fall around a linear relationship pointing to the fact that in terms of crank angle

the standard deviation values are independent of speed but behave systematically with change in equivalence ratio, i.e increase as the fuel is made leaner. This indirectly shows that the turbulence increases linearly with speed.

The correlation coefficient between x values at two distinct values of x determine how strongly they are related to each other. A value of 1 indicates a strong positive linear relationship and a value of 0 indicates no relationship at all. The correlation coefficient between the burning times at $x= 0.07$ and $x = 0.10, 20, 30, 40$ and 50 is shown in Fig 32 for an equivalence ratio of 1.05 at 3000 rpm and WOT condition. A high correlation exists between the initial burning times and the burning times at a later stage. This high value of the correlation coefficient indicates that the standard deviation in burning time in the later stages of burning is strongly related to the standard deviation in burning time in the initial stages. This sample case is a true representative of most of the test cases considered.

6.4 EFFECT OF SPARK PLUG GEOMETRY:

Fig 33 shows a modified spark plug used to determine the effect of electrode shape and size on cyclic variations.

Fig 34 and 35 show the linear behaviour of the standard deviation in burning time with mass-fraction-burned for different equivalence ratios at 3000 rpm and WOT.

Fig 36 shows the plot of σ_o values for different equivalence ratios and is compared with the standard configurations at the same speed. They exhibit a similar trend of change in standard deviation with change

in equivalence ratio with a minimum at near stoichiometric fuel-air ratio. This figure does not show any significant improvement in the standard deviations in burning times with the modified spark plug point.

This test shows that the size of the shape and size electrode has little effect on cyclic variations.

6.5 EFFECT OF SPARK GAP WIDTH :

Figure 37 shows the modified spark plug used to study the effects of long sparks at ignition on the cyclic variations in engines.

Fig 38 and 39 show the linear behaviour of the standard deviation in burning time with x for different equivalence ratios at 3000 rpm and WOT. The case of $\phi = 0.6739$ has misfiring cycles in the sample data and it demonstrates how misfiring can affect the linear relationship between σ_0 and x .

Fig 40 which shows the plot of σ_0 for different equivalence ratios and compared to the standard configuration at the same speed. They exhibit a similar trend of change in standard deviation with change in equivalence ratio with a minimum at near stoichiometric. This curve does not show any significant change in σ_0 with the modified spark plug gap.

Thus, this test shows that there is a weak relationship between wide spark gaps (2.3mm) and cyclic variations.

6.6 EFFECT OF PART THROTTLE

Tests with partly open throttle were conducted to study the effects of increased residuals on cyclic variations.

Fig 41 and 42 show the linear variation with x of the standard deviation in burning time for different equivalence ratios at 3000 rpm.

Fig 43 shows the plot of σ_o for different equivalence ratios at 3000 rpm for the standard configuration and the partly open throttle. They exhibit a linear relationship of increase in standard deviation with change in equivalence ratio with a minimum at near stoichiometric. This curve does not show any significant change for the part throttle.

It shows a weak relationship with change in throttle setting from WOT to partly open throttle. This weak effect could be due to the combined effect of high compression ratio and MBT spark timing.

6.7 Disc Combustion Chamber

This section discusses the results from the disc-shaped combustion chamber. Most of the tests were conducted for similar operating conditions as with the "bath-tub" combustion chamber. Figs 44-50 shows the behaviour of standard deviation in burning time with mass-burned-fraction values for different operating conditions of speeds (2400, 3000, 3600 and 4200 rpm), spark plug geometry, spark plug gap and partly open throttle respectively. These plots have one fundamentally different operating parameter such as speed, electrode shape or electrode gap and throttle opening. All these plots show that there exists an increasing linear relationship between x and standard deviation in burning time.

Fig 51 shows the effect of change in speed and equivalence ratio on the σ_o . The influence of equivalence ratio on standard deviation has a distinctive pattern with a minimum value near the stoichiometric air-fuel ratio and increases with change in equivalence ratio for both rich and lean mixtures. The influence of speed on standard deviation is

not very distinct with a small amount of decrease in standard deviation for increase in speed from 2400 to 3600 rpm. Further increase in speed over 3600 rpm shows an increase in engine variations. Thus there is a weak relationship of speed with standard deviation for a whole range of speeds.

The influence of the equivalence ratio on standard deviation could be related to the effect of flame speed. Near stoichiometric air-fuel ratio the flame speeds are the fastest and hence combustion rate is increased. This flame speed is a function of the temperature and pressure with a maximum near the stoichiometric air-fuel ratio. As the equivalence ratio is changed the maximum temperature in the combustion chamber is less than the maximum value near the stoichiometric value and this reduces the flame speed which increases the combustion duration and hence the variations. The turbulence level increases linearly with speed and hence decreases the combustion duration which shows up as an improvement in standard deviation. At higher level of speed the increase in combustion rate is made more complex by an increase of residuals due to the decreased volumetric efficiency and this may explain the increased values of standard deviation.

Fig 52 shows the effect of spark plug geometry on cyclic variations at 3000 rpm, WOT and MBT spark timing. From the plot it can be seen that there is no improvement in standard deviation for the two different shapes of spark plug points, which is in agreement with the results of bath-tub chambers and other researchers that the effect of spark plug point geometry is insignificant in reducing cyclic variations.

Fig 53 shows the effect of an increased spark plug gap on cyclic variations at 3000 rpm, WOT and MBT spark timing. The spark gaps considered were the standard gap of 0.7mm and modified spark plug gap of 1.5mm. The influence of equivalence ratio on σ_o appears to be similar for both types of spark plugs. The Figure shows a decrease in extrapolated standard deviation with increased spark gap (1.5mm). This behaviour could be due to the increased size of the kernel which needs small amounts of initial travel time to interact with the turbulence (This phenomenon is better explained in chapter 8).

Fig 54 shows the effect of residuals due to partly open throttle on combustion variations at 3000 rpm and MBT spark timing. This figure shows a significant increase in σ_o for lean mixtures and a decrease in standard deviation for rich mixtures. The increase in standard deviation for lean mixtures may be due to effects of increased residuals which influence the flame speed and hence decrease the combustion rate and hence increases the combustion variations. The effect of reduced volumetric efficiency due to part open throttle and the residuals in the rich mixture seem to have an effect of increase in flame speed and hence reduces cyclic variations in standard deviation.

Thus, the effect of part-open throttle is such that there is a increase in value of σ_o compared to the fully open throttle condition at 3000 rpm.

Figures 55 to 61 shows the effect of two different combustion chambers on cyclic variations. The two chambers are the simple combustion chamber (disc-shaped) and the bath-tub chamber which has

squish at TDC.

These figures shows that

- a) There is a distinct improvement in σ_o for different values of equivalence ratio and speed.
- b) the minimum value of σ_o occurs at leaner equivalence ratio for the "bath-tub" chamber as compared to the disc chamber.
- c) σ_o decreases with increased speed as speed is proportional to the turbulence level.

This behaviour could be due to the increased level of turbulence in the "bath-tub" chamber as compared to the simple disc-shaped combustion chamber. The higher turbulence level increases the combustion rate which affects the phasing and gives decreased value of σ_o for higher turbulence level.

6.8 Summary

In summary the experimental results computed from the engine pressure data shows that

- 1) The pressure data shows randomness at all operating conditions.
- 2) The ensemble-averaged peak pressures for a sample data at any speed shows a maximum value near the stoichiometric air-fuel ratio and changes with change in speed.
- 3) The COV in peak pressure shows a minimum value near the stoichiometric air-fuel ratio and changes with change in speed.
- 4) The x values calculated from the pressure data seem to suggest a substantial randomness in the burning times during combustion.
- 5) The standard deviation in burning times increases linearly as the

x increases and shows a minimum set of values near the stoichiometric air-fuel ratio.

6) Extrapolated values of standard-deviation in burning times vary with speed and shows a minimum near the stoichiometric air-fuel ratio.

7) Extrapolated standard deviation shows less dispersion when plotted in terms of crank angle.

8) A high correlation exists between the values of x at initial stages and the later stages..

9) The shape of the electrode has no significant effect on cyclic variations for both "disc" shaped and "bath-tub" chamber.

10) The spark gap width has no significant effect on cyclic variations in "bath-tub" combustion chamber but has a stabilization effect on cyclic variations in the disc chamber, by showing lower values of σ_o as compared to the standard spark plug gap values of σ_o .

11) The increased residuals had no effect on cyclic variations when the volumetric efficiency is changed from 85% to 64% at MBT spark timing in "bath-tub" chamber but for the "disc" chamber there is a deterioration in cyclic variations as seen by the higher values of the σ_o compared to the case of full throttle.

12) The corresponding values of standard deviation in burning times in the disc shaped combustion chamber has higher values than the "bath-tub" combustion chamber.

An inference that can be drawn from these results is that the "bath-tub" chamber generates more turbulence than the "disc" chamber.

7. TURBULENCE AND IGNITION IN ENGINES

7.1 Introduction

This chapter reviews the available literature on turbulence structure within the engine during the combustion period. The chapter considers

- a) the nature of the turbulent structure in spark ignition engines.
- b) the distribution of the major turbulence parameters viz: turbulence intensity, and turbulent scales and their dependence on speed.
- c) the model of the small scale structure of turbulence as presented by Tenneekes.
- d) optical data on the initial flame kernel.
- e) the theoretical step-by-step development of the initial flame kernel following spark (as deduced from the turbulent structure model) and the nature of the early flame propagation.
- f) the laminar burning velocity of methane (a major constituent in natural gas).

7.2 Homogeneity And Isotropy in Engine Turbulence

The flow field in an engine is primarily governed by the valve events and piston motion. During the early part of the compression process the influence of the intake process is dominant; the combustion chamber shape (eg. pre-combustion chamber), inlet swirl and effective valve area are mainly important in establishing the initial levels of turbulence from which the decay process begins. Combustion in an engine occurs mostly in the vicinity of Top Dead Centre (TDC) during the compression and expansion process. Measurements of turbulence have been in this region.

Semenov [29] did extensive work on the distribution of mean

velocity and turbulent intensity across a disc-shaped combustion chamber. Using hot wire anemometry in a motored engine he made measurements at various points in the combustion chamber at different running conditions. He noted that during the compression stroke in the vicinity of TDC the turbulence intensity at a given point does not vary with time by more than 10% and it does not change by more than 15% with increasing distance from the chamber centre. Semenov thus concluded that combustion proceeds under conditions of practically constant turbulence.

Whitelaw et al. [52] made measurements of three velocity components using a forward-scatter laser doppler anemometer in the transparent cylinder motored with a disc type chamber having a compression ratio of 7.4. They found that the turbulence showed a tendency towards isotropy at TDC.

Lancaster [16] used single point measurements with a tri-axial probe and obtained close agreement between the intensities measured by the three sensors near TDC; he concluded that the turbulence tended towards isotropy. The results of several other investigations [4][20] imply that in chambers with no squish the turbulence is nearly homogeneous and isotropic. Daneshyar and Fuller [5] for example conclude that "When averaged over many cycles the turbulence is virtually homogeneous and isotropic towards the end of compression in swirling and non swirling flows (except near the chamber walls)".

The general consensus, on the turbulent structure for the engine operating conditions, is that approximately constant conditions of homogeneous, isotropic turbulence prevail in the engine during

combustion.

7.3 Turbulence Measurements in Engines

Turbulence is defined as the fluctuating velocity component super-imposed on the mean velocity of a viscous flow. The velocity fluctuations which are measured at a fixed point in space can be envisioned as the result of turbulent eddies passing that point. Three parameters- mean velocity ,turbulent intensity and turbulent scale- can be used to describe the observed turbulence.

Mean Velocity

The mean velocity is the average velocity measured during a specified time interval and it has both direction and magnitude. This definition is dependent on the time interval for which it is defined and this leads to stationary analysis of turbulence data. The mean velocity is then defined as

$$U = \bar{U} + u \quad \dots\dots\dots(7.1)$$

where U is the instantaneous velocity, \bar{U} is the time averaged value and u is the fluctuation component.

If the mean velocity varies slowly with time the mean velocity could be defined as

$$U(t,i) = \bar{U}(t) + \bar{U}(i) + u(t,i) \quad \dots\dots\dots(7.2)$$

where U(t,i) is the instantaneous velocity at any time t in record i, $\bar{U}(t)$ is the ensemble-averaged mean velocity at any time t and $\bar{U}(i)$ is the time-averaged mean velocity for a portion ("window") of record i after $\bar{U}(t)$ has been subtracted from the instantaneous velocity at each time in the record. The turbulent component of velocity is u(t,i). This definition of mean velocity is used for non-stationary analysis of

engine data.

Turbulence Intensity

Turbulence intensity is defined as the root mean square value of the velocity fluctuations about the mean. Whitelaw et al. [51] made measurements of three velocity components using a forward-scatter laser doppler anemometer in the transparent cylinder motored engine with a "disc" type chamber having a compression ratio of 7.4. Using stationary analysis they found that the ratio of average turbulence intensity and the mean piston speed at TDC of compression increased from 0.47 to 0.59 in the absence of induction swirl along the cylinder diameter with similar values being 10-25% lower in the presence of swirl.

Bracco et al [51] noted that for a "disc" shaped combustion chamber the ratio of turbulence intensity to the mean piston speed has a upper limit of about 0.5 at TDC.

Boisvert [37] used a numerical model of the combustion process incorporating all the combustion implications of Tennekes model and found that the ratio of values of turbulence intensity to the mean piston speed are in the range of 0.47 to 0.60.

Hall and Bracco [51] used laser doppler velocimetry to make cycle-resolved velocity and turbulence measurements under motoring conditions in a "pancake" chamber engine having a compression ratio of 7.5. They found that the turbulence intensity had a linear relationship with the engine speed and the magnitude of TDC turbulence intensity has a maximum value of about 0.5 times the mean piston speed for this simple chamber.

Semenov [29] reported that turbulent intensity was relatively constant with time during the end of compression and beginning of expansion with

the value of the constant depending on the geometry of the combustion chamber. Lancaster [50] showed that turbulence intensity increased with increasing speed.

There is substantial variation in the reported measurements of the turbulence intensity mainly because of different methods of analysis (stationary and non-stationary analysis). The mean velocity signal from the engine is non-stationary and non ergodic. The results of ensemble-averaged values of turbulence intensity (stationary analysis) differ substantially from values obtained by non-stationary averaging with windows of various sizes [37]. Since the ensemble-averaged analysis for the engine contains fluctuations due to the mean velocity it produces values of turbulence intensity which are larger than similar values obtained using non-stationary analysis. Thus though the experiments carried out so far seem to point out the lack of sufficient engine data, a consensus conclusion reported by Heywood [39] is that for chambers without swirl the turbulence intensity at TDC has a maximum value of about half the mean piston speed and the turbulence intensity increases with increase in engine speed.

7.4 Turbulence Scales

Direct measurements of length scale requires simultaneous 2 point measurement of the spatial correlation coefficient from which integral and perhaps microscales can be calculated. The spatial correlation of simultaneous velocity measurements at two points x_0 and (x_0+x) is given by

$$R(x) = \frac{1}{N-1} \sum_{i=1}^N \frac{u(x_0) u(x_0+x)}{u'(x_0) u'(x_0+x)} \dots (7.3)$$

where i refers to the i^{th} measurement, N is the total number of

measurements, u is the velocity fluctuation, and u' is the RMS velocity fluctuations. The integral length scale L_x is defined by

$$L_x = \int_0^{\alpha} R(x) dx \quad \dots\dots\dots(7.4)$$

Due to the difficulty in applying the technique of two point measurement to engine studies, single point autocorrelation has been widely used to calculate the integral length scale. This method first calculates the integral time scale defined by the correlation between two velocities at a fixed point in space but separated in time

$$\tau_L = \int_0^{\alpha} R\tau dt \quad \dots\dots(7.5)$$

where,

$$R\tau = \frac{1}{N} \sum_{i=1}^N \frac{u(\tau) u(\tau+t)}{u'(\tau) u'(\tau+t)} \quad \dots\dots(7.6)$$

where i refers to the i^{th} measurement, N is the total number of measurements, u is the velocity fluctuation, and u' is the RMS velocity fluctuations.

The integral length scale is then related to the integral time scale by the relation

$$L_x = \bar{U} \tau_L \quad \dots\dots(7.7)$$

where \bar{U} is the mean velocity, and τ_L is the integral time scale.

However equation 7.7 is approximately valid only for stationary, homogeneous and low turbulence intensity flows. It therefore cannot be used for engine studies.

The Taylor microscale, λ , is defined by the second derivative of the of the auto correlation coefficient $R(x)$ evaluated at the origin x_0 .

$$\lambda^2 = -2/(\delta^2 R(x)/\delta x^2)_{x_0} \quad \dots\dots\dots(7.8)$$

where $R(x)$ is the auto correlation coefficient differentiated w.r.t

distance x .

For single point auto correlation the micro time scale r_m is defined from the auto correlation function of equation 7-6 evaluated at the origin to.

$$r_m^2 = -2/(\delta^2 R_r / \delta t^2)_{t_0} \dots\dots\dots(7.9)$$

For homogeneous, isotropic turbulence the micro time and length scales are related by

$$\lambda = \bar{U} r_m \dots\dots\dots(7.10)$$

The turbulent scale is a parameter representative of the size of the eddies in the flow. In turbulent flows there is a distribution of energy over a continuous range of eddy sizes. The large eddies whose sizes are limited by the system boundaries are called the integral length scales. These scales create velocity gradients in the flow which result in turbulent stresses. These turbulent stresses create smaller eddies which in turn create still smaller eddies until the kinetic energy of flow is dissipated into heat through viscous action. Dissipation occurs at the smallest length scale in the energy cascade. Turbulence length scales are of fundamental importance in the characterization of turbulent flows and in the formulation of turbulent models.

For isotropic and homogeneous turbulence the three length scale relationships are as calculated below.

For isotropic, homogeneous turbulence the rate of production of turbulent energy is proportional to the kinetic energy per unit mass of large eddies divided by the time scale of the large eddies L/u' . For steady state this production is equal to the rate of viscous dissipation

therefore

$$\epsilon \propto (u'^3/L) \quad \dots\dots\dots(7.11)$$

where ϵ is the rate of dissipation of turbulent kinetic energy per unit mass due to viscosity, u' is the turbulence intensity and L is the integral length scale

Taylor [7] has shown that for isotropic turbulence the rate of energy dissipation per unit mass is

$$\epsilon = 15\nu \left(\frac{u'}{\lambda}\right)^2 \quad \dots\dots(7.12)$$

where u' is the RMS value of the fluctuating velocity component, ν is the kinematic viscosity and λ is the Taylor microscale.

Kolmogorov's length scale η , velocity v for isotropic turbulence are based upon ϵ and v . They are $\eta = (\nu^3/\epsilon)^{1/4}$ and $v = (\epsilon\nu)^{1/4} = \nu/\eta$ from the definition of the Kolmogorov length scale $\epsilon = \nu^3/\eta^4$.

The scaling rules for locally isotropic turbulence can thus be derived from the above as

$$\epsilon = \frac{u'^3}{L} = 15\nu \left(\frac{u'}{\lambda}\right)^2 = \nu \frac{v^2}{\eta^2} \quad \dots\dots\dots(7.13)$$

where ϵ is the rate of dissipation of turbulent kinetic energy per unit mass due to viscosity, ν is the kinematic viscosity and L , λ and η are the integral length scale, Taylor microscale and the Kolmogorov scales of turbulence respectively. These relationships imply that

$$\frac{L}{\lambda} = \frac{1}{\sqrt{15}} R_L^{1/2} = \frac{1}{15} R_\lambda \quad \dots\dots\dots(7.14)$$

$$\frac{\lambda}{\eta} = \sqrt{15} R_L^{1/4} = (\sqrt{15})^{1/2} R_\lambda^{1/2} \quad \dots\dots\dots(7.15)$$

in which $R_L = \frac{u' L}{\nu}$

and $R_\lambda = \frac{u' \lambda}{\nu}$

Fraser et al [38] made direct measurements of the lateral fluctuations integral length scale by means of LDV in a motored engine with a disc shaped chamber and operated with swirl. They found that the fluctuation integral length scale L reaches a minimum within 10 degrees BTDC and rises thereafter, reaching approximately one-fifth the chamber height near TDC. At TDC the integral length scale was found to be about 2.25mm and it scales with the instantaneous clearance height and varies little with speed.

Lancaster [50] noted that the integral scale normalized by TDC clearance height had values in the range of 0.175 to 0.275 and reached a minimum at TDC, and was independent of speed. There seems to be some similarity in the results obtained by using hot wire and laser doppler velocimetry. Lancaster [50] from his measurements in a motored CFR engine using hot wire anemometry calculated the Taylor microscales in the range of 0.63mm to 0.84mm. He also noted that the temporal microscale was nearly independent of engine variables other than the engine speed.

In summary, it is shown by almost all researchers that the integral length scale is about one-fifth the chamber height and it is independent of speed. Heywood [39] in his review paper has reported a range of 2-5 mm for the integral length scales in an automotive engine.

7.5 Small Scale Structure Of Turbulence

Given that during ignition and combustion the turbulence within the engine is homogeneous and isotropic and that we have approximate knowledge of the turbulence intensity and integral length scale, we can make estimates concerning the small scale structure of turbulence.

Tests conducted in the wind tunnels by various researchers using hot wire anemometry reveal that the flow may not be continuously turbulent on a very small scale but it may exhibit intermittency. The intermittency factor at a point is defined as that fraction of time for which the flow is turbulent. This phenomenon has been found to be characteristic of all turbulent flows.

To explain this intermittency Tennekes used a hypothesis that "the small scale structure of turbulence may be modelled as vortex tubes of diameter η which are stretched by eddies of size λ where η is the Kolmogorov scale and λ is the Taylor microscale".

Tennekes proposal of the small scale structure of turbulence is indicated in Fig 62 in which a single vortex tube is shown with typical spacings λ and more or less uniform velocity u' within these λ -sized regions where the flow is laminar. The dissipation process is concentrated in the vortex tube of characteristic size η . The Taylor microscale is consistent with the experimental observations of the length scale corresponding to the zero crossing frequency. This model, with regions of concentrated dissipation in the vortex tubes and the intermittency in between, is dimensionally compatible with the scaling rules. The dissipation rate per unit mass within the tube will be of the order of

$$\epsilon = c\nu \left(\frac{u'}{\eta}\right)^2 \quad \dots\dots(7-16)$$

where c is a constant. The ratio of the mass within the tube to the total will be proportional to

$$\frac{\eta^2 \lambda}{\lambda^3} = \frac{\eta^2}{\lambda^2} \quad \dots\dots(7-17)$$

so the average dissipation rate in the fluid as a whole will be

$$\epsilon = c\nu \left(\frac{u'}{\eta}\right)^2 \frac{\eta^2}{\lambda^2} = c\nu \left(\frac{u'}{\lambda}\right)^2 \quad \dots(7-18)$$

which is in agreement with the relationship (7-11) above.

The Taylor microscale is given a physical meaning by showing it as the spacing of the spaghetti-like structure the vortex tubes of Kolmogorov thickness assume. The Tennekes model implies that all of the dissipation takes place within the vortex tube.

In brief, the Tennekes model implies that a large eddy of the size of integral length scale contains several λ -sized regions in which the burning rate is slow, probably at laminar burning velocity, but the boundaries of these regions are rapidly inflamed because of the rapid flame propagation along the vortex tubes of size η .

7.6 Initial Flame Propagation

Before the turbulent flame propagation process can begin the existence of a viable flame kernel must be established. Theoretical analysis of the ignition process requires estimation of the heat generated by ignition and combustion and the heat loss due to heat conduction from burned to the unburned gases. The minimum ignition energy is usually determined by balancing the heat produced by chemical reaction and the heat dissipated via turbulence. Of critical importance is the size of the flame kernel when its temperature has fallen to the adiabatic flame temperature of the mixture. At this point the criterion for successful ignition is that the rate of heat release from the reaction zone be greater than the heat loss from the volume.

We now review the available optical data for the early flame

development period.

Khalghatgi [45] studied the effects of change in compression ratio from 3.5 to 7 and fuels like propane, methane, and iso-octane on the early flame development in a spark ignition engine using an optical technique. This optical technique times the passage of the flame front across two parallel adjustable laser beams. Khalghatgi observed that cyclic variations in combustion are reduced if the flame kernel reaches a critical size more quickly i.e. if the laminar burning velocity is increased. In his experiments laminar burning velocity was increased by increasing compression ratio and by using different fuels. Increase in compression ratio increased the laminar burning velocity due to a decrease in residual mass-fraction. Laminar burning velocity varies from propane to iso-octane to methane in the descending order.

Visualization techniques are particularly useful in the very early stages of combustion. Parameters like pressure and burning times can only yield limited information. Photographs of the combustion chamber during the combustion process show that although a substantial volume fraction is occupied by burned gas, the corresponding mass burned fraction is too small to be measured. It is interesting to note that when the outer flame radius is of the order of 10 mm the mass-fraction-burned is still well below 1%.

Gatowski, Heywood and DeLeplace [26] examined schlieren photographs of the early stages of flame development in a square cross section engine taken at 1400 rpm using premixed propane (0.9 equivalence ratio) as the fuel. They observed that the flame started at the spark plug as a smooth surfaced roughly spherical kernel and this initially spherical

kernel about 1mm diameter interacts with the turbulent flow field to produce a wrinkled and convoluted outer surface of the flame within the first few degrees. They also noted that the direction of motion of the kernel varies from cycle to cycle.

Tagalian and Heywood [47] used a square piston engine and schlieren photography at 1400 rpm using premixed propane at 0.9 equivalence ratio. An enlarged view of the spark plug region permits the study of flame travel during the first few crank angle degrees after spark. They noted that the flame started from a smooth-surfaced spherical kernel about 1 mm in diameter formed during the first crank angle degree following the spark and grows spherically for the next few degrees. They found that the flame radius was found to increase linearly with time over the first 15°. During this period of 15° following spark the amount of mass burned is small and the burning speed can be derived from the flame speed (dr/dt) and the ratio of densities i.e. $S_b = \left[\frac{\rho_b}{\rho_u} \frac{dr}{dt} \right]$. This burning speed for small amount of mass burned is found to be similar to the laminar burning speed for the fuel considered (propane in this case). Thus concluding that laminar like burning process immediately follows the spark discharge.

Keck, Heywood and Noske [48] analysed the high speed schlieren photographs of Gatowski and Heywood to obtain information on early flame development in their square piston, premixed, spark-ignition engine. They suggested that the variations in the growth rate of the flame kernel and its location in the initial stages were the major causes of cyclic variations in spark-ignition engines. They fitted a theoretical

circle on the schlieren photographs from the engine such that they had the same area and the centre as the schlieren shadows to give a theoretical shadow radius $r_f = (A_f/\pi)^{1/2}$. Similarly they obtained the burned radius r_b from the burned gas volume. They calculated shadow radius r_f and its rate of change from the optical data. Similarly they calculated the burned gas radius and its rate of change from the pressure data. By plotting these two they found that for regions less than 1 cm the shadow expansion speed approaches the burned gas expansion speed. Extrapolating to zero size of the shadow radius the value of the flame speed is approximately the laminar burning velocity for the different design configurations. The burning speed is also shown to be linearly dependent on the kernel size for radii less than 20mm. They also concluded that variation in flame speed at the spark plug is the major source of cyclic variations.

Opinions differ on the development character of the kernel in the very early stages of combustion. Zur Loye and Bracco [49] suggested that the integrating nature of the schlieren technique makes it very difficult to draw firm conclusions about the structure of the kernel. Their technique produced a two dimensional image of a thin slice of the flame front rather than an image which corresponds to an integration along the path of the light. A pulsed laser sheet was passed through the engine and Mie scattering by TiO_2 seeding particle was collected by a 100x100 pixel diode array with a field of view of 1cm x 1cm and later digitized. They noted the influence of turbulence on the structure of the kernel at all engine speeds and even at 0.6° after spark at 300rpm. They observed flame kernels at different speeds 300, 1200, and 3000 rpm

and at different times and noticed that the shape of the flame kernel was far from spherical and the shape and size varied considerably from cycle to cycle and the convolutions increased with speed. One particular frame at 3000rpm and 100 μ s after spark showed a kernel of 2-3mm from end to end but only 0.2-0.5mm wide in certain protruding ligaments.

The principal shortcoming of these observations is that even a size as small as 1mm is too large in scale to show the early flame development. The critical (self-sustaining) kernel size is about $10\alpha/U_f$, where α is the thermal diffusivity which under engine conditions is of the order of 0.01mm. The Taylor microscale is of the order of $(15\nu L/u')^2$, where ν is the kinematic viscosity and L is the integral length scale, which under engine conditions is of the order of 0.2mm. Extrapolation with the present diagnostic and visualization techniques is required to infer the random behaviour of the earliest stages of flame kernel growth.

An important inference from the research done in the early flame development period is that the flame propagation during this period is approximately at the laminar burning velocity of the fuel.

7.7 Laminar Burning Velocity

The laminar burning velocity or flame velocity is the velocity at which unburned fuel air gas mixture moves through the combustion wave in the direction normal to the wave surface.

For a given fuel, the laminar burning velocity is a function of the mixture strength, the unburned mixture temperature and pressure. The wholly empirical correlation proposed by Guilder [35] was used in this

research

$$S_u(\phi, T, P) = S_{u0}(\phi) \cdot (T_u/T_0)^\alpha \cdot (P/P_0)^\beta \dots\dots\dots 7.19$$

S_{u0} is the velocity measured at $T_u = T_0$ and $P = P_0$ for a given mixture strength, α and β are constants or mixture strength dependent terms and subscripts u and o represent the unburned and standard conditions.

Extensive experimental values for the laminar burning velocity of methane are available but not enough evidence of these values for natural gas, since methane constitutes over 94% of natural gas the laminar burning velocity values for methane are used here. Comparison of the laminar burning velocity values from different sources is compiled in appendix C.

7.8 Summary

In summary, based on the literature review undertaken the general findings on engine turbulence measurements are:

- a) Turbulence is nearly homogeneous and isotropic near TDC.
- b) Turbulence intensity varies linearly with speed.
- c) Turbulence intensity varies from about 0.4 to 0.6 times the mean piston speed.
- d) The integral length scale is about one fifth the chamber height at TDC.
- e) There is some uncertainty in determining the size of the kernel following spark from the schlieren and other modes of photography.
- f) Flame travels with laminar burning velocity following spark until it hits the vortex tubes whereby it travels at turbulent velocity.

8. COMPARISON OF MEASUREMENTS AND THEORETICAL ESTIMATES OF STANDARD DEVIATION.

8.1 Introduction: This chapter compares a characteristic from the experimental data with a characteristic estimated value of the nature of turbulence within the engine. The nature of the turbulence is deduced from the trends of continuing experimental research as discussed in chapter 7. The comparison is made in accordance with the hypothesis presented by Hill [55]. The hypothesis states that "Cyclic variations in Combustion in Spark Ignition engines are mainly due to (and predictable from) the small scale structure of turbulence and can be correlated with the Taylor microscale and the laminar burning velocity."

where the Taylor microscale is a characteristic length scale of turbulence, and the laminar burning velocity is the burning velocity of the fuel-air mixture in the engine, as discussed in appendix C.

To have a comparable characteristic of the turbulence with the experimental value of the standard deviation in burning time during the early stages of combustion following spark or for zero mass-fraction-burned we calculate the mean random time delay $\lambda/4U_t$ from the Tennekes model of turbulence.

In the following sections we first determine a comparable characteristic mean random time delay. Then we compare the two characteristic time values for zero mass-fraction-burned i.e for the region following spark.

8.2 Mean Random Time Delay

From the small scale structure model and the initial flame

development review we can now picture the flame development stages following spark in an engine.

Chomiak [2] pointed that a flame should propagate rapidly along a vortex tube owing to the collapse of the vortex tube caused by the density change associated with the flame. Daneshyar and Hill [9] showed by a simple model that the propagation velocity produced by this hydrodynamic effect should be of the order of the square root of the density ratio across the flame (unburned to burned gas density ratio) times the turbulent fluctuating velocity $u_t = u_1 + \sqrt{2/3 \rho_u / \rho_b} u'$ and this quantity is much faster than the laminar speed. This implies that the flame propagates rapidly along the vortex tube of diameter η and relatively slowly in the quiescent regions of length scale λ . The flame kernel in the λ -sized region propagates at the laminar burning velocity u_ℓ but once the kernel hits the vortex boundary the flame propagates at the turbulent rates that are much faster than the laminar burning rates.

Assuming spark ignition as almost a point source then the randomness of ignition is related as to where the effective point source is located near to or far from the vortex tubes of diameter η . In the λ -sized region the flame is taken to propagate at the laminar velocity U_ℓ . So the maximum difference in time for the flame to reach the fast burning zone of the turbulence structure will range from 0 to $\lambda/(2U_\ell)$. The mean value of the random time delay is then $\lambda/(4U_\ell)$. There is an equal probability of location of the spark within these extreme values. Figure 73, which shows time at $x=10\%$ on probability paper, indicates normal distribution of the sample test of 100 cycles, except perhaps for

some cycles towards the end of the data set. Thus in this study, the distribution of the mean random time delay is assumed to be normally distributed.

Based on this identifiable structure of homogeneous, isotropic turbulence we can calculate the random time delay period $\lambda/4U_\ell$ as

$$\frac{L}{\lambda} = \frac{1}{15} \left(\frac{u' \lambda}{\nu} \right) \quad (\text{Homogeneous Isentropic relationship})$$

$$\frac{\lambda}{4u_\ell} = \frac{1}{u_\ell} \sqrt{\frac{15 \nu L}{16 u'}}$$

where

u' is the characteristic turbulence RMS velocity

L is the integral length scale

ν is the kinematic viscosity

λ is the Taylor microscale

u_ℓ is the laminar burning velocity

The value of u' is assumed to be 0.5 times the mean piston speed in the case of the "Bath-tub" chamber and 0.42 times the mean piston speed in the case of the disk chamber being considered. The uncertainty in the calculation of u' can be +30% for both the chambers. The calculation of U_ℓ is made from the results presented by Guilder [35] as shown in section 8.5 and the uncertainty in the value of the laminar burning velocity can be of the order of 2. The calculation of L is based on the general consensus that it is one-fifth the chamber height and the uncertainty in this value is of the order of 2. Typical length and velocity scales of a spark ignition engine are shown in Table 4.

Table 4. Typical length and velocity scales for engine turbulence.
(3000 RPM).

u' m/sec	$0.5 \bar{U}_p$	4.41
Re_L	$\frac{u' L}{\nu}$	1654
U_ℓ m/sec		0.48
u'/U_ℓ		9.2
L mm	0.2H	2.25
λ mm	$\sqrt{15} L \left(\frac{\nu}{u' L} \right)$	0.213
η mm	$\frac{\lambda}{\sqrt{15} Re_L}$	0.0087
δ_q mm	$\frac{10\alpha}{(St - 0.63u')}$	0.01
δ_c mm	$\frac{2\alpha}{St} \left[1 + 10 \left(u' \delta_L / S_L L \right)^{0.75} \left(u' / S_L \right)^{0.375} \right]$	0.004

In the above table u' is the turbulent intensity, Re_L is the Reynolds number for the integral length scale, U_ℓ and St are the laminar and turbulent burning velocities, L, λ, η are integral, Taylor and Kolmogorov scales respectively, δ_q [58] is the quenching distance, δ_c is the width of the flame kernel, and α is the thermal diffusivity.

The random time delay theoretically calculated above for the turbulent structure in an engine has a distribution of values for negligible mass-fraction-burned. The experimental data shows a spread in burning times for zero mass-fraction burned by extrapolation. It would be interesting to examine the relationship if any between these two. This comparison is done in the following sections.

Figure 63 shows the trend in the estimated values of the mean random time delay with equivalence ratio for different speeds. Increase in speed tends to decrease the value of the mean random time delay. This is due to the increase in turbulence level with increase in speed. Increase in turbulence level decreases the value of λ as it is inversely proportional to the Reynolds number (Chapter 7). Also an increase in speed increases the temperature and pressure which increases the value of the laminar burning velocity. Thus there is a decrease in the value of $\lambda/4U_\ell$ with increase in speed. Recollect that a similar phenomenon of decrease in the value of extrapolated standard deviation is observed for the experimental data and also similar to the experimental data there exists a minimum value of $\lambda/4U_\ell$ near the stoichiometric fuel-air ratio.

8.3 Comparison of Data

In this section we compare the value of extrapolated standard deviation and the mean random time delay for different speeds and operating conditions.

Figures 64 to 67 show the behaviour of the two characteristic time constants at different speeds and equivalence ratio. These Figures show that in the lean fuel region the two curves follow the same trend for all the speeds and configurations considered. Also the magnitudes of the two variables correspond very closely to each other. There seems to be no similar relationship for rich mixtures.

Finally, a comparison of the estimated value of the mean random time delay is made with the extrapolated standard deviation in burning time, for both the "bath-tub" and "disc" chamber. The fuel-air ratio considered in these comparisons is $\phi < 1.05$. Figures 68 and 69 show

these comparisons for the "bath-tub" and "disc" chamber respectively. From these plots we observe that there exists a simple relation between the extrapolated standard deviation and the mean random time delay for both the chambers. This relation is

$$\sigma_{\circ} = 0.75 \lambda/4u_{\ell} \quad \text{for the bath-tub chamber, and}$$

$$\sigma_{\circ} = 0.85 \lambda/4u_{\ell} \quad \text{for the disc chamber.}$$

where σ_{\circ} is the extrapolated standard deviation in burning time from the experimental data and $\lambda/4u_{\ell}$ is the estimated mean random time delay. These simple relations suggest that the distribution of extrapolated standard deviation σ_{\circ} falls around the mean value of $\lambda/4U_{\ell}$ where the mean value of random time delay is normally distributed.

8.4 Summary

- a) The random time delay period $\lambda/4U_{\ell}$ in the early stages of burning can be estimated from the Tennekes model of the small scale structure of turbulence.
- b) Combining the Tennekes model of small scale structure of turbulence, Chomiak's concept of rapid flame travel along the vortex tubes and the approximate point source of ignition we can give an explanation of the initial flame propagation within an engine.

9. CONCLUSIONS.

The objective of this research was to investigate the origin of cyclic variations in combustion by relating the mass-fraction-burned values calculated from the experimental data to the small scale structure of turbulence prevalent in the engine.

The conclusions, based on the experiments and estimates of turbulence parameter are:

- 1) Standard deviation in burning time increases linearly with increase in the value of x and the mass-fraction-burned (x) values in the later stages of combustion are strongly dependent on the x values in the initial stages.
- 2) The values of the standard deviation in burning time, extrapolated to kernels of vanishing sizes, are significant and show that randomness exists at zero mass-fraction-burned.
- 3) At the same speed, the extrapolated standard deviation values at different equivalence ratios shows a minimum value near the stoichiometric air-fuel ratio and this value increases as the air-fuel ratio is increased both towards lean and the rich side (in the absence of misfiring).
- 4) The modified spark plug electrode shape did not show any change in combustion variation as compared with the standard spark plug.
- 5) The modified spark plug spark gap decreases combustion variation in case of a disc shaped combustion chamber, but it shows no combustion improvement in case of a Bath tub combustion chamber.
- 6) The effect of the part-open-throttle on the change in standard deviation was negligible in the case of Bath tub combustion chamber but

an increase in the values of standard deviation was observed in the case of a disc shaped combustion chamber. An increase in mean time for complete combustion was observed in both cases.

7) Comparison of the bath-tub and the disc chamber at different speeds and configurations at similar operating conditions show that the Bath tub chamber has lower values of extrapolated standard deviation.

8) The minimum value of extrapolated standard deviation shifts towards the leaner equivalence ratio (around the stoichiometric air-fuel ratio) with increase in turbulence levels.

9) The mean random time delay shows a linear relationship when compared to the extrapolated standard deviation in burning time value for both the bath-tub and the disc chamber. The simple relationship suggests that the distribution of values of extrapolated standard deviation fall around the normally distributed values of mean random time delay.

The mean random time delay estimated from the Tennekes model of small-scale-structure of turbulence resulted from the following assumptions:

- a) Turbulence is nearly homogeneous and isotropic near TDC.
- b) Turbulence intensity varies from about 0.4 to 0.6 times the mean piston speed for chambers with no swirl.
- c) The integral length scale is about one fifth the chamber height at TDC.
- d) Flame travels with laminar burning velocity following spark until it hits the vortex tubes whereby it travels at turbulent velocity.
- e) Chomiak's concept of rapid flame travel along the vortex tubes and the approximate point source of ignition can give an explanation of the

initial flame propagation within an engine.

The results presented above do not prove that these assumptions are true, nevertheless the results have shown that the origin of cyclic variations can be predicted from the small-scale-structure of turbulence in the engine during spark.

RECOMMENDATIONS

It is suggested that further work be conducted in order to determine the turbulence parameters such as the turbulence intensity, length scales and the nature of turbulence during combustion using the Laser Doppler Anemometry for the "Bath-tub" and "Disc" combustion chamber that have been used in these studies.

Further, pressure data should be collected for the modified spark-plug gaps with both an increase and decrease in spark-gap size for the Bath-tub and Disc shaped combustion chamber. Also the effect of gradually increasing residuals on cyclic variations should be observed by changing the throttle opening.

Finally, a study of the visualization of initial flame growth following spark will be highly useful in determining the initial flame growth.

REFERENCES

1. Young, Michael B., "Cyclic Dispersion in the Homogeneous-charge Spark-Ignition Engine", A Literature Survey Society of Automotive Engineers Paper, SAE 810020 , 1981.
2. Chomiak, J., "Flame Development from an Ignition Kernel in Laminar and Turbulent Homogeneous Mixtures", The Combustion Institute, Seventeenth Symposium (International) on Combustion, 255-263,1979.
3. Amann, C.A., "Cylinder Pressure Measurement and its use in Engine Research", SAE 852067.
4. Dent, J.C., and Salama, N.X., "The Measurement of the Turbulence Characteristics in an Internal Combustion Engine Cylinder", SAE 750886 Automobile Engineering Meeting, Detroit, (1975).
5. Daneshyar, H., and Fuller, D.E., "Mixture Motion in an Engine Cylinder", Cambridge University Engineering Department/A/Thermo/TR.15 (1981).
6. Smith, J.R., "The Influence of Turbulence on Flame Structure in an Engine", ASME conference Phoenix, Arizona, Paper W014-19 (1982).
7. Taylor, G.I., "Production and Dissipation of Vorticity in a Turbulent Fluid", Proc. Roy. Soc. A, 1938.
8. Tennekes, H., "Simple Model for the Small Scale Structure of Turbulence", The Physics of Fluids, vol. 1, No. 3. (1968).
9. Daneshyar, H., and Hill, P.G., "the Structure of Small Scale Turbulence and its Effects on Combustion in Spark Ignition Engines", Proc. in Energy and Combustion Science.
10. Soltau, J.P., "Cylinder Pressure Variations in Petrol Engines," Proceedings of the Institute of Mechanical Engineers, No. 2, 1960-1961.
11. Karim, G.A., "An Examination of the Nature of the Random Cyclic Pressure Variations in a Spark ignition Engine," J. of the Institute of Petroleum, vol. 53, No 519, March 1967.
12. Peters, B.D., Borman, G.L., "Cyclic Variations and Average Burning Rates in a S.I.Engine," SAE 700064, 1970.
13. Harrow, G.A., Orman, P.L., "A Study of Flame Propagation and Cyclic Dispersion in a Spark-Ignition Engine," Advanced School of Automotive Engineering (Part IV) Combustion Processes in the Spark Ignition Engine, Pergamon Press, July 1965.
14. Barton, R.K., Kenemuth, D.K., Lestz, S.S., Meyer, W.E., "Cycle-by-Cycle Variations of a Spark Ignition Engine- A Statistical

Analysis," SAE 700488, 1970.

15. Winsor, R.E., Patterson, D.J., "Relationship of Cyclic Combustion Variations and Mixture Motion in a Spark-Ignition Engine," Tech. Report No.1, Dept. of Mechanical Engineering, University of Michigan, September 1972.

16. Lancaster, D.R., "Effects of Engine Variables on Turbulence in a Spark-Ignition Engine," SAE 761059, 1976.

17. Lancaster, D.R., Krieger, R.B., Sorenson, S.C., Hull, W.L., "Effects of Turbulence on Spark-Ignition Engine Combustion," SAE 760160, 1976.

18. Andrews, G.E., Bradley, D., Lwakabamba, S.B. "Turbulence and Turbulent Flame Propagation -A Critical Appraisal," Combustion and Flame, Vol. 24, 1975.

19. Hansel, H.G., "A Turbulent Combustion Model of Cycle-to-Cycle Combustion Variations in Spark-Ignition Engines," Combustion Science and Technology, Vol. 2, 1970.

20. Winsor, R.E., Patterson, D.J., "Mixture Turbulence-A key to Cyclic Variations," SAE 730086., 1973.

21. Annand, W.J.D., "Heat Transfer in the Cylinder of Reciprocating Internal Combustion Engines," Proc. Instn. Mech. Engrs., Vol. 177, No. 36, pp.973-996, 1983.

22. Beretta, G.P., Rashidi, M., Keck, J.C., "Turbulent Flame Propagation and Combustion in Spark-Ignition Engines," Combustion and Flame, Vol. 52, pp 217-245, 1983.

23. Bopp, S., Vafidis, C., and Whitelaw, J.H., "The Effect of Engine Speed on the TDC Flow field in a Motored Reciprocating Engine," SAE 860023, 1986.

24. Chomiak, J., "Dissipation Fluctuations and the Structure and Propagation of Turbulent Flames in Premixed Gases at high Reynolds Numbers," Sixteenth Symposium (International) on Combustion, The Combustion Institute, pp 1665-1673, 1977.

25. Fraser, R.A., Felton, P.G., Bracco, F.V., and Santavicca, D.A., "Preliminary Turbulence Length Scales Measurements in a Motored IC Engine," SAE 860021, 1986.

26. Gatowski, J.A., Heywood, J.B., and Delaplace, C., "Flame Photographs in a Spark-Ignition Engine," Combustion and Flame, Vol. 56, pp 71-81, 1984.

27. Kuo, A.Y.S., and Corrsin, S., "Experiments on Internal Intermittency and Fine Structure Distribution Functions in Fully

- Turbulent Fluid," Journal of Fluid Mechanics, Vol. 50, Part 2, pp. 285-319, 1971.
28. Lancaster, D.R., Krieger, R.B., Lienesch, J.H., "Measurement and Analysis of Engine Pressure Data," SAE 750026, 1975.
 29. Semenov, E.S., "Studies of Turbulent Gas Flow in Piston Engines," NASA Technical Translation F-97, 1963.
 30. Tabaczynski, R.J., "Turbulence and Turbulent Combustion in Spark-Ignition Engines," Prog. Energy Combustion Science, Vol. 2, pp. 143-165, 1976.
 31. Tabaczynski, R.J., "Turbulence Measurement and Modelling in Reciprocating Engines-An overview," I Mech. Eng. 1983.
 32. Taylor, G.I., "Statistical Theory of Turbulence," Proceedings of Royal Society (London), Ser.A., Vol. 151, pp 421, 1935.
 33. Andrews, G.F., Bradley, D., "The Burning Velocity of Methane Air Mixtures," Combustion and Flame, Vol. 19, pp 275-288, 1972.
 34. Sharma, S.P., Agarwal, D.D., Gupta, C.P., "The Pressure and Temperature Dependence of Burning Velocity in a Spherical Combustion Bomb," Eighteenth Symposium (International) on Combustion, The Combustion Institute, pp 493-501, 1981.
 35. Gulder, O.L., "Correlations of Laminar Combustion Data For Alternative S.I.Engine Fuels," SAE 841000, 1984.
 36. Belmont, Hancock and Buckingham "Statistical Aspects of Cyclic Variability," SAE 860324.
 37. Boisvert, J., "Turbulent Combustion of Gas-Air Mixtures in a Spark-Ignition Engine." M.A.Sc Thesis U.B.C. AFL-86-05 1986.
 38. Fraser, Felton, Bracco and Santavicca "Preliminary Turbulence Length Scale Measurement in a Motored IC Engine." SAE 860021.
 39. Heywood, J.B., "Fluid Motion within the Cylinder of Internal Combustion Engines. - The 1986 Freeman Scholar Lecture". J. of Fluids Engineering March 1987 Vol 109/3.
 40. Patterson, D.J., "Pressure Variations, A fundamental Combustion Problem". SAE paper No.660129, 1966.
 41. Hirao, O., Kim, Y., "Combustion Variation Analysis on Flame Propagation in 4 Cycle Gasoline Engines". Japan Automobile Research Institute, Inc., 1970.
 42. Broeze, J.J., "Combustion in Internal Combustion Engines. II. The Spark Ignition Engines,". Engineering Vol. 169, April 28, 1950.

43. Van Wylen. G.J., Sonntag. R.E., "Fundamentals in Classical Thermodynamics".
44. Warren, J.A., Hinkamp. J.B., "New Instrumentation For Engine Combustion Studies", SAE Transactions, Vol 64, 1956.
45. Kalghatghi, G., "Early Flame Development in a Spark-Ignition Engine", Combustion and Flame 60, 299,308, 1985.
46. Gatowski, J.A., Heywood, J.B. and DeLePlace, C., "Flame Photographs in a Spark-Ignition Engine"., Combustion and Flame, 56, 71-81, 1984.
47. Tagalian, J., and Heywood, J.B., "Flame Initiation in a Spark-ignition Engine", Combustion and Flame, 64, 243-246, 1986.
48. Keck, J.C., and Heywood, J.B., "Early Flame Development and Burning Rates Spark-ignition Engines and Their Cyclic Variability", SAE 870164 (1987).
49. Zur Loye, A.O. and Bracco, F.V., "Two-Dimensional Visualisation of Ignition Kernels in an IC Engine"., Combustion and Flame, 69, NO.1 60-69, 1987.
50. Lancaster, D.R., "Effects of Engine Variables on Turbulence in a Spark-Ignition Engine". SAE 760159.
51. Bracco, F.V., and Hall, M.J, "A Study of Velocities and Turbulence intensities in Firing and Motored Engines". SAE 870453.
52. Whitelaw, J.H., Vafidis, Bopp, S., "The Effect of Engine Speed on TDC Field in a Motored Reciprocating Engine". SAE 860023.
53. Albrecht, H., Bloss, W.H., Herden, W., Maly, R., Saggan, B., and Wagner, E., "New Aspects on Spark Ignition". SAE 770853.
54. Starkman, E.S., Strange. F.M., and Dahm. T.J., "Flame Speeds and Pressure Rise Rates in Spark Ignition Engines." SAE paper 83V, 1959.
55. Hill. P.G., "Cyclic Variations and Turbulence Structure in Spark Ignition Engines". Combustion and Flame.
56. "The Ricardo/Cussons Standard Hydra Engine and Test Bed Manual".
57. Hung. J., "Effects of Propane and Ethane Addition on the Laminar Burning Velocity Of Methane".

APPENDIX A. CALIBRATION CURVES

This appendix presents the calibration curves for a) the Meriam laminar flow element, used to monitor the natural gas flow b) the Meriam Laminar flow meter to monitor the air flow to the Ricardo engine, and c) the calibration curve for the piezo-electric transducer.

LAMINAR FLOW ELEMENT

The calibration curves for the two Meriam laminar flow elements a) air model 50MC2-4F and b) fuel model 50MW20-1.5 are supplied by the manufacturer with the instrument giving the relation between pressure head across the meter elements in inches of water and the volume flow in ft^3/min . To calculate the standard cubic feet per minute temperature and pressure correction factors from charts supplied by the manufacturer are used.

QUASI-STATIC CALIBRATION OF PIEZO-ELECTRIC PRESSURE TRANSDUCER

The pressure transducer was calibrated in the laboratory to confirm the calibration constant supplied by the manufacturer. The pressure transducer was attached to its sleeves [56] and installed in the deadweight tester. The piezo-electric transducer is calibrated quasi-statically on a deadweight tester using a Kistler 5001 charge amplifier. The charge amplifier was set on its "long" time constant to provide high input resistance. The large input resistance of the charge amplifier makes it suitable to calibrate this dynamic response producing pressure transducer. The sensitivity and the range are set to the settings normally used on the engine. The sensitivity (calibration constant) is provided by the manufacturer and the calibration range of pressures is between 10-110 bars (this is the pressure range within the

engine).

After the preliminary installation is done the dead weight tester is loaded with known weights. These weights provide a hydraulic pressure on the pressure transducer which gives an output signal. The value of the output signal is determined using the oscilloscope. Thus the values of the voltages corresponding to the known pressure are collected. A plot is then made of the charge output versus pressure applied. The best fitting straight line is then drawn through the points and the gradient of the line gives us the sensitivity. If the gradient is different from the one supplied by the manufacturer the calibration is repeated with the sensitivity set at the new value of the gradient. The calibration curve supplied by the manufacturer and the calibration curve determined from the measurements obtained in the laboratory are both reported.

The values of the pressure and the output from the charge amplifier are as shown in Table A.1.

Table A.1: Pressure and Voltage Values for Calibration of Piezo-electric Pressure-Transducer.

Pressure Input (psi)	Voltage Output (mV)
15	99
25	168
35	240
45	297
55	359
105	695
155	1017
205	1363

APPENDIX B. COMBUSTION-VOLUME PHASING

This appendix examines the effect of the piston movement on combustion within the engine. The piston position changes while the combustion occurs within the engine. This change in piston motion being small at TDC, when the velocity of the piston approaches zero and then increases sinusoidially on the expansion stroke with the maximum velocity occuring midway between the stroke.

The Engine simulation model by Boisvert [37] calculates the pressure in an engine from BDC prior to compression to TDC and into the expansion stroke. The calculations for the compression stroke until the occurrence of the spark are the same as in the program XPRESS described in chapter 4 but the calculations following spark in the combustion period are done combining a thermodynamic analysis of the cylinder contents coupled with the turbulent entrainment model.

This program was used to show the importance of combustion volume phasing.

The input to the program is the initial conditions of intake and ambient temperature, ambient pressure, speed, residual fraction, spark advance and the equivalence ratio. To understand the effect of the pressure occuring at or near TDC we maintain all the conditions of input the same but change the value of the spark advance such that the peak pressure occurs over a range of crank angles after spark.

The results of this experiment are shown in Table B.1

Table B.1: Peak-Pressure and its Crank Angle Occurrences for Changes in Phasing.

Spark Advance Before TDC	Crank Angle at Peak Pressure	Peak Pressure
26	16	5340.80
28	14	5705.94
30	12	6068.03
32	10	6394.30
34	8	6658.30
36	6	6940.91
38	4	7128.25

If we consider these cycles to be true for a particular set of operating conditions then we can see that the cycle which has the peak pressure near the TDC shows the highest value of the pressure or conversely if the cycle is faster burning i.e it travels faster in the chamber then most of the heat release occurs near TDC and subsequently the value of the peak pressure is higher.

The phasing of the pressure and the volume position plays an important role in determining the character of the pressure and the output variations. For fast burning cases a large fraction of the energy release occurs near TDC when the combustion chamber volume is changing very slowly. As a result the pressure variations are due mainly to the combustion variations. For the slower burning cases a large part of energy release occurs later in the cycle, the variations in pressure due to the combustion variation is augmented by the changing

pressure due to rapidly varying cylinder volume during this part of the cycle. By burning most of the mixture while the piston is at or very near TDC i.e by faster burning the cyclic variations have been known to decrease. Obviously then to minimize cycle to cycle variations in an engine combustion variations should be minimized and or combustion rates maximized.

APPENDIX C. Laminar Burning Velocity

This appendix reviews some of the literature on the laminar burning velocity of methane at high temperatures and pressures as presented by various authors. engine.

The laminar burning velocity or flame velocity is the velocity at which unburned fuel air gas mixture moves through the combustion wave in the direction normal to the wave surface.

For a given fuel, the laminar burning velocity is a function of the mixture strength, pressure and the unburned mixture temperature. Guilder [35] suggested that closed vessel explosions techniques accompanied by density corrections can give good possibilities for the accurate measurement of burning velocity. Various forms of empirical relationships have been proposed for laminar burning velocities and the simplest form of the wholly empirical correlation proposed by Guilder is

$$S_u(\phi, T, P) = S_{u_0}(\phi) (T_u/T_0)^\alpha (P/P_0)^\beta$$

S_{u_0} is the velocity measured at $T_u = T_0$ and $P = P_0$ for a given mixture strength, α and β are constants or mixture strength dependent terms and subscripts u and o represent conditions of the unburned gases and at standard conditions respectively.

Guilder made measurements in a constant volume bomb. He proposed empirical expression to represent the room temperature burning velocity of methane

$$S_{u_0}(\Phi) = W \Phi^n \exp [-\xi(\Phi-1.075)^2]$$

where the $n=0.15$, $\xi=5.18$, $W=0.422$ m/sec are for methane.

The effect of pressure and temperature on the burning velocity of methane and propane have been correlated by various kinds of relationships including the power law. Guilder proposed the following relations for temperature and pressure.

Pressure Dependency

For the pressure dependence of the laminar burning velocity a power law expression is deduced by Guilder from the available data from various sources

$$S_u(\Phi, P) = S_{u0}(\Phi) [P/P_0]^\beta$$

for methane this pressure exponent β is around -0.5 in the range of 4-100 pressure in kpa.

Temperature dependency

For the temperature dependency of the burning velocity the power law proposed by Guilder is

$$S_u(\Phi, T) = S_{u0}(\Phi) [T_u/T_0]^\alpha$$

for the temperature exponent of methane the proposed values of α ranges from 1.37 to 2.33 at various pressure ranges and equivalence ratios. This value is taken to be 2 in our case.

Andrew and Bradley [33] obtained the value of laminar burning velocity using bomb hot wire and corrected density ratio techniques. They proposed separate formulae for the dependence of methane laminar burning velocity on unburned gas pressure and temperature

$$S_{\ell} = 43 P_u^{-0.5} \quad (\text{constant } T_u)$$

$$S_{\ell} = (10 + 0.000371 T_u * T_u) \quad (\text{constant } P_u)$$

where P is in atm.

Combing these two equations to get the laminar burning velocity we have

$$S_{\ell} = (10 + 0.000371 T_u * T_u) P_u^{-0.5}$$

this is justified by Sharma Aggarwal and Gupta who show that the rate of increase of burning velocity with temperature does not vary with increasing pressure.

Sharma, Aggarwal and Gupta [34] obtained laminar burning velocity of methane-air for pressures of 0.5 to 8 atm, temperature of 300 to 600°K and equivalence ratio in the range of 0.8 to 1.2. They correlated the pressure, temperature and mixture strength dependence in to the relations given by

$$S_{\ell} = C_4 (T_u / 300)^{1.68/\phi} \quad \phi < 1.0$$

$$S_{\ell} = C_4 (T_u / 300)^{1.68*\phi} \quad \phi > 1.0$$

where $C_4 = -418 + 1287/\phi - 1196/\phi^2 + 360/\phi^3 - 150(\log P_u)$

they stated that though the working fuel was natural gas they computed the burning velocity assuming this gas to be

Methane.

Hung [57] obtained laminar burning velocity of stoichiometric mixtures of methane-air and methane with ethane or propane additives by making measurements in a constant volume chamber for pressures of 1 to

80 atm and with unburnt gas temperature in the range of 300 to 500°K. She correlated the pressure and temperature dependence of the burning velocities for the whole range of experimental conditions by the relation

$$S_u = S_{u0} [T_u/T_0]^\alpha [P/P_0]^\beta$$

where $S_{u0} = 33.7$, $\beta = -.315$ and $\alpha = 1.87$ for methane.

She also reported that the greatest relative increase in burning velocity was at the highest pressure, for a given temperature and trace amounts of propane and ethane do not appear to have significant effects on the burning velocity.

APPENDIX D - PROPERTIES OF B.C. NATURAL GASComposition (Volume %)

Methane	94.00
Ethane	3.30
Propane	1.00
Iso-Butane	0.15
N-Butane	0.20
Iso-Pentane	0.02
N-Pentane	0.02
Nitrogen	1.00
Carbon-Dioxide	0.30
Hexane	0.01

Water content: 3 to 4 lbs/million cubic feet.

APPENDIX E - SENSITIVITY ANALYSIS

The effect of uncertainty in the pressure data in determining the mass-fraction-burned values w.r.t the crank angles in the initial stages after spark is illustrated in the following discussion.

The sensitivity of raw pressure data w.r.t time (after spark) can be established from the relationship

$$\Delta t = \frac{\Delta P}{\delta P / \delta t}$$

where Δt is the uncertainty in time corresponding to the uncertainty ΔP in the pressure data. The derivative $\delta P / \delta t$ is the slope of the combustion pressure (less motored pressure) w.r.t time after spark. The term ΔP is the minimum uncertainty in the pressure corresponding to the digitization error of ± 1 units. For the transducer assembly, the digitization of analog data was such that a digital value of 4096 at the data acquisition system corresponded to 100 bars of pressure within the engine. Thus 2 units of raw pressure data would equal 5 kPa.

Figure 74 shows the typical fired and motored pressure curves. Figure 75 shows the difference between the combustion pressure and the motored pressure and (in a broken curve) the same curve plus the digitization error of 100 bar / 4096 = 5 kPa. The full curve is used to estimate $\delta P / \delta t = \frac{P_{i+1} - P_i}{t_{i+1} - t_i}$. This estimate becomes unreliable when $\delta P / \delta t$ is small.

Figure 76 shows both the mass-fraction growth with crank angle (computed from the fired pressure curve) and the estimate of the time uncertainty $\Delta t = \frac{\Delta P}{\delta P / \delta t}$ corresponding to the digitization error and affected by the fluctuations in the estimate of $\delta P / \delta t$.

This graph shows the estimates of burning time uncertainty are necessarily unreliable for $x < 2\%$.

TABLE 1 RICARDO HYDRA ENGINE SPECIFICATIONS

Number of Cylinders	1
Bore	80.26 mm
Stroke	88.90 mm
Con-rod Length	158.0 mm
Swept Volume	0.45 l
Clearance Volume	0.0563 l
Compression Ratio	9:1
Max Speed	90 rev/sec
Max Power	15 kW
Max Cylinder Pressure	120 bar

Valve Timing:

Inlet Opens	12° BTDC
Inlet Closes	56° ABDC
Exhaust Opens	56° BBDC
Exhaust Closes	12° ATDC

Normal Working Temperatures:

Oil	80°C
Water	80°C

CYCLIC PRESSURE VARIATIONS IN A SPARK IGNITION ENGINE
Speed = 3000 RPM $\phi = 1.00$

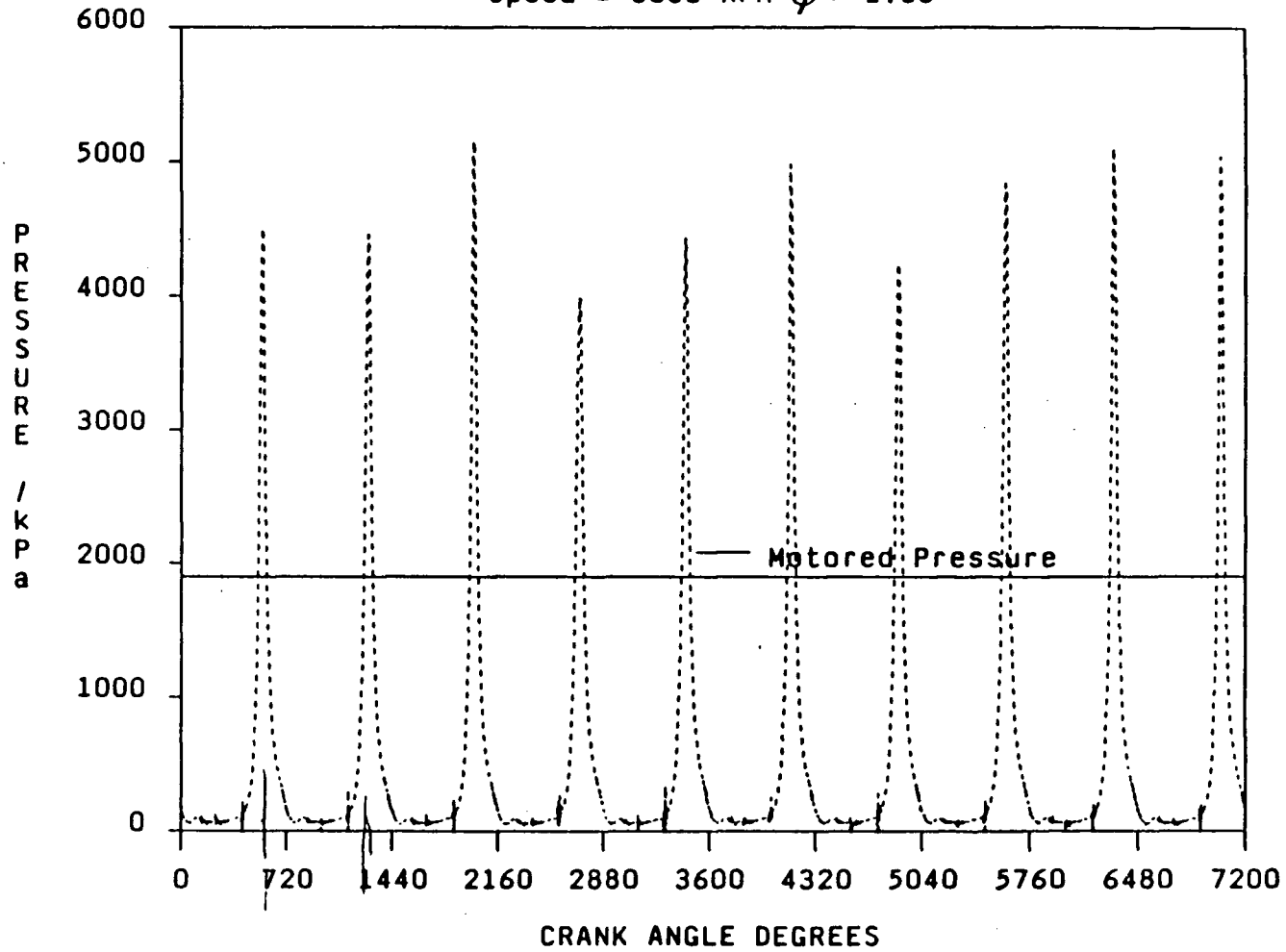


Fig 1. Cyclic Pressure Variations in a Spark Ignition Engine.

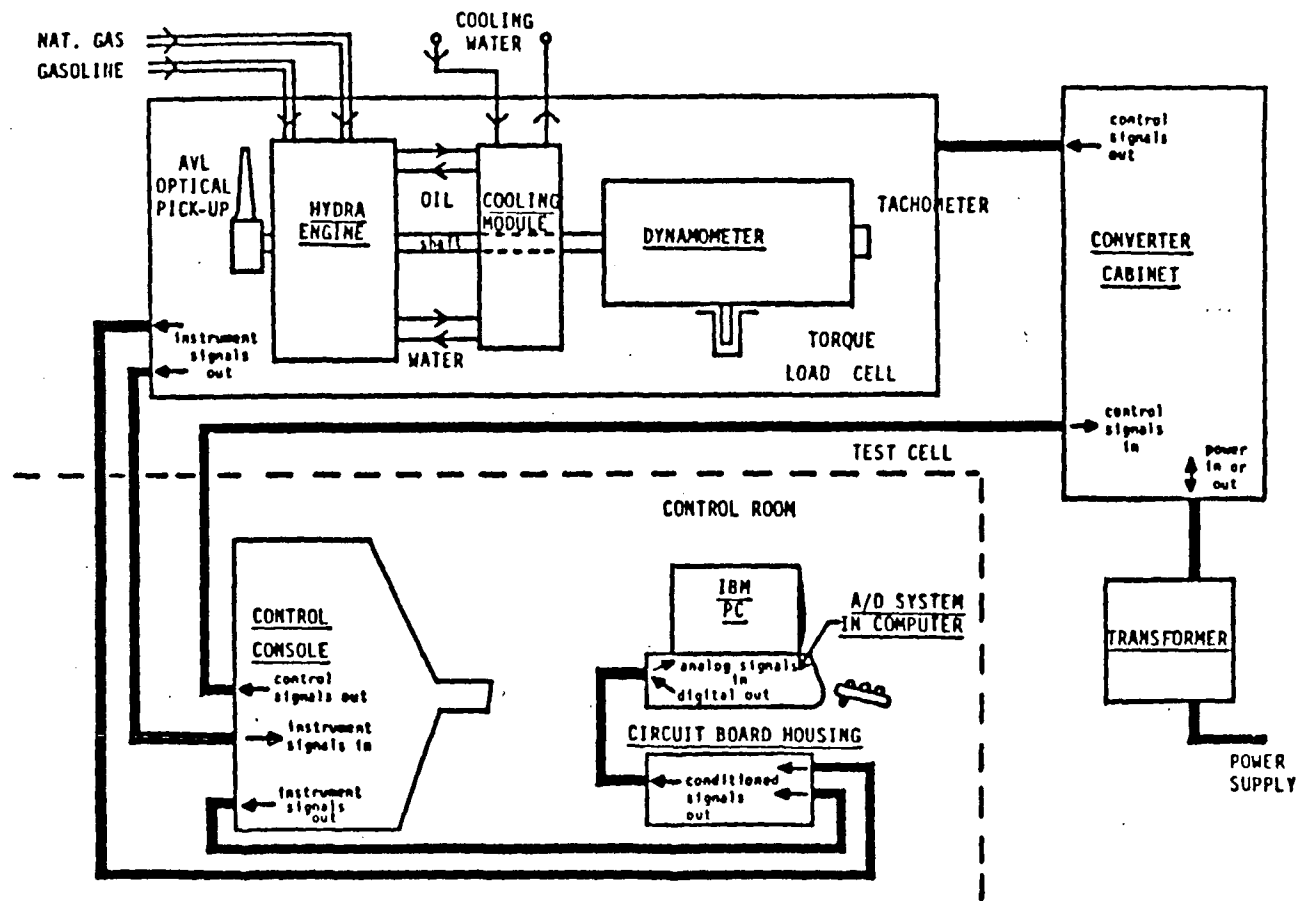


Fig 2. Engine, Dynamometer and Control Systems Layout.

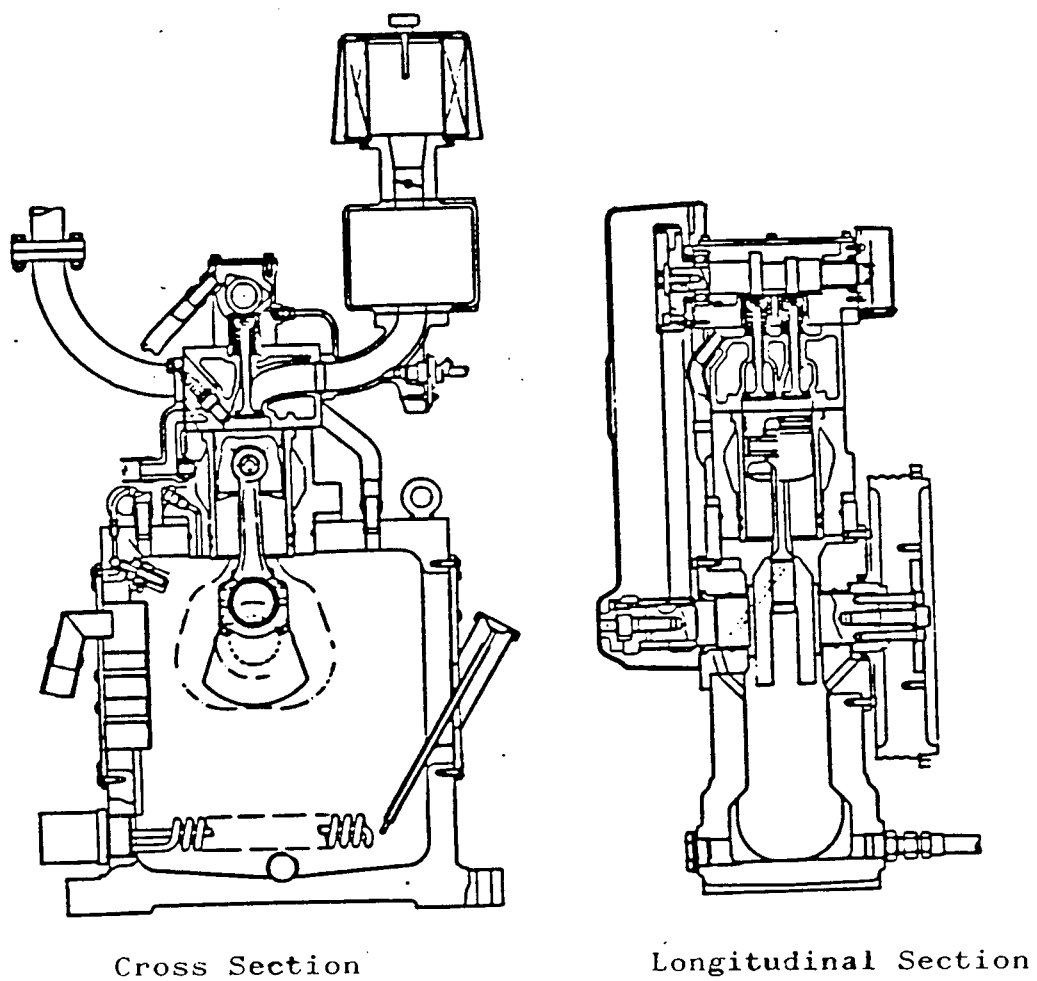


Fig 3. Ricardo Hydra Engine Cross-Sectional Views.

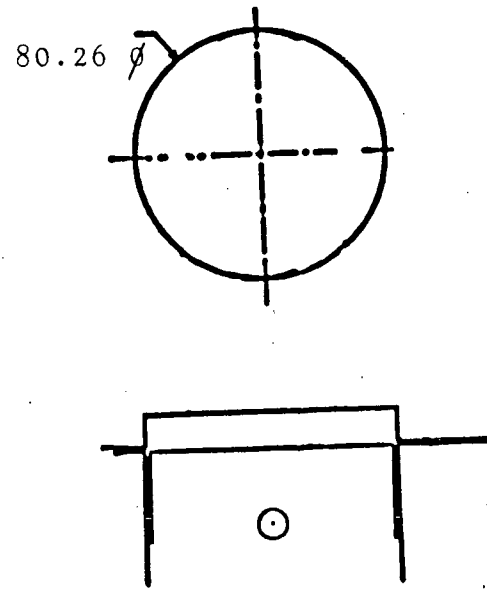
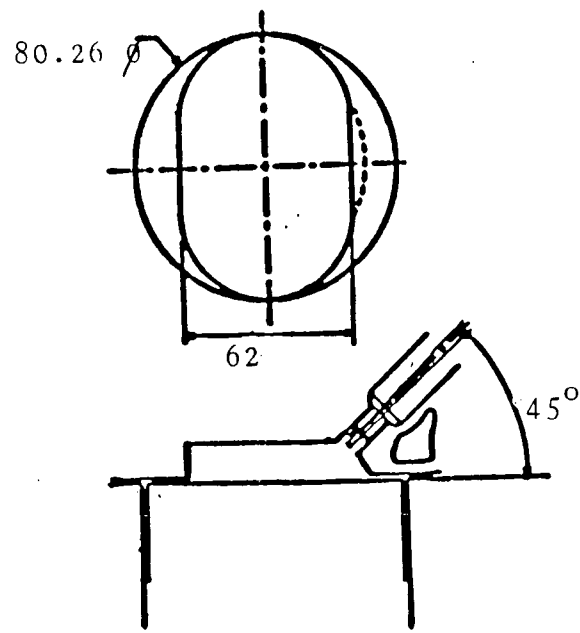


Fig 4. Combustion Chamber Shapes a) Bath-Tub Chamber. b) Disc Chamber.

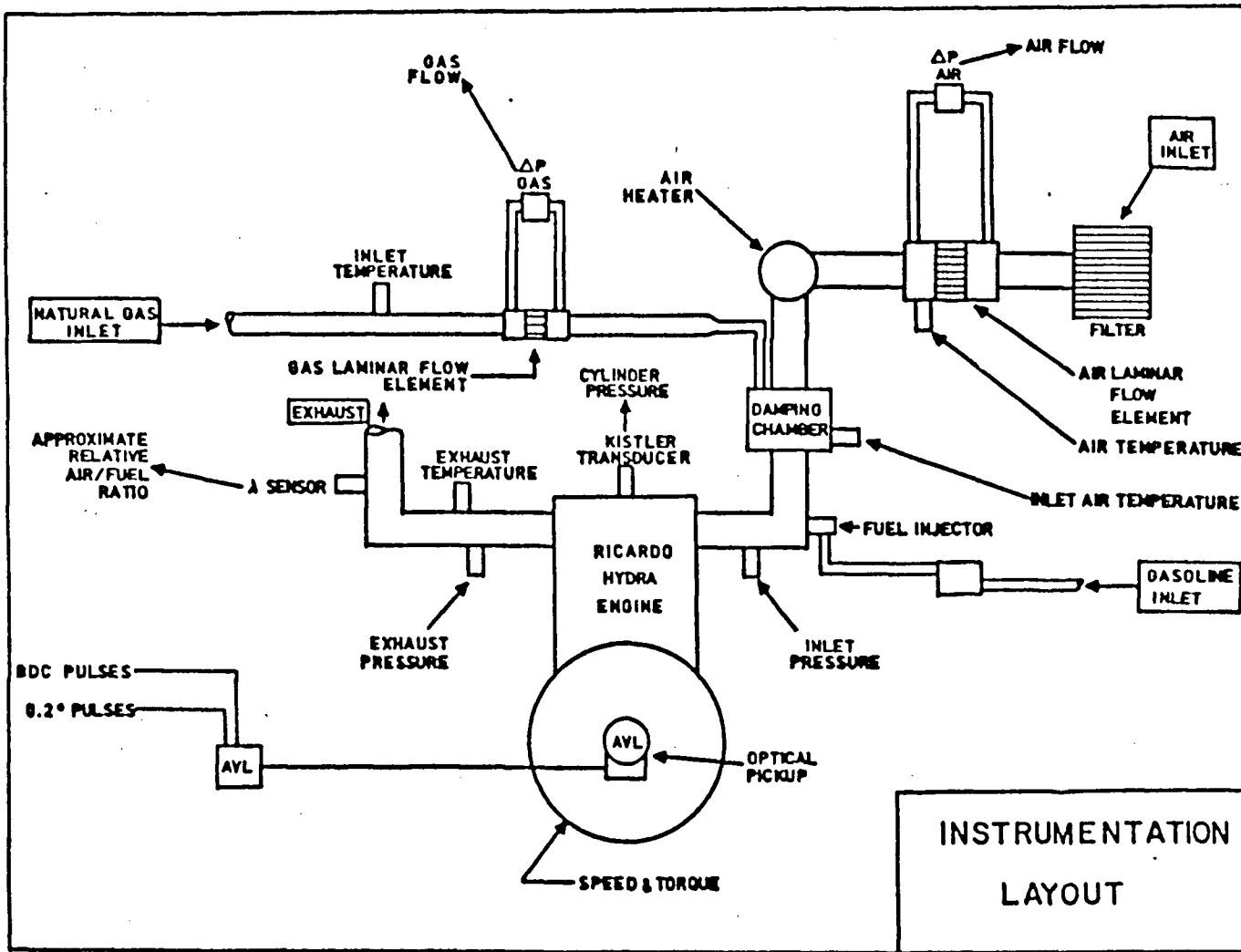


Fig 5. Instrumentation Layout.

FIGURE 6 - HARDWARE ARRANGEMENT

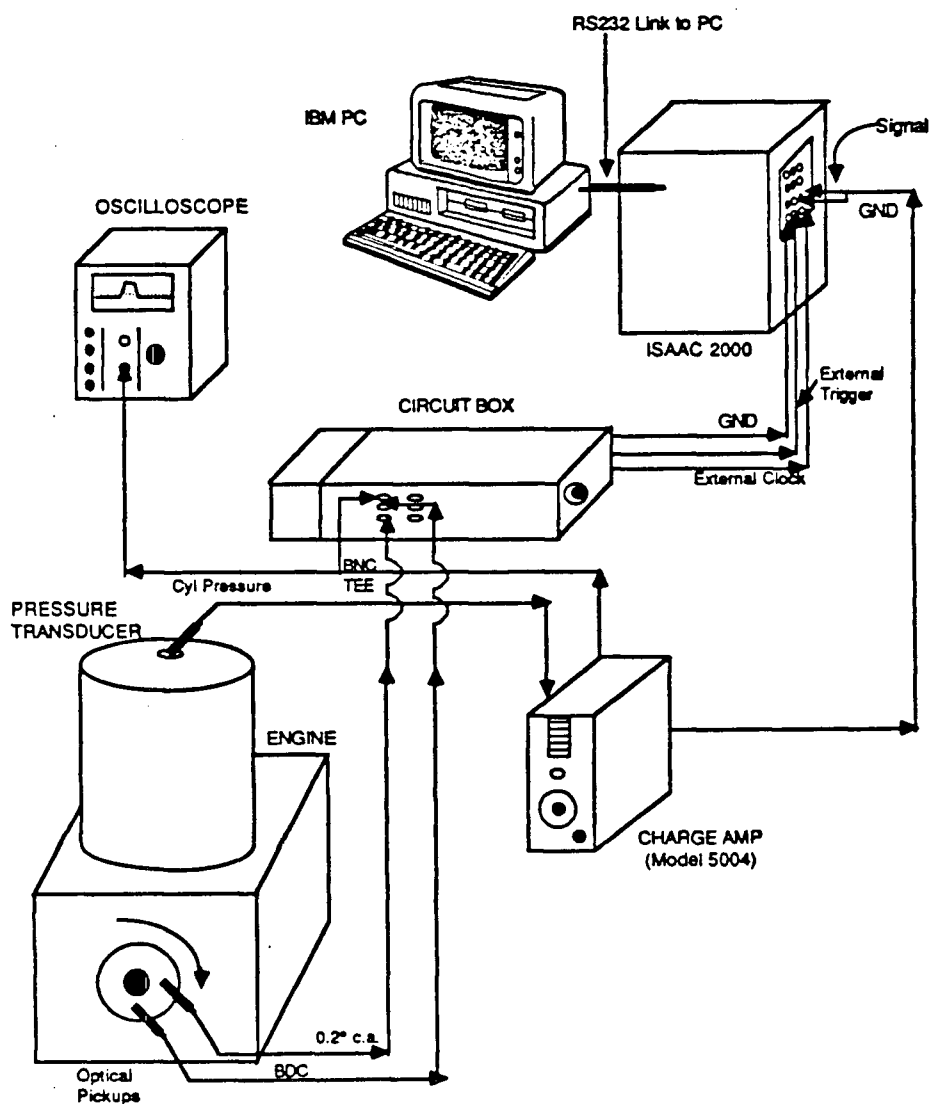


Fig 6. Hardware Arrangement.

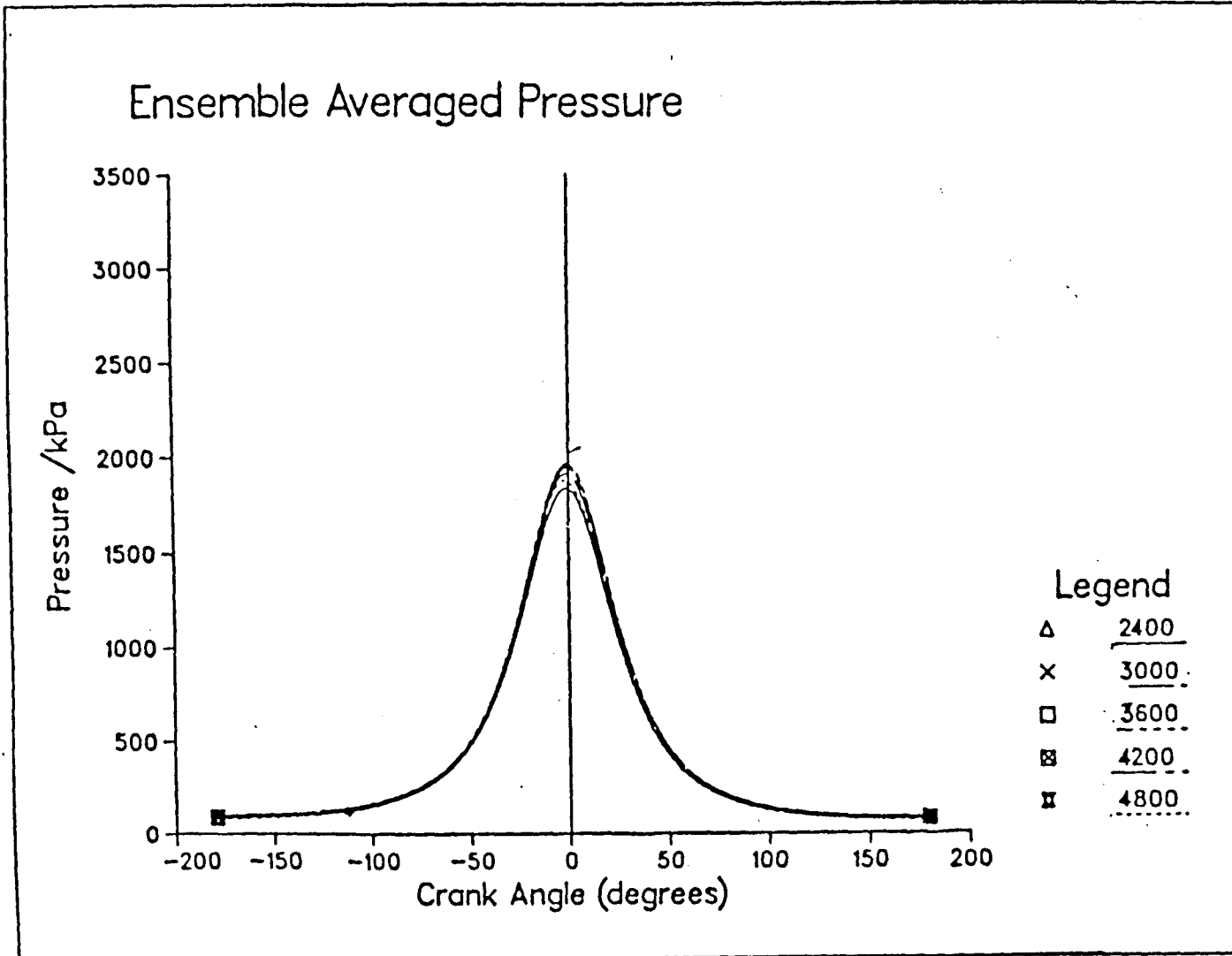


Fig 7. Ensemble-Averaged Pressure [Motored Engine]

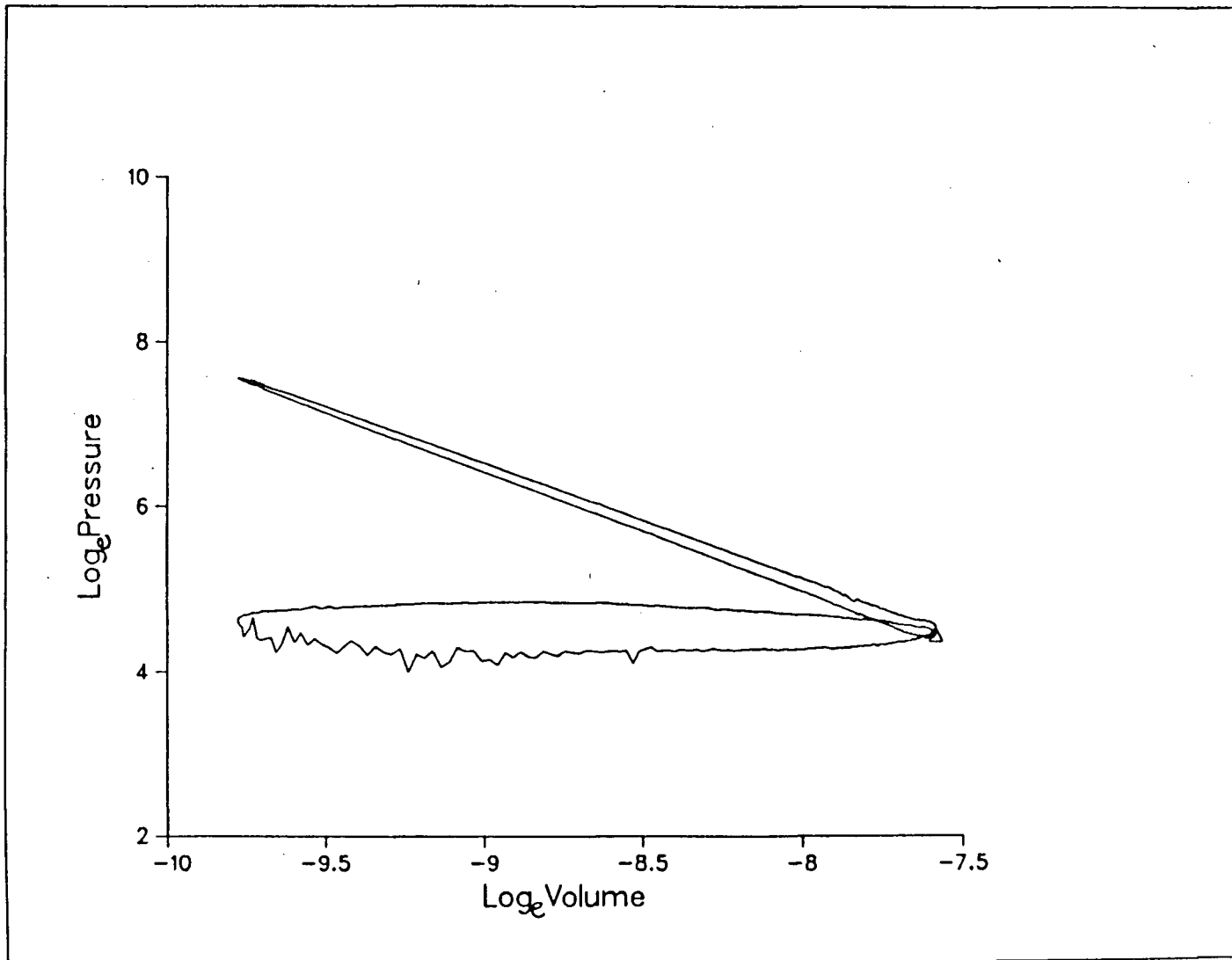


Fig 8. Indicator Diagram on Logarithmic Scale [Motored Engine]

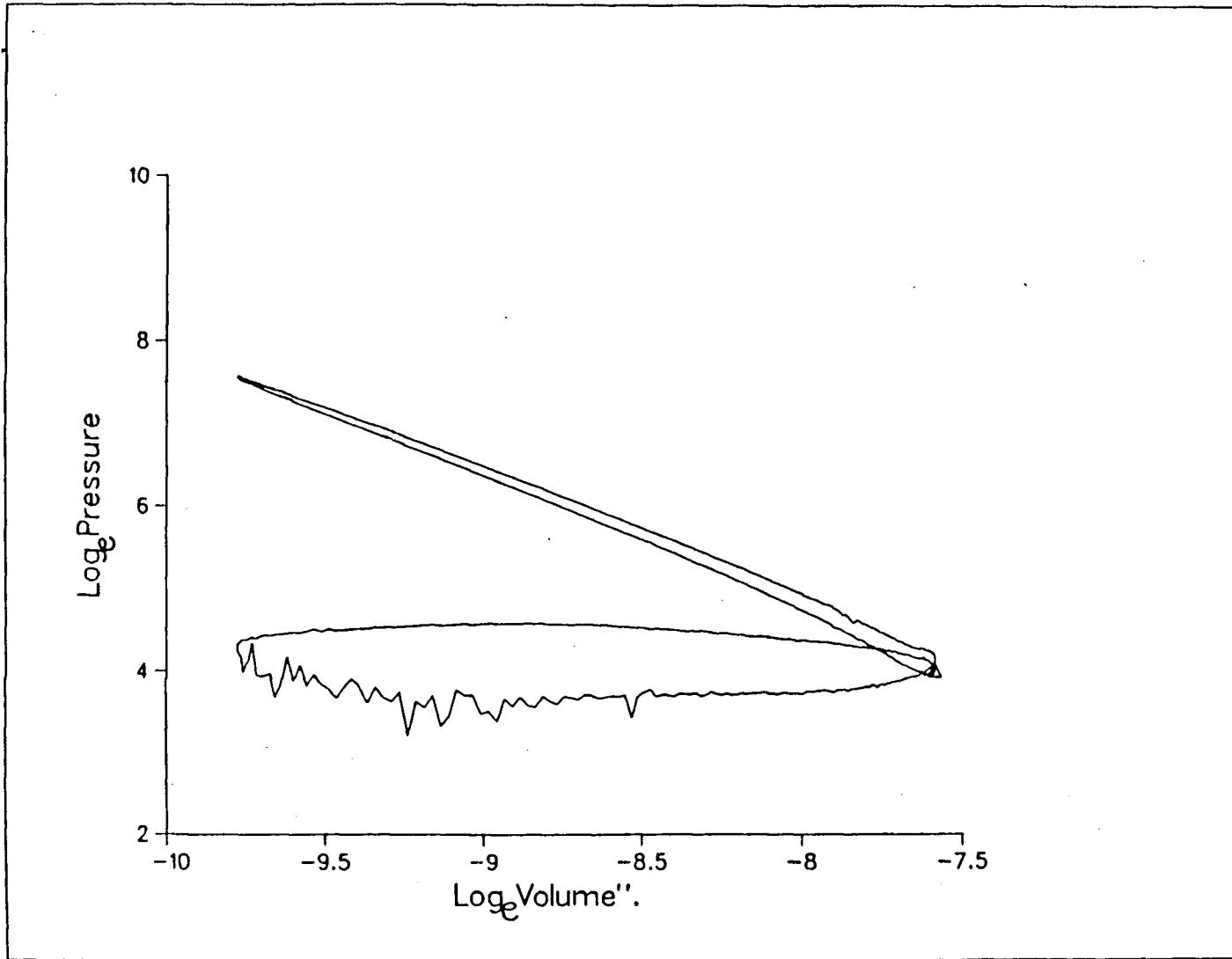


Fig 9. Indicator Diagram on Logarithmic Scale [Incorrect reference Pressure]

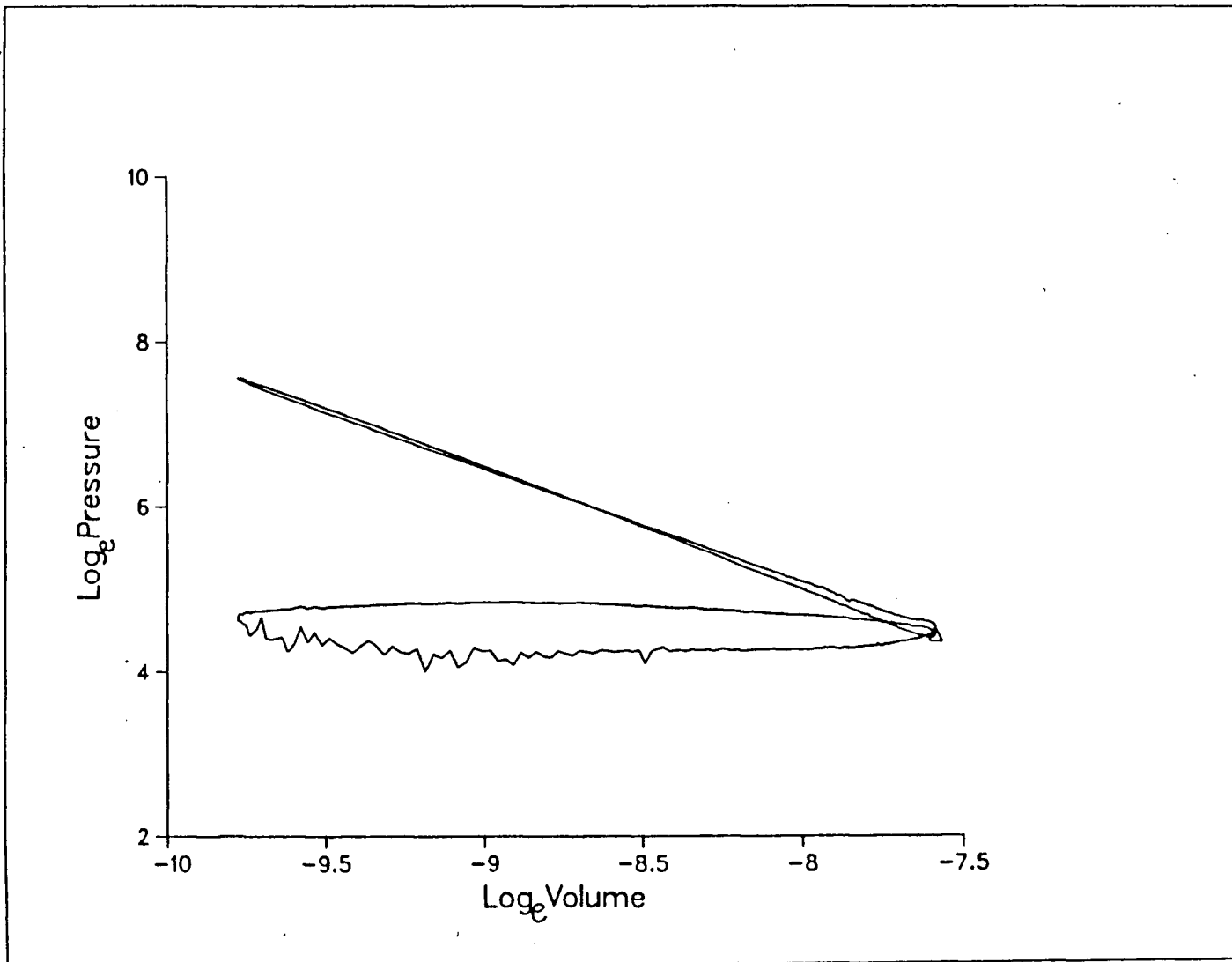


Fig 10. Indicator Diagram on Logarithmic Scale [Pressure Retarded]

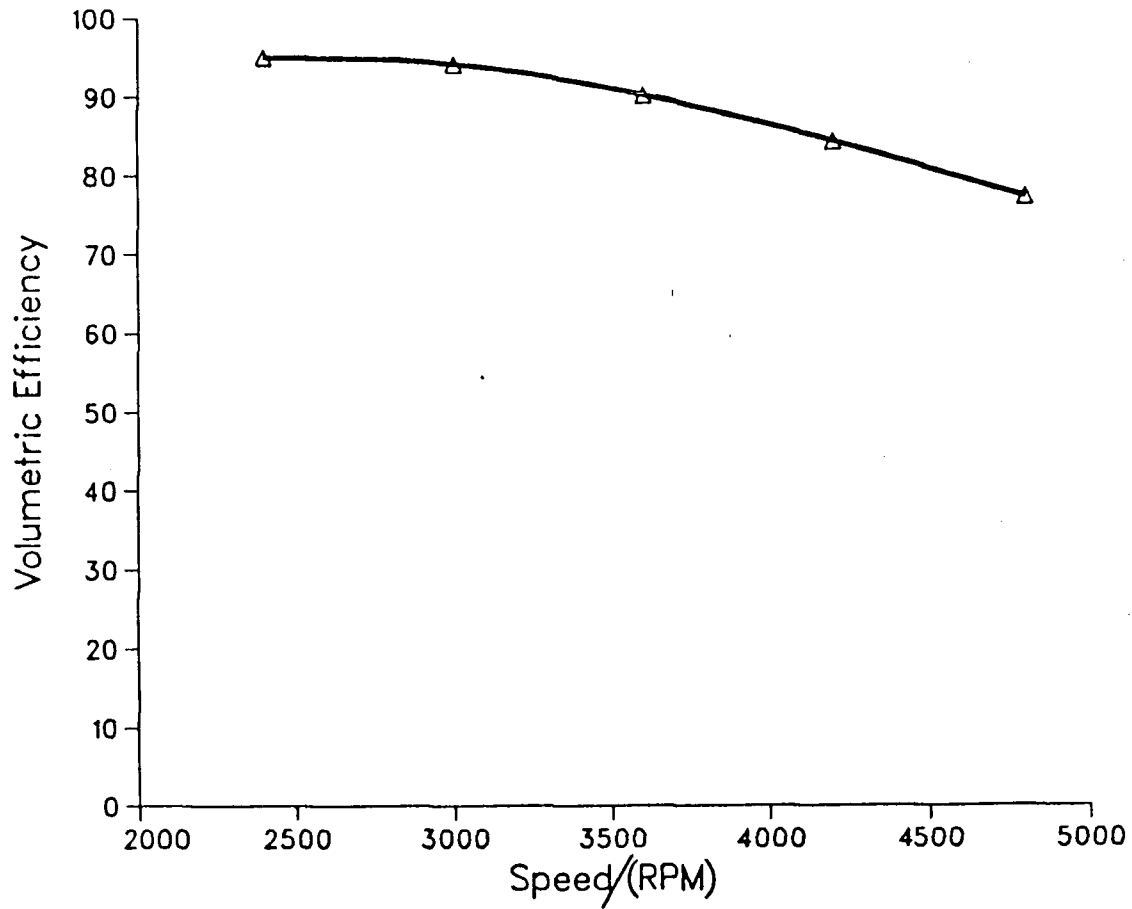


Fig 11. Volumetric Efficiency in a Motored Engine.

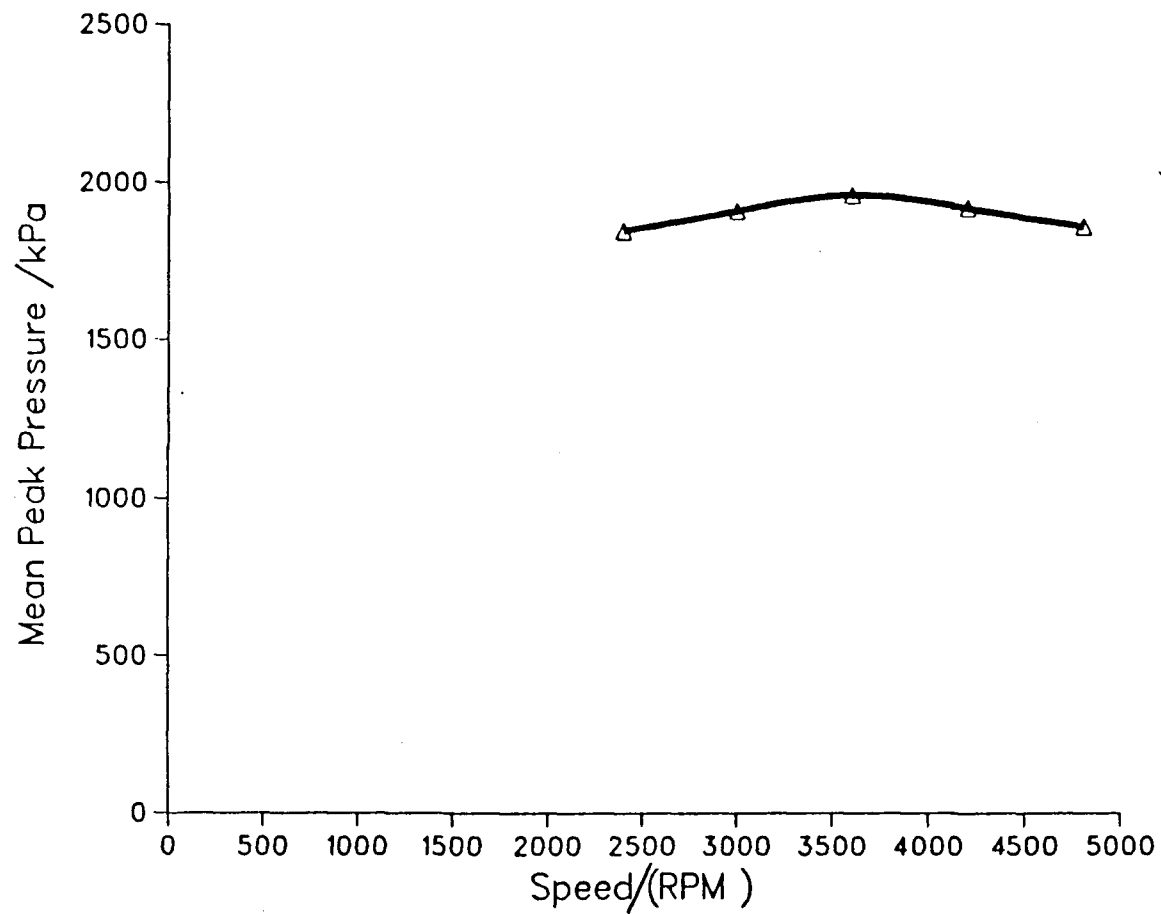


Fig 12. Ensemble-Averaged Peak Pressure in a Motored Engine.

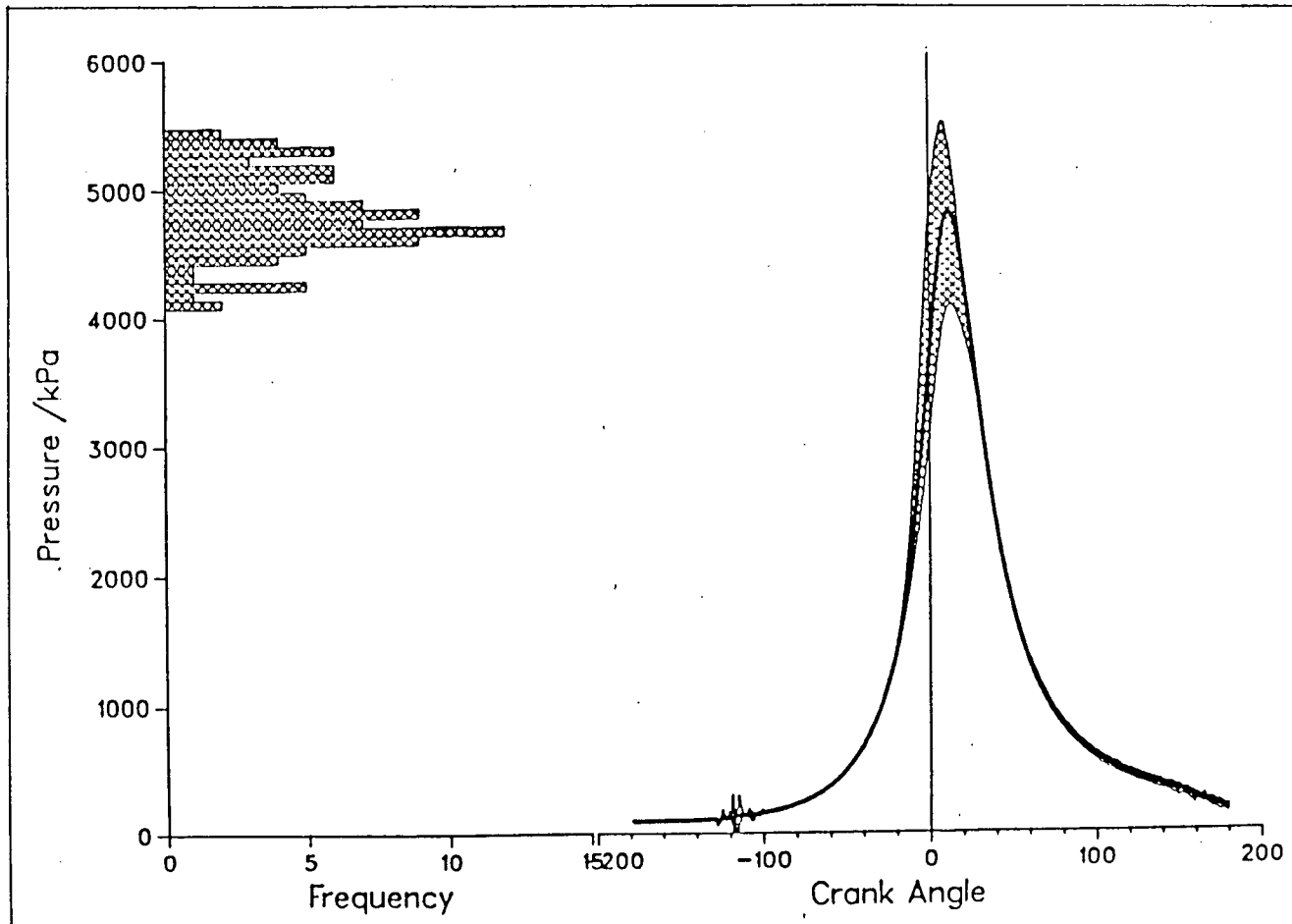


Fig 13. Typical Pressure Variations and Frequency Histogram for Peak Pressure.
 Speed - 3000 RPM, ϕ - 1.015.

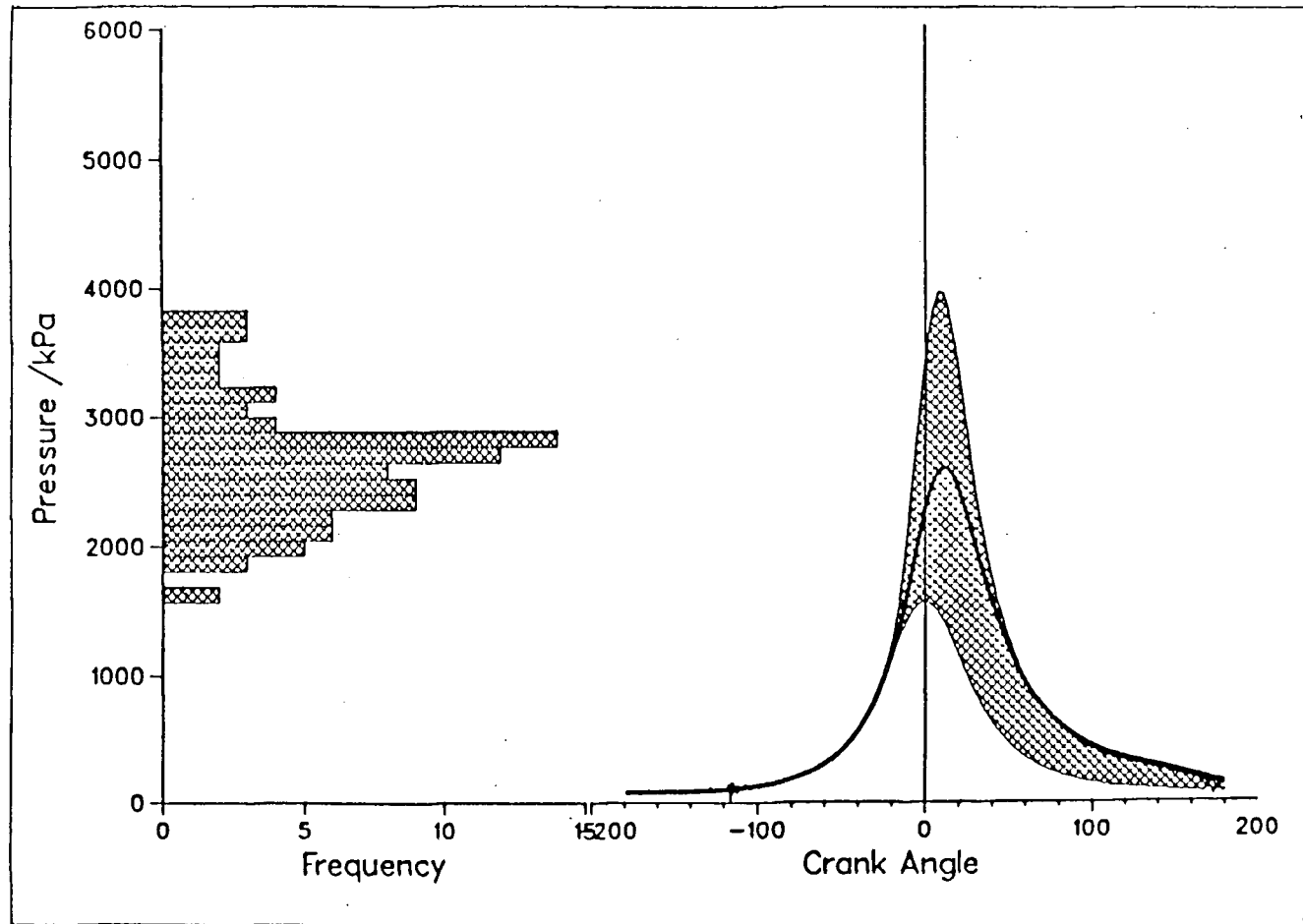


Fig 14. Typical Pressure Variations and Frequency Histogram for Peak Pressure.
 Speed - 3000 RPM, ϕ - 0.674.

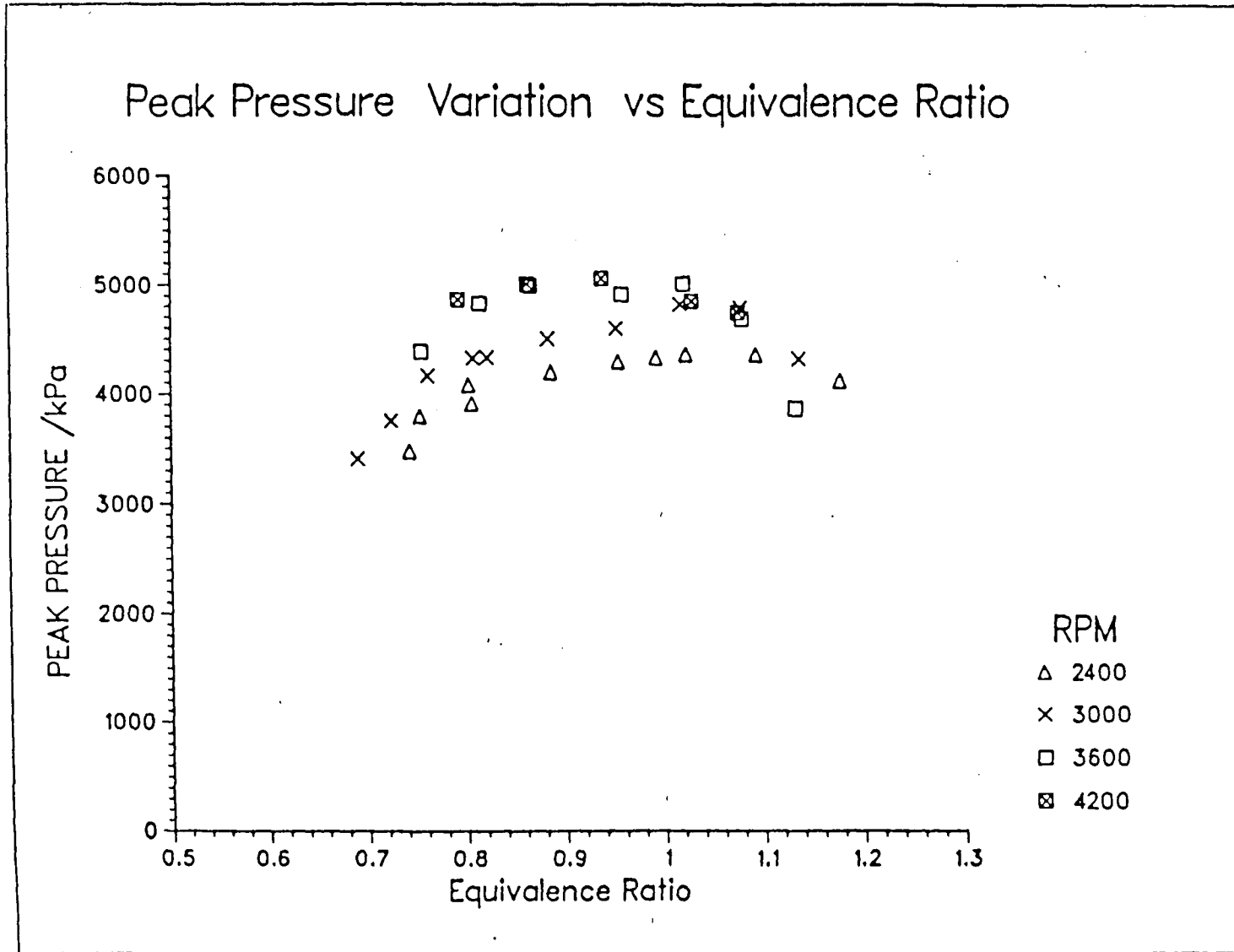


Fig 15. Ensemble-Averaged Peak Pressure Variation with Speed and Equiv. Ratio.

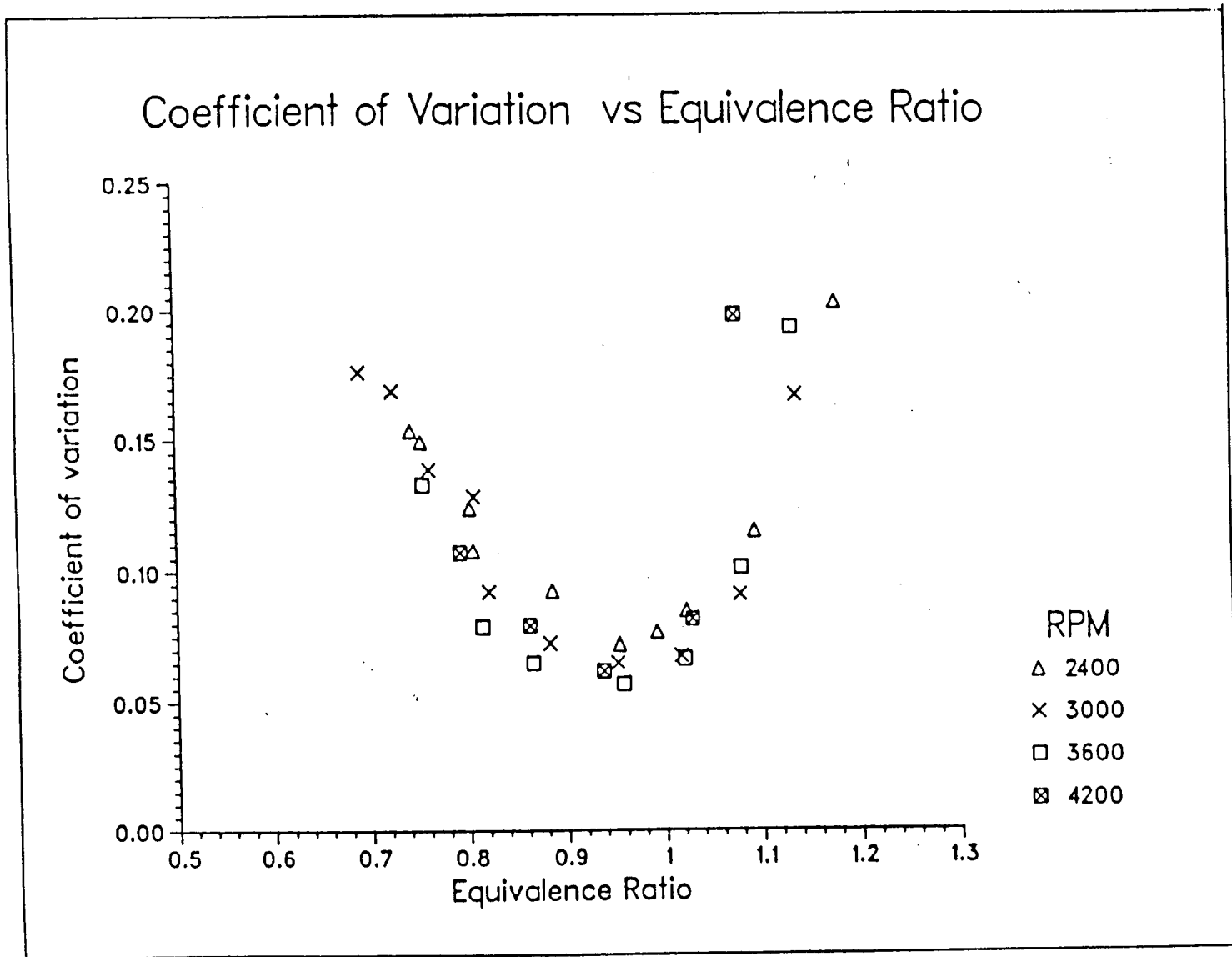


Fig 16. Coefficient of Variation for Different Speeds and Equivalence Ratios.

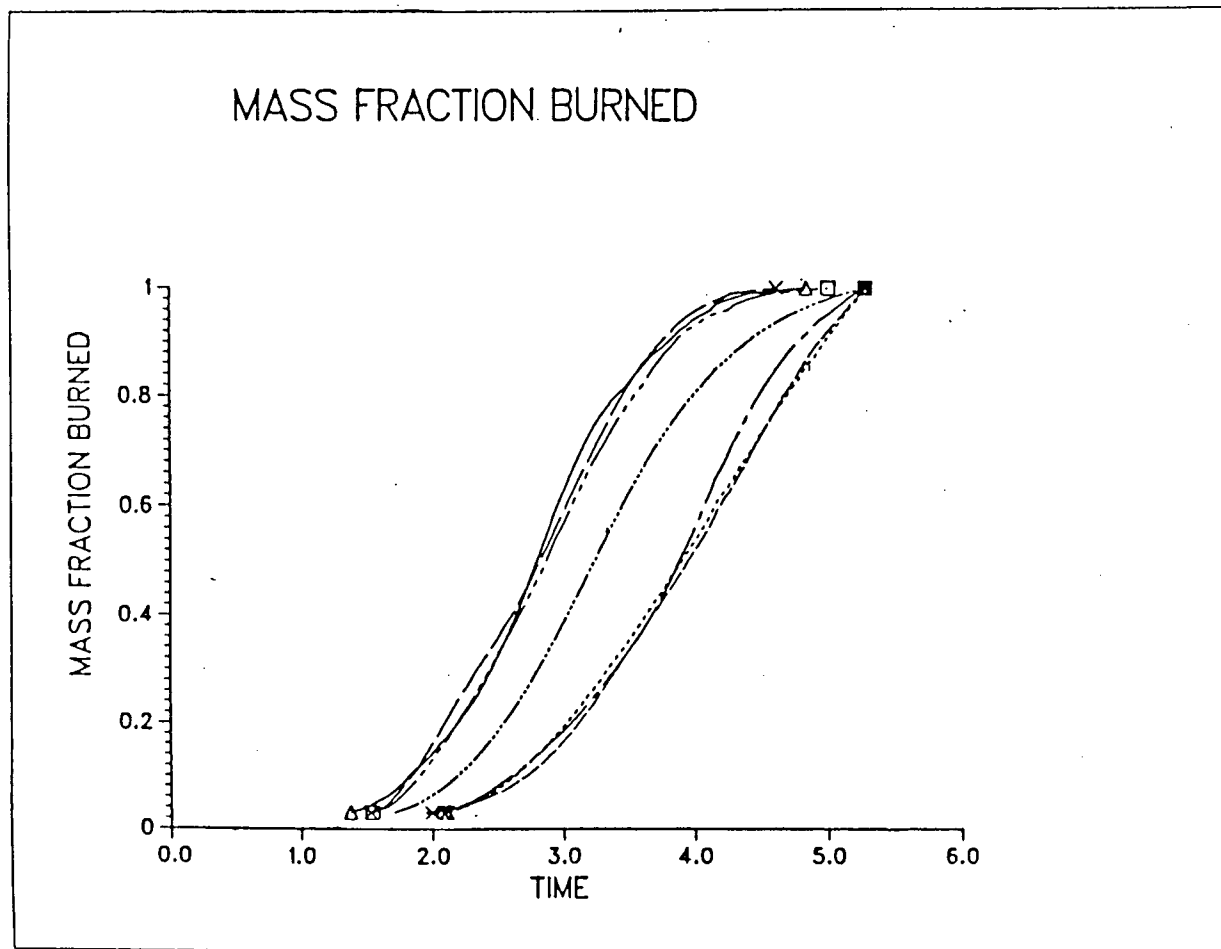


Fig 17. Typical Mass-Fraction-Burned Variation with Time, From Ignition.

N=3000 RPM. $\phi = 1.37$

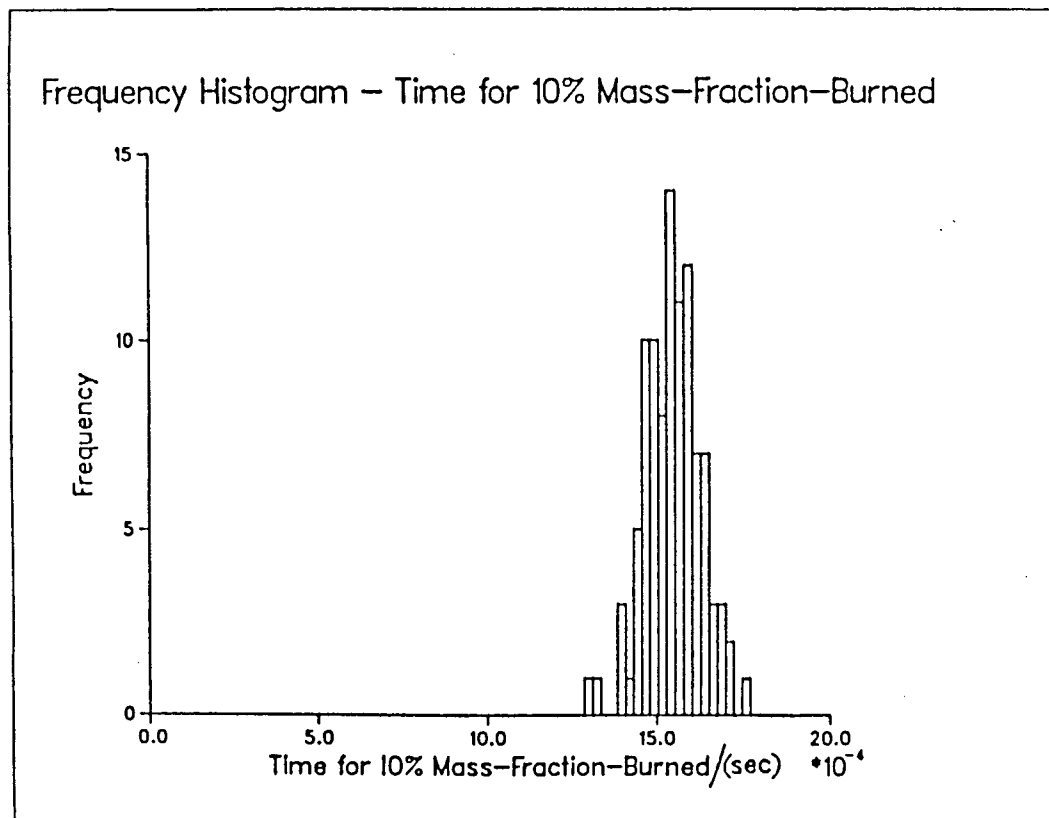


Fig 18. Typical Frequency Histogram for Burning Times
 ($X=0.10$, $N = 3000$, $\phi = 1.105$.)

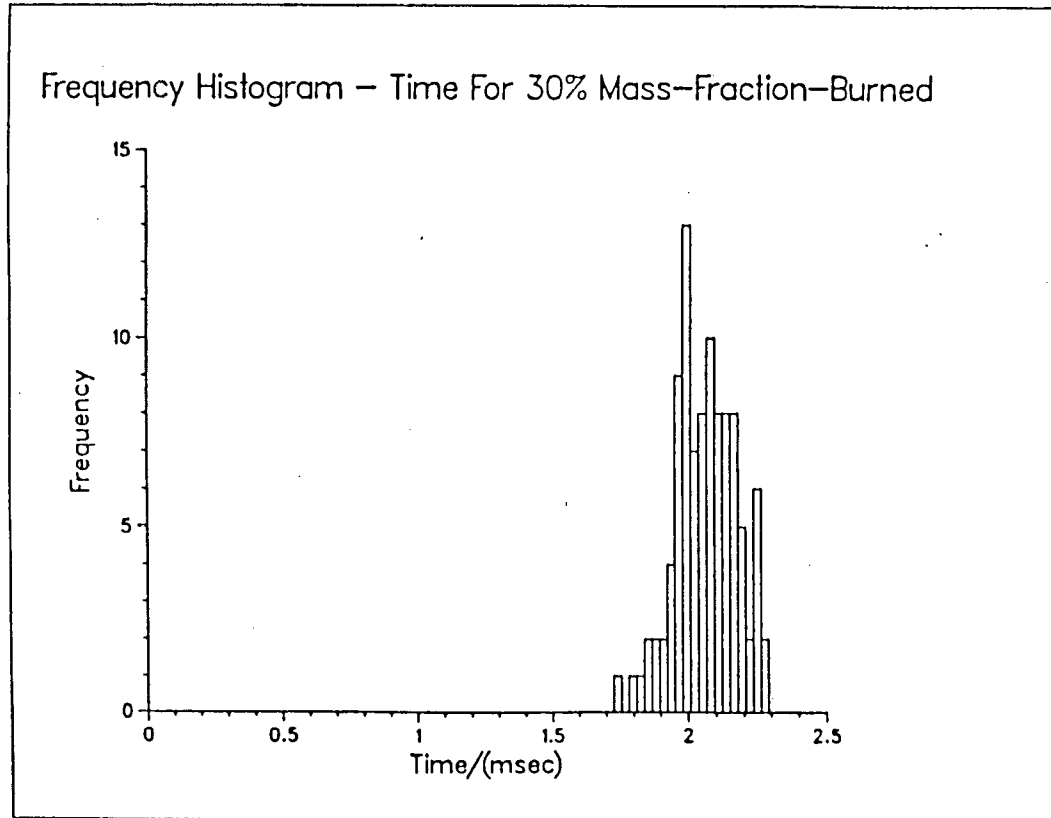


Fig 19. Typical Frequency Histogram for Burning Times
($X=0.30$, $N = 3000$ RPM. $\phi = 1.05$.)

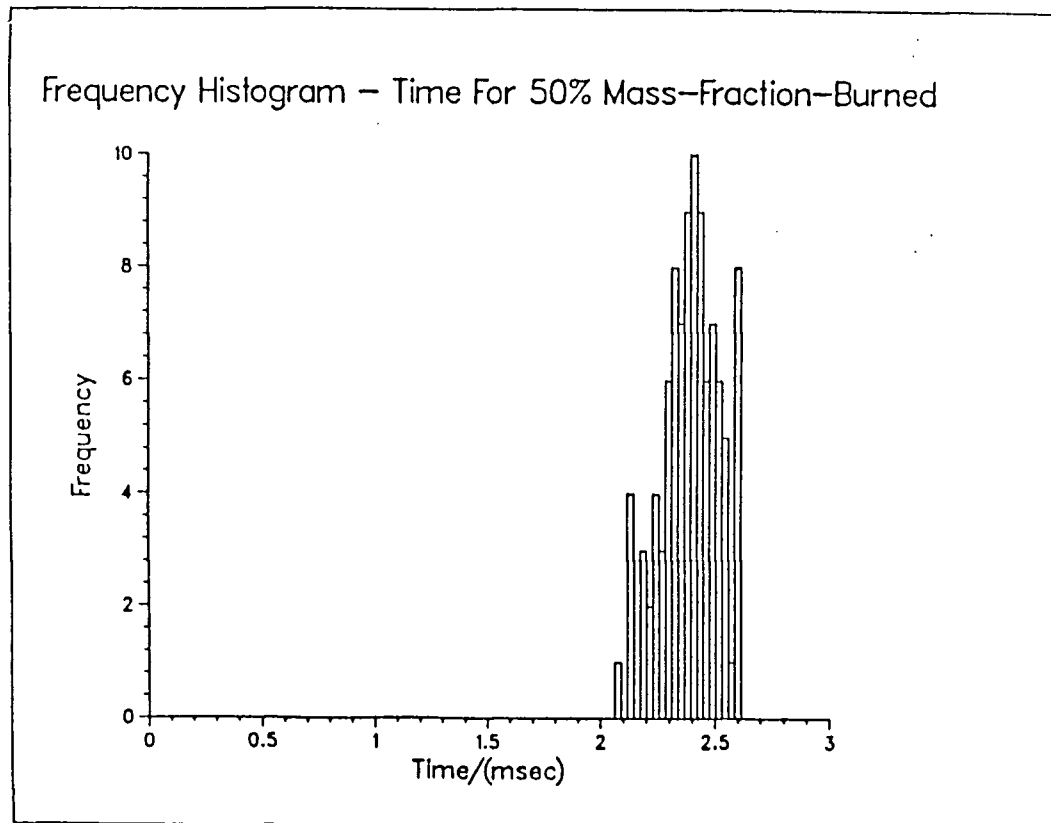


Fig 20. Typical Frequency Histogram for Burning Times
($X=0.50$, $N = 3000$ RPM. $\phi = 1.05$.)

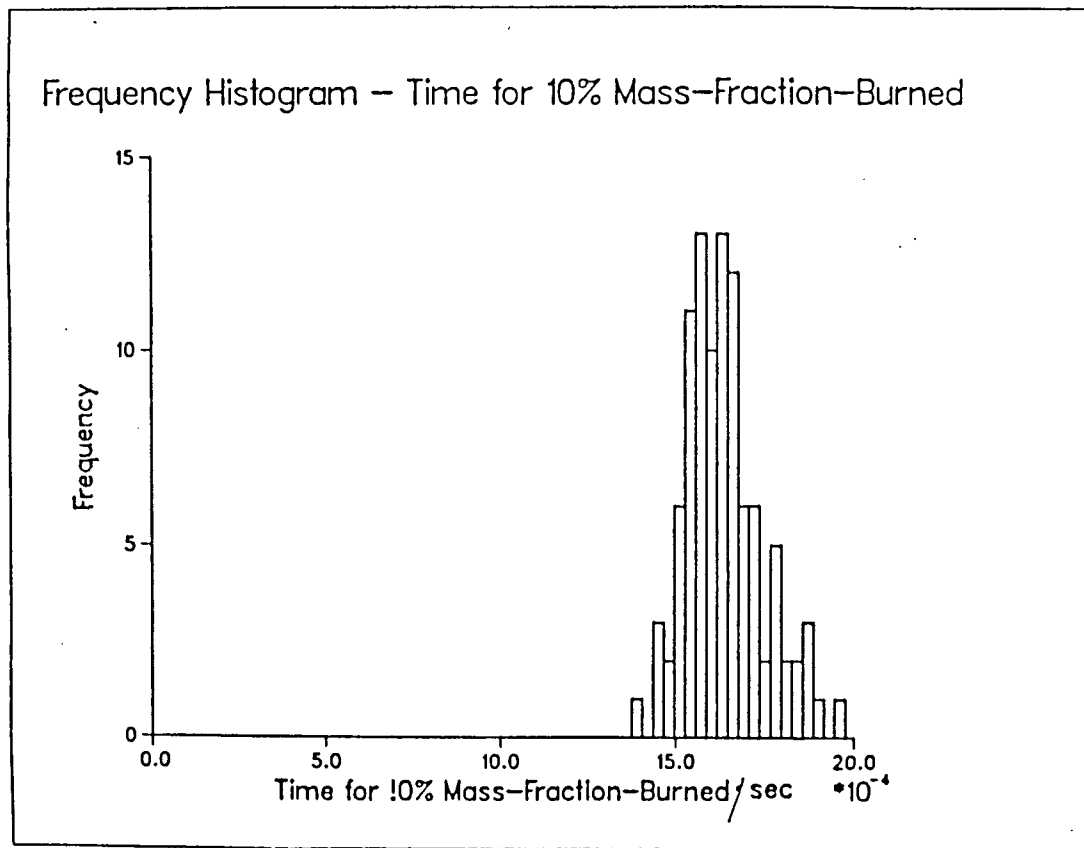


Fig 21. Typical Frequency Histogram for Burning Times
 (X=0.10, N = 3000 RPM. ϕ = 1.22.)

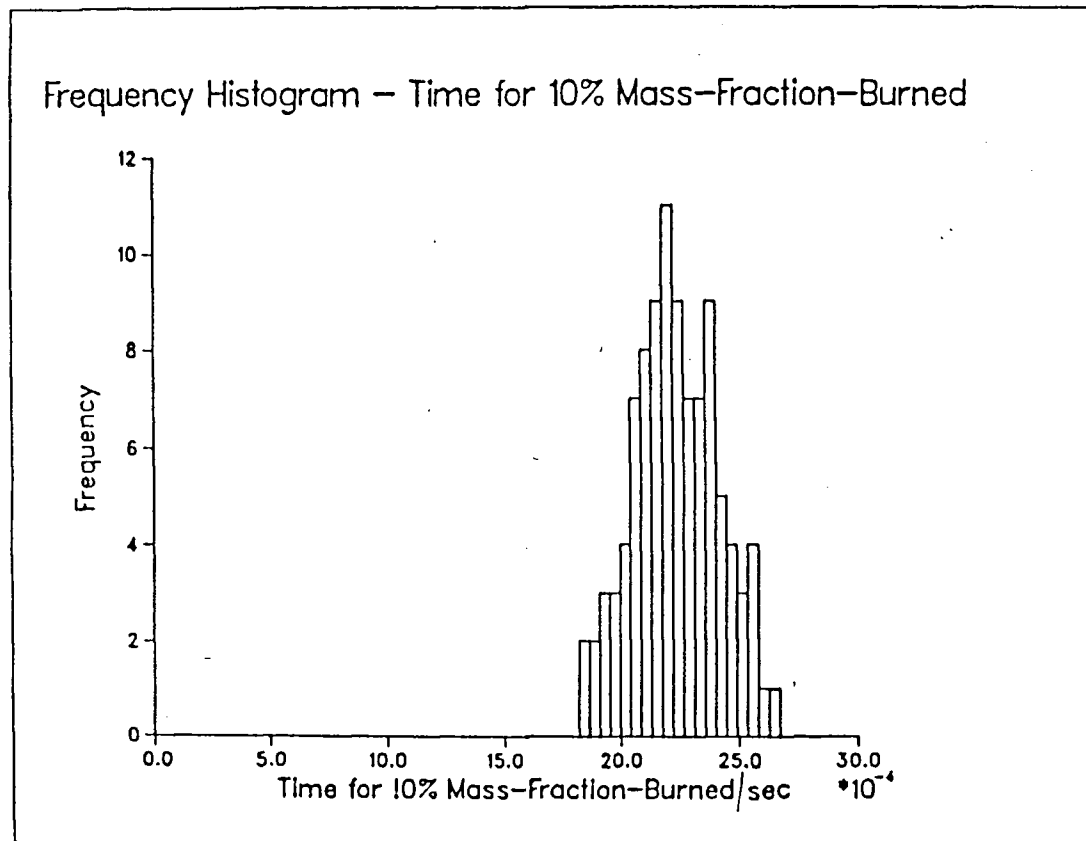


Fig 22. Typical Frequency Histogram for Burning Times
 (X=0.10, N = 3000 RPM. ϕ = 1.38.)

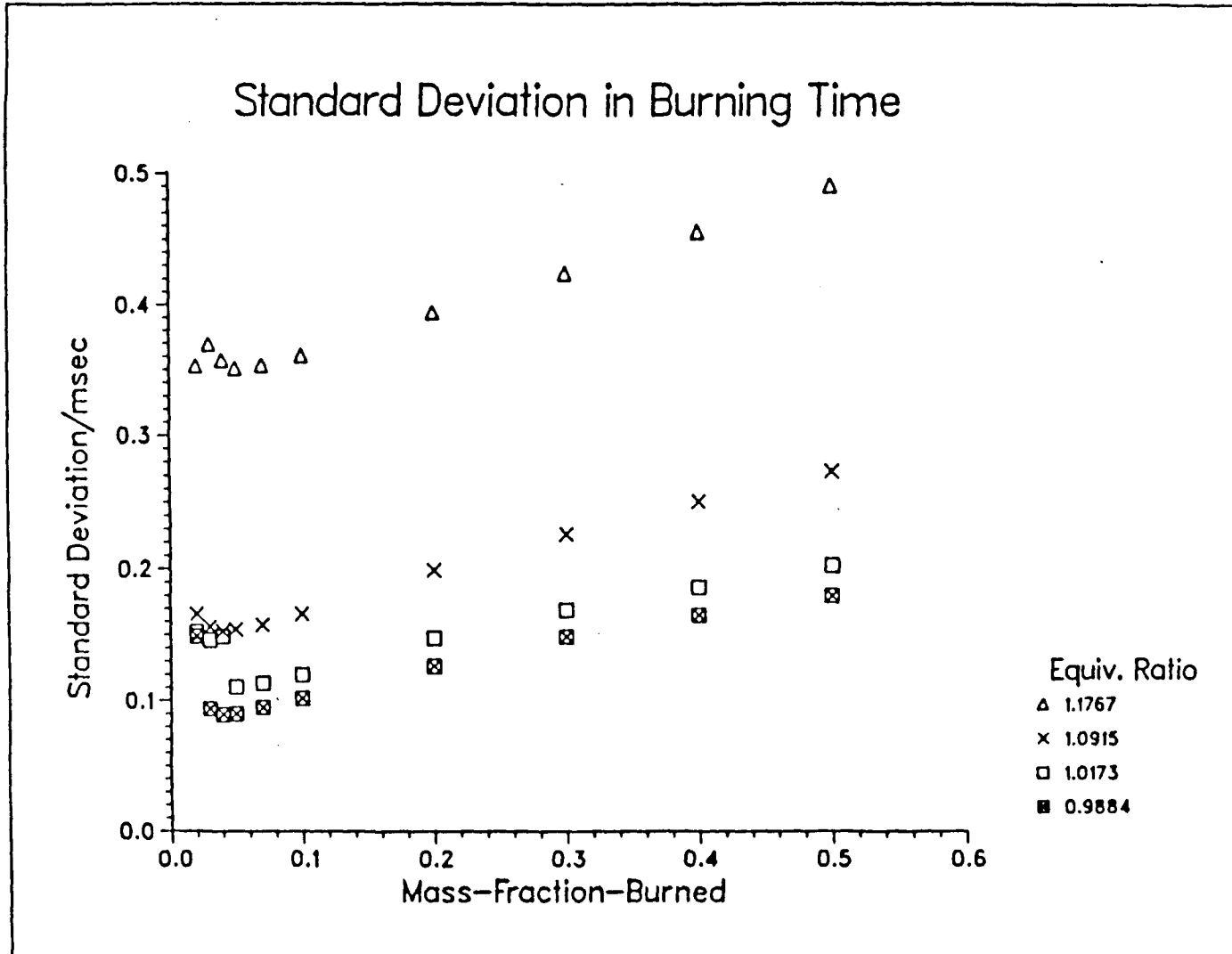


Fig 23. Standard Deviation in Burning Time. N = 2400 RPM. (Bath Tub Chamber).

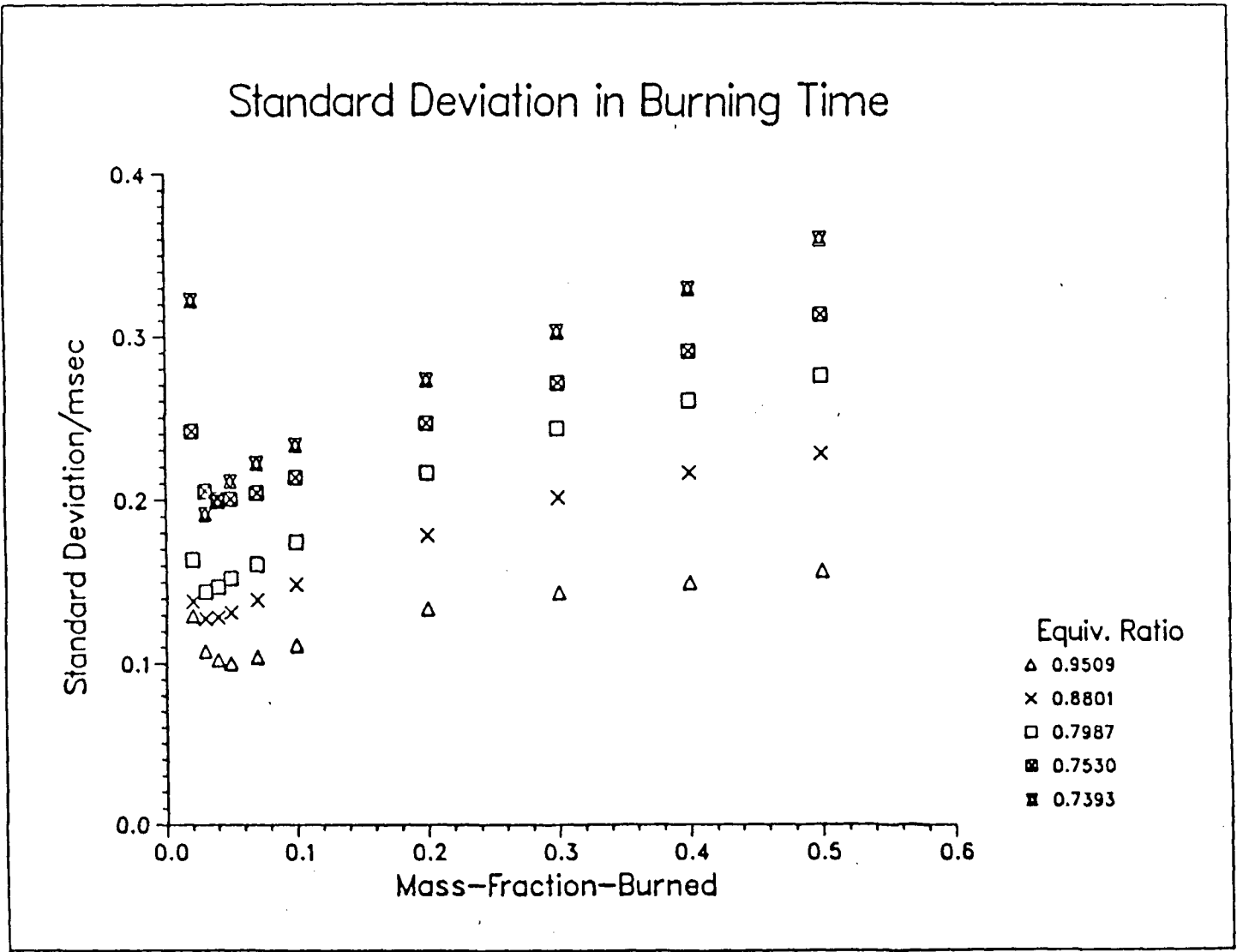


Fig 24. Standard Deviation in Burning Time. N = 2400 RPM. (Bath Tub Chamber).

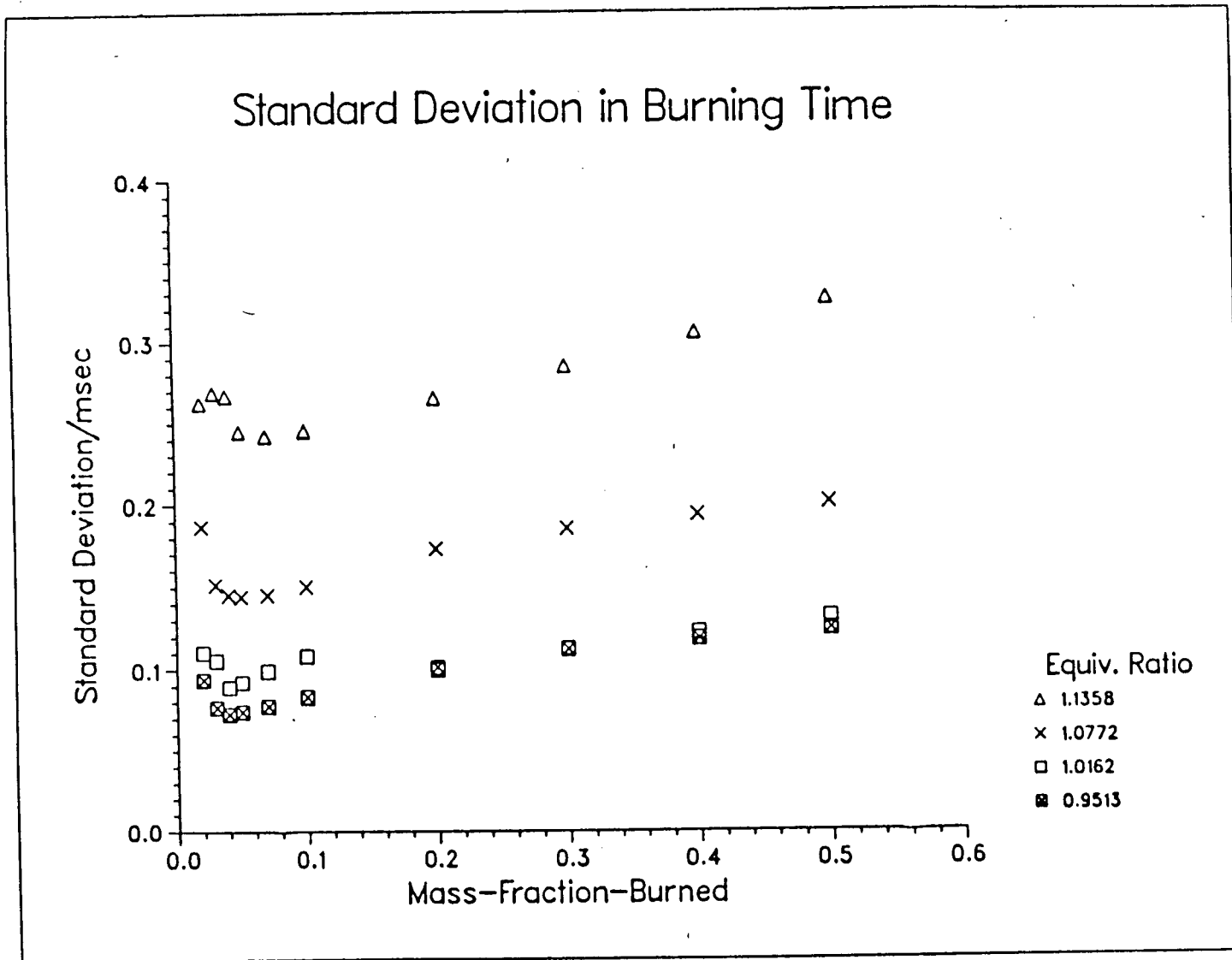


Fig 25. Standard Deviation in Burning Time. N = 3000 RPM. (Bath Tub Chamber).

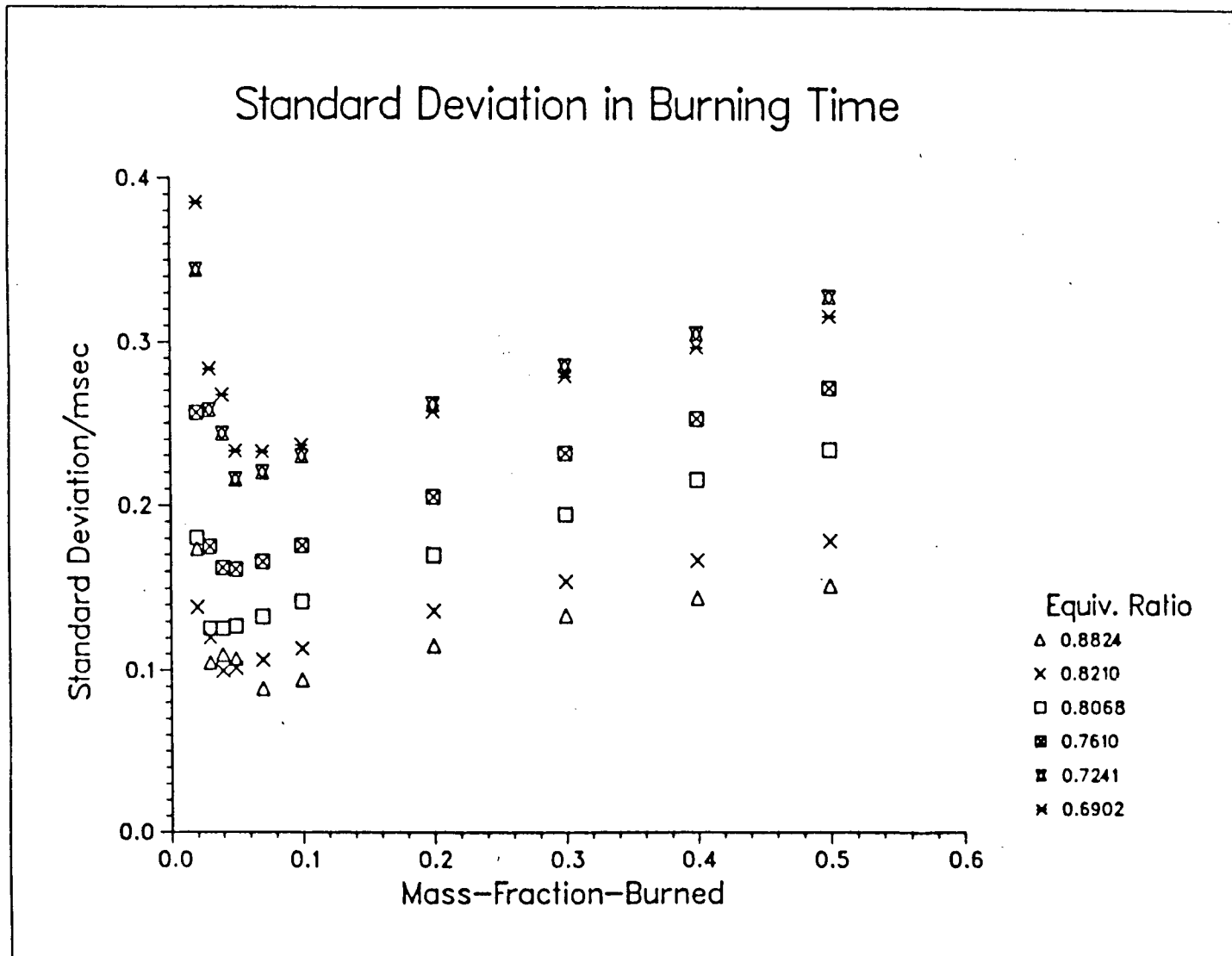


Fig 26. Standard Deviation in Burning Time. N = 3000 RPM. (Bath Tub Chamber).

Standard Deviation in Burning Time

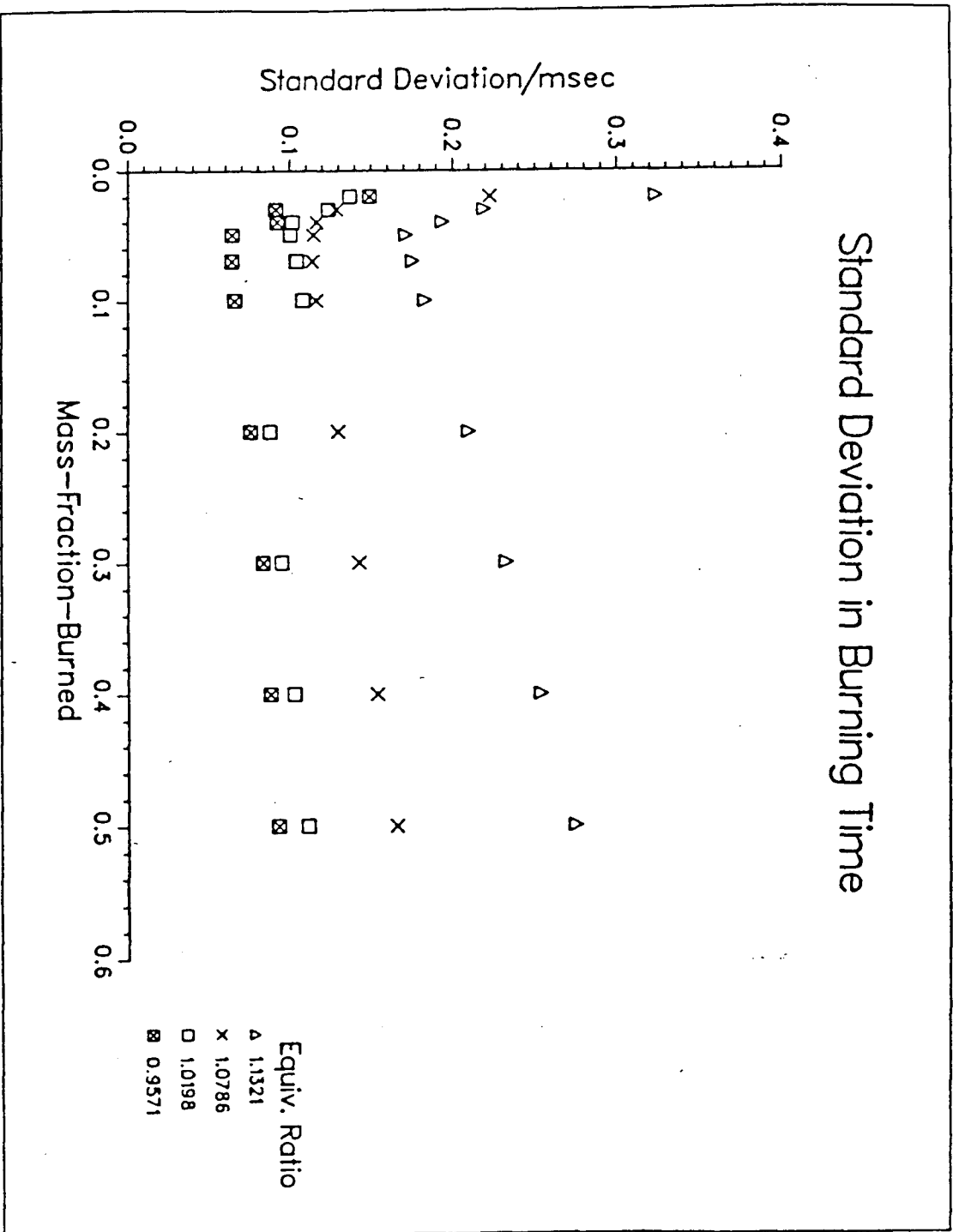


Fig 27. Standard Deviation in Burning Time. N = 3600 RPM. (Bath Tub Chamber).

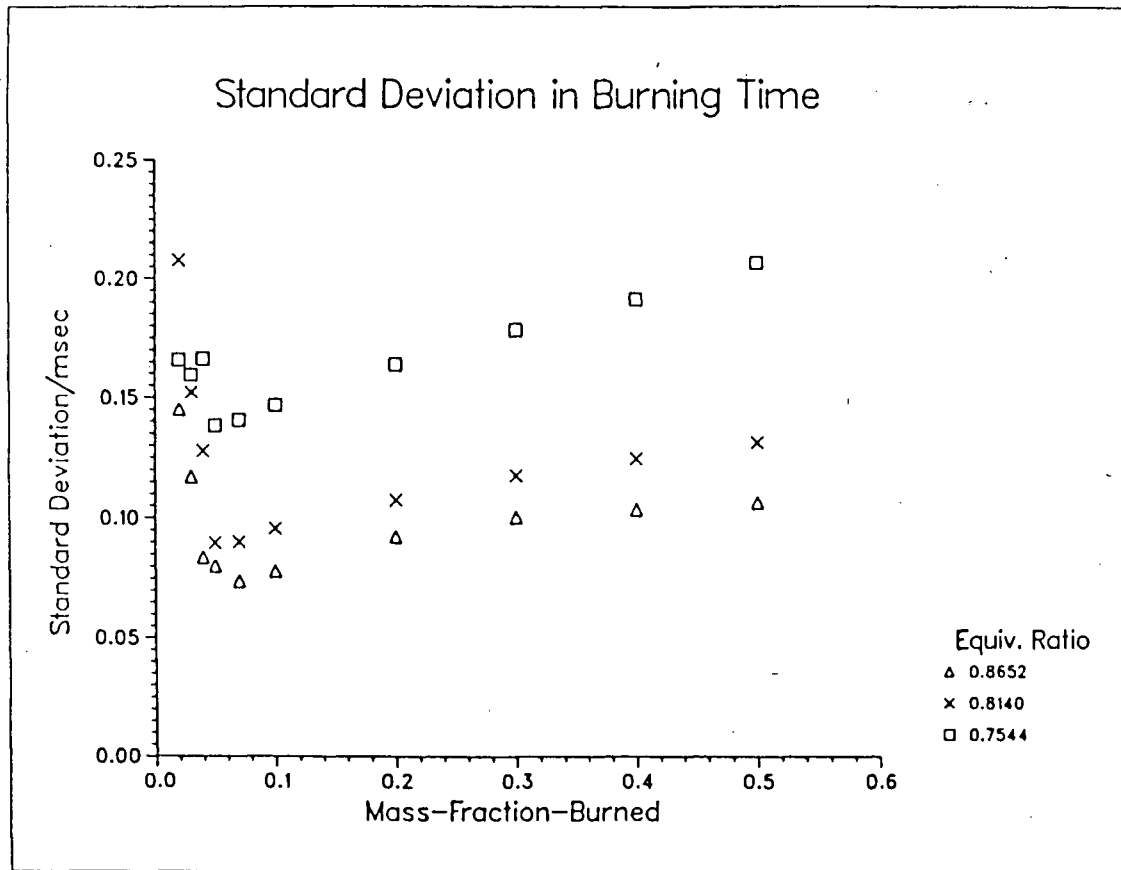


Fig 28. Standard Deviation in Burning Time. N = 3600 RPM. (Bath Tub Chamber).

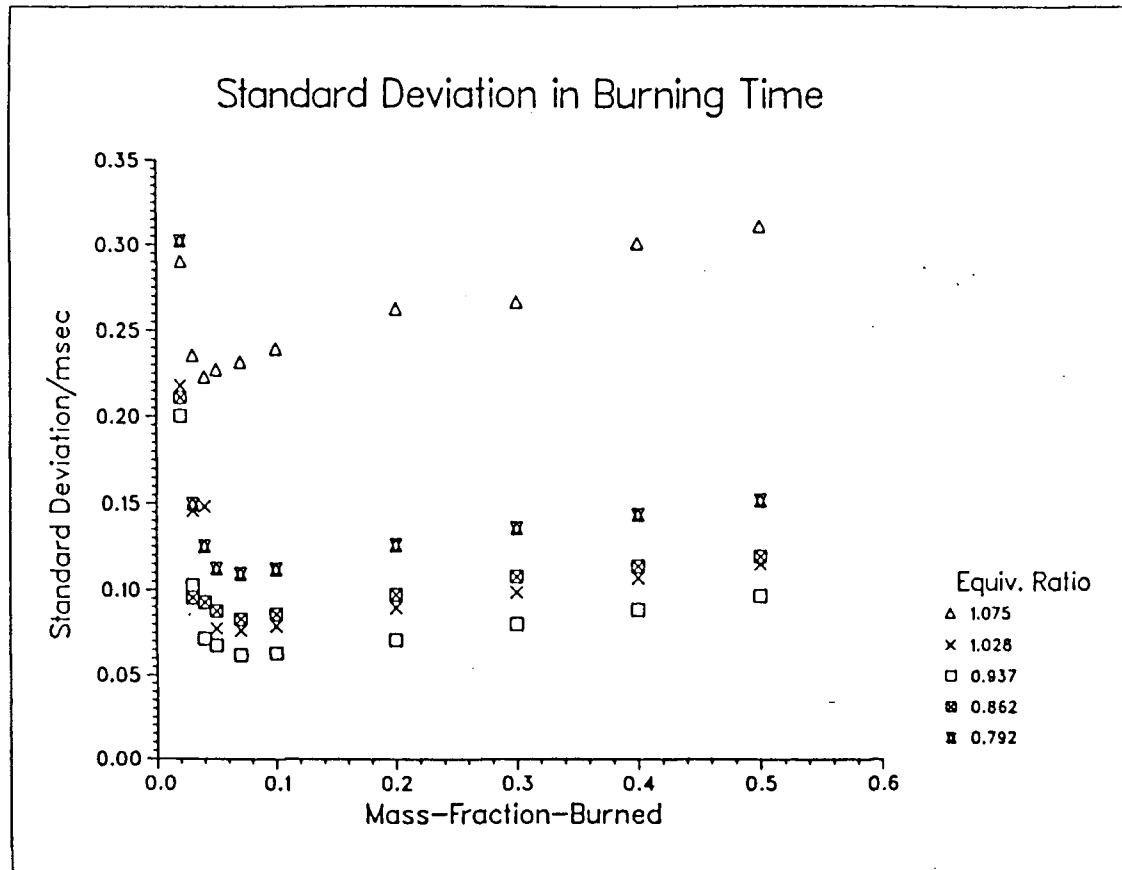


Fig 29. Standard Deviation in Burning Time. N = 4200 RPM. (Bath Tub Chamber).

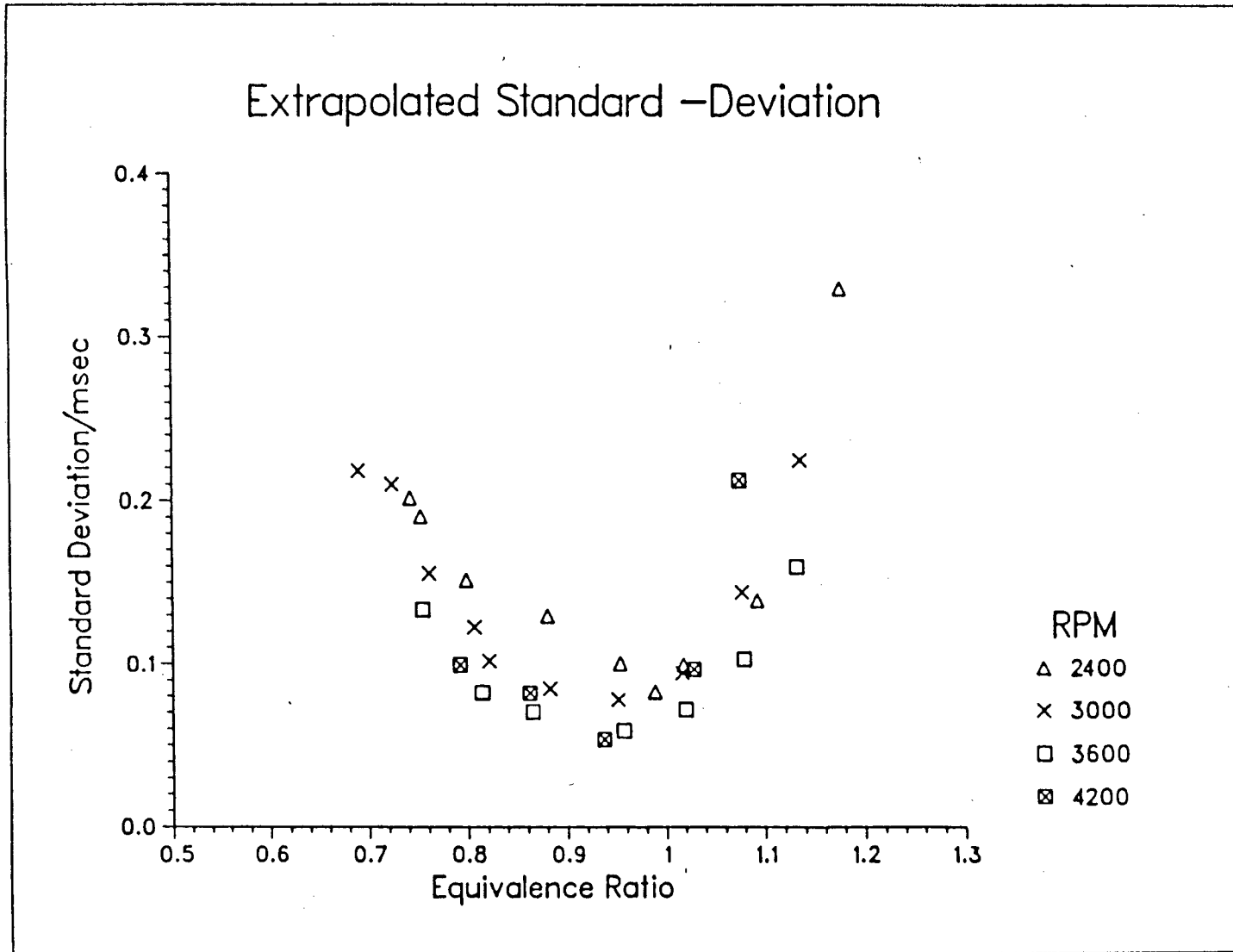


Fig 30. Extrapolated Standard Deviation in Early Burning Time.

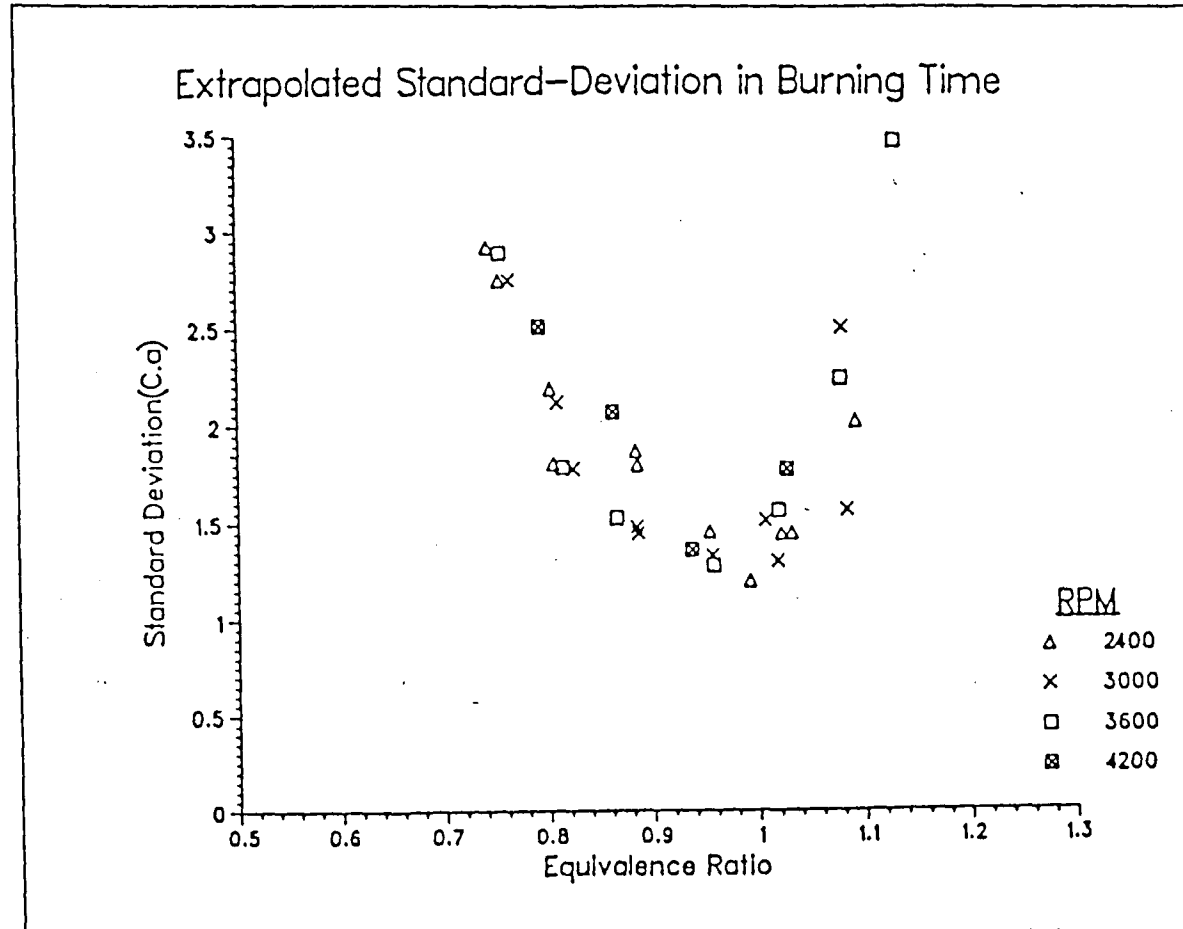


Fig 31. Extrapolated Standard Deviation in Early Burning Crank Angle Interval

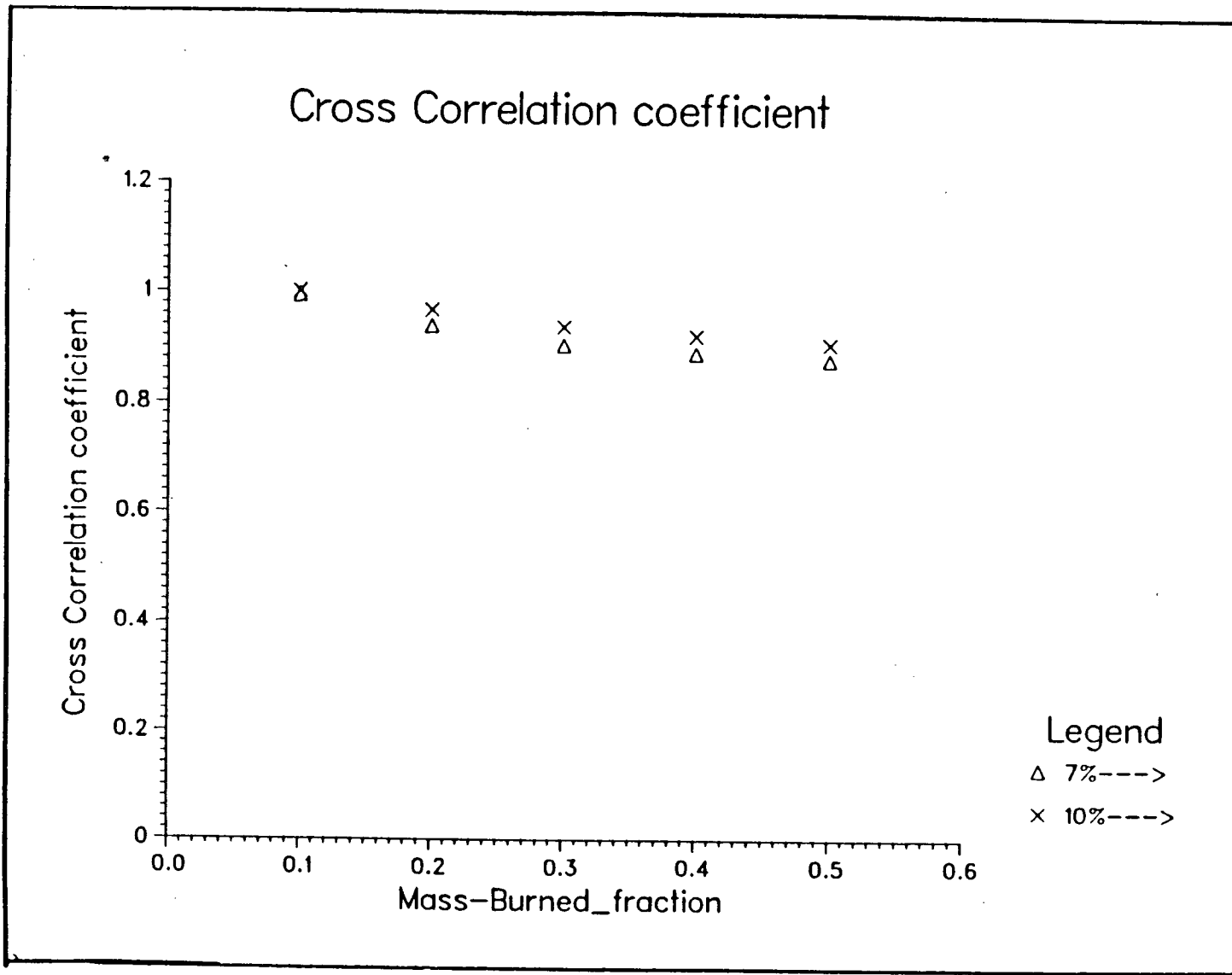


Fig 32. Cross Correlation Coefficient Of Standard Deviation In Burning Time.

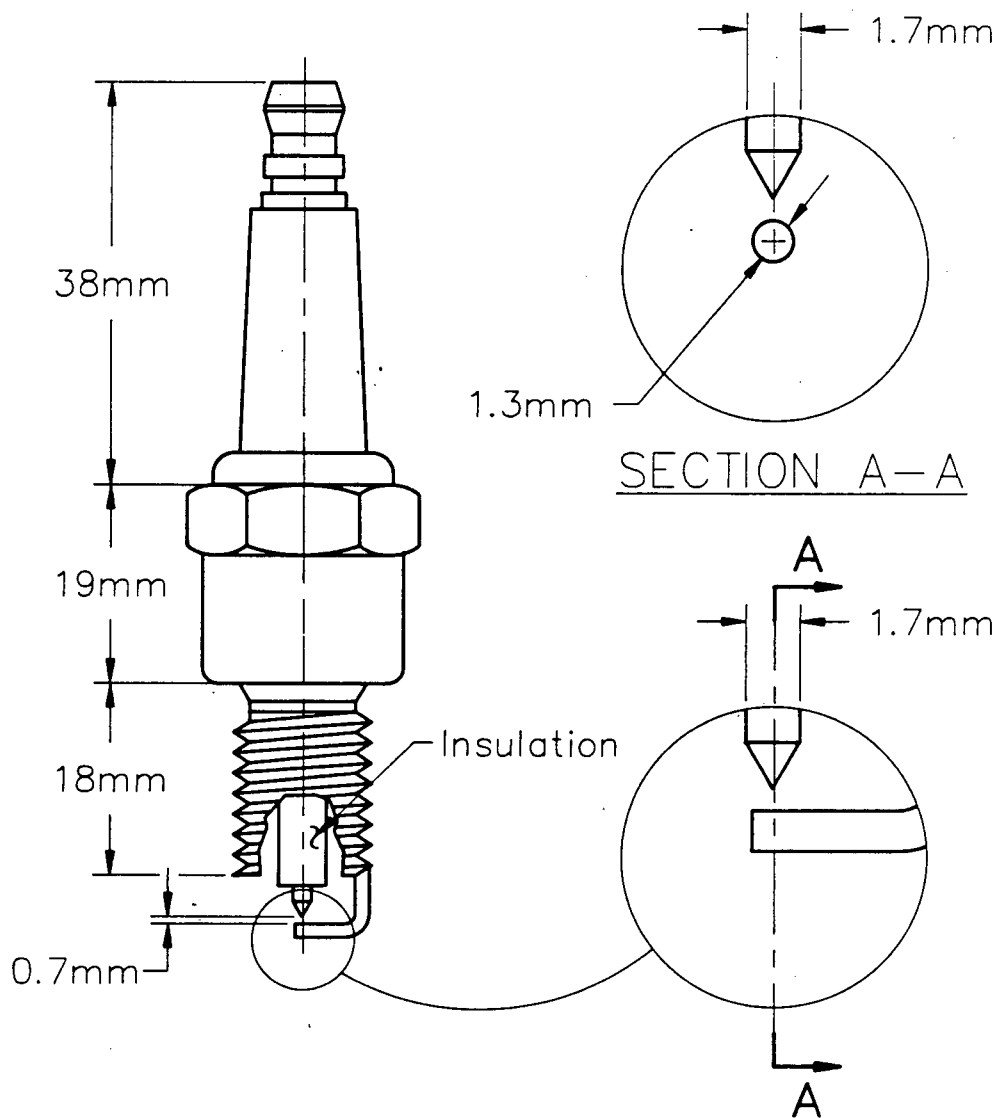


FIG 33. Modified Spark Plug with Fine Point Electrodes
Spark Plug Gap 0.7mm.

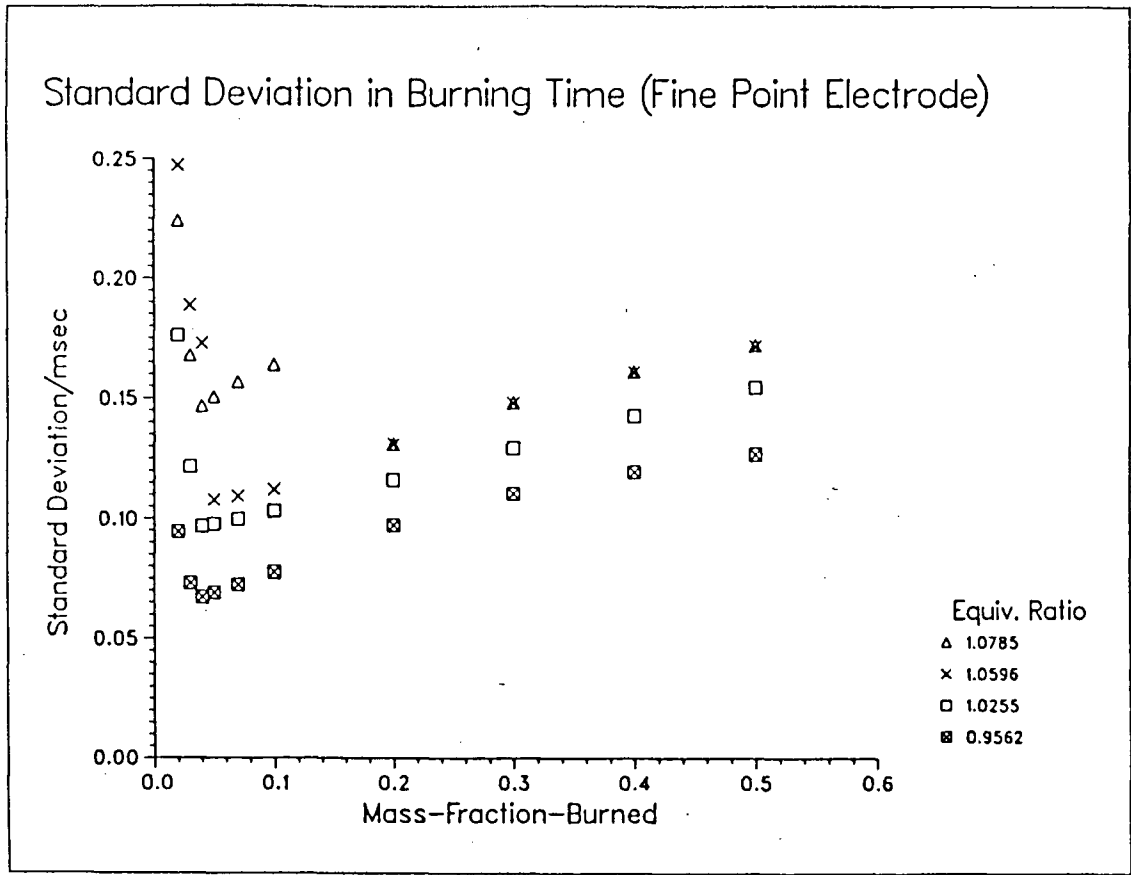


Fig 34. Standard Deviation in Burning Time. N = 3000 RPM.
(Needle Point Electrode Geometry).

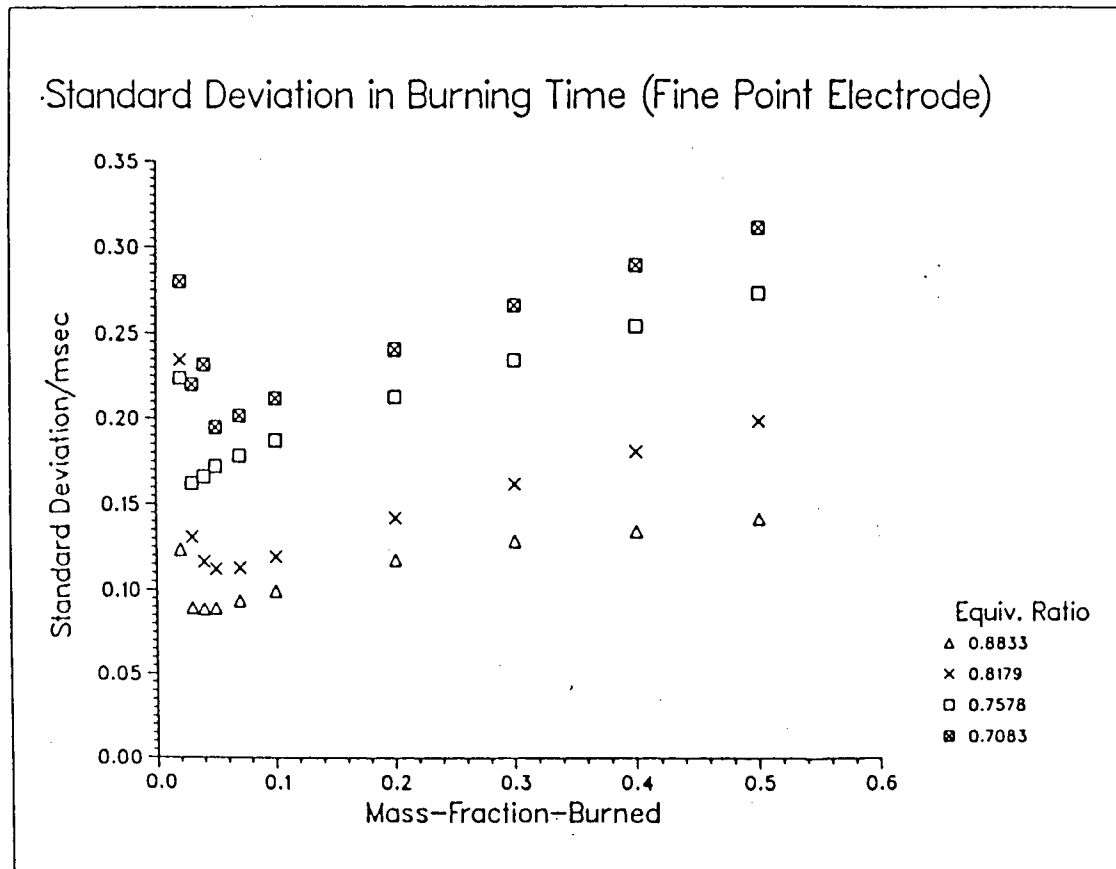


Fig 35. Standard Deviation in Burning Time. N = 3000 RPM.
(Needle Point Electrode Geometry).

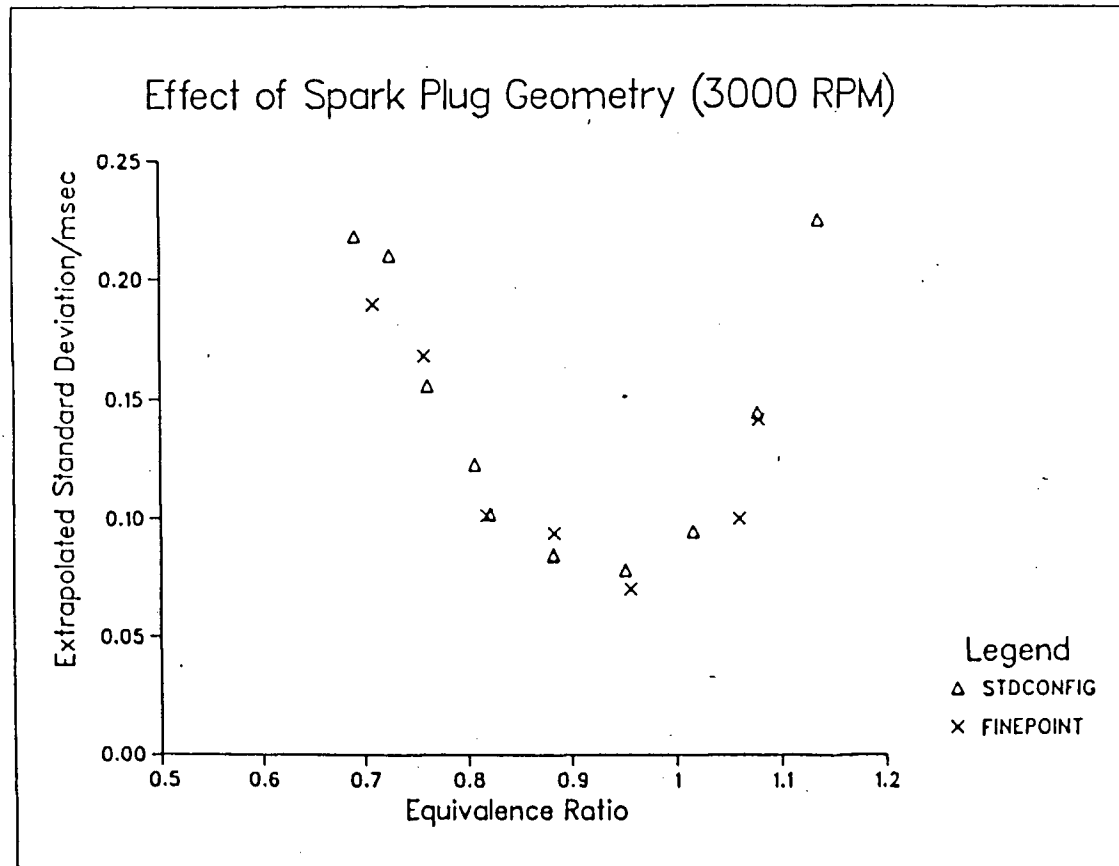


Fig 36. Extrapolated Standard Deviation in Early Burning Time.
 Different Electrode Geometries N = 3000 RPM.

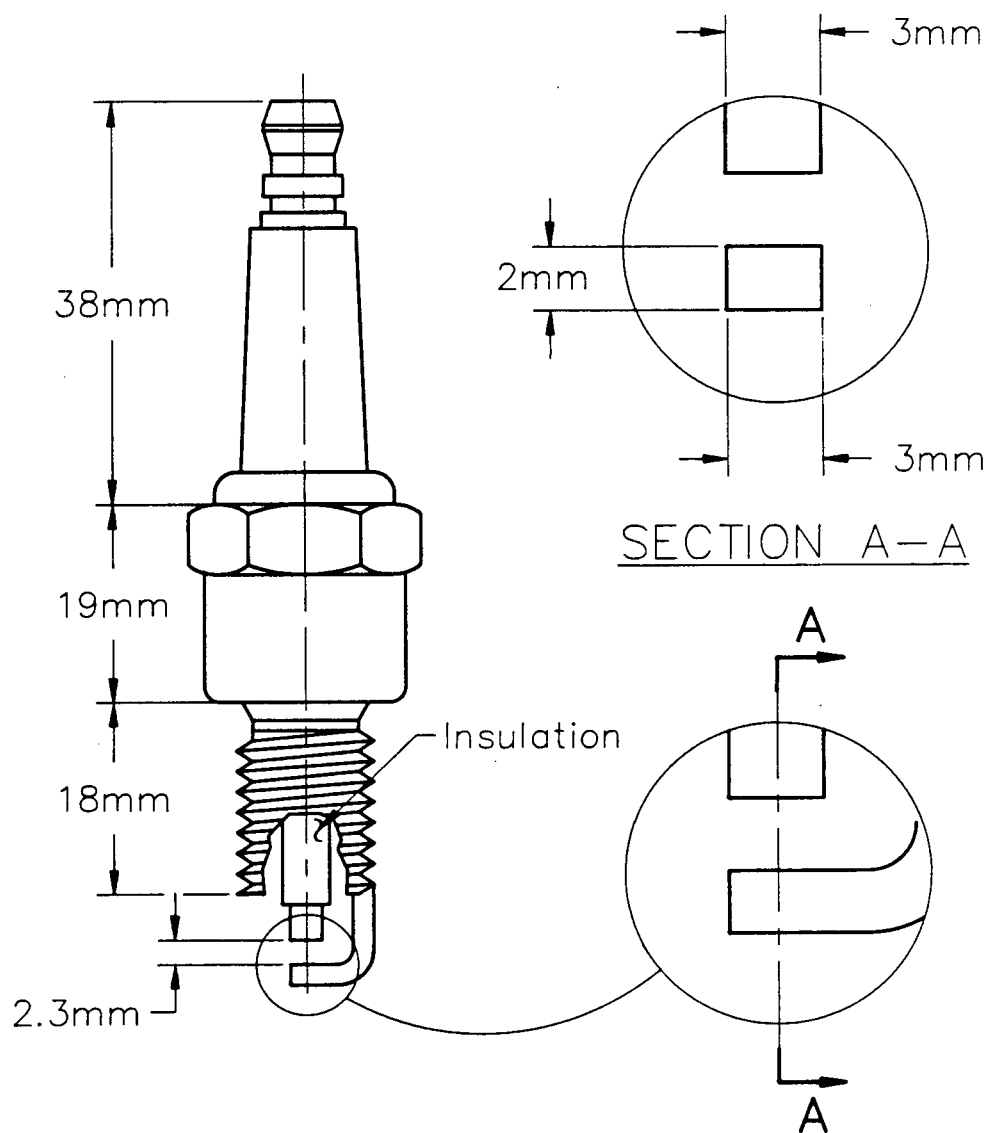


FIG 37. Modified Spark Plug with Wide Gap Electrodes
Spark Plug Gap 2.3mm.

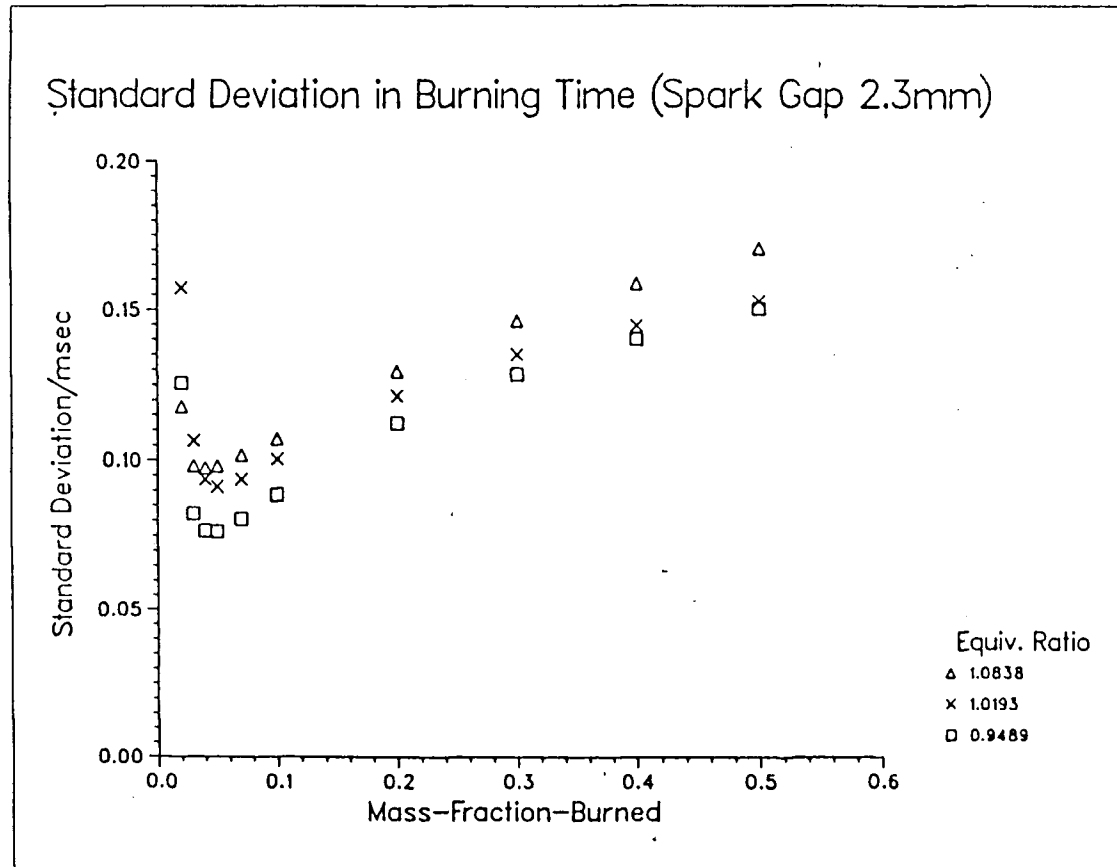


Fig 38. Standard Deviation in Burning Time. N = 3000 RPM.
(Spark Plug Gap = 2.3 mm)

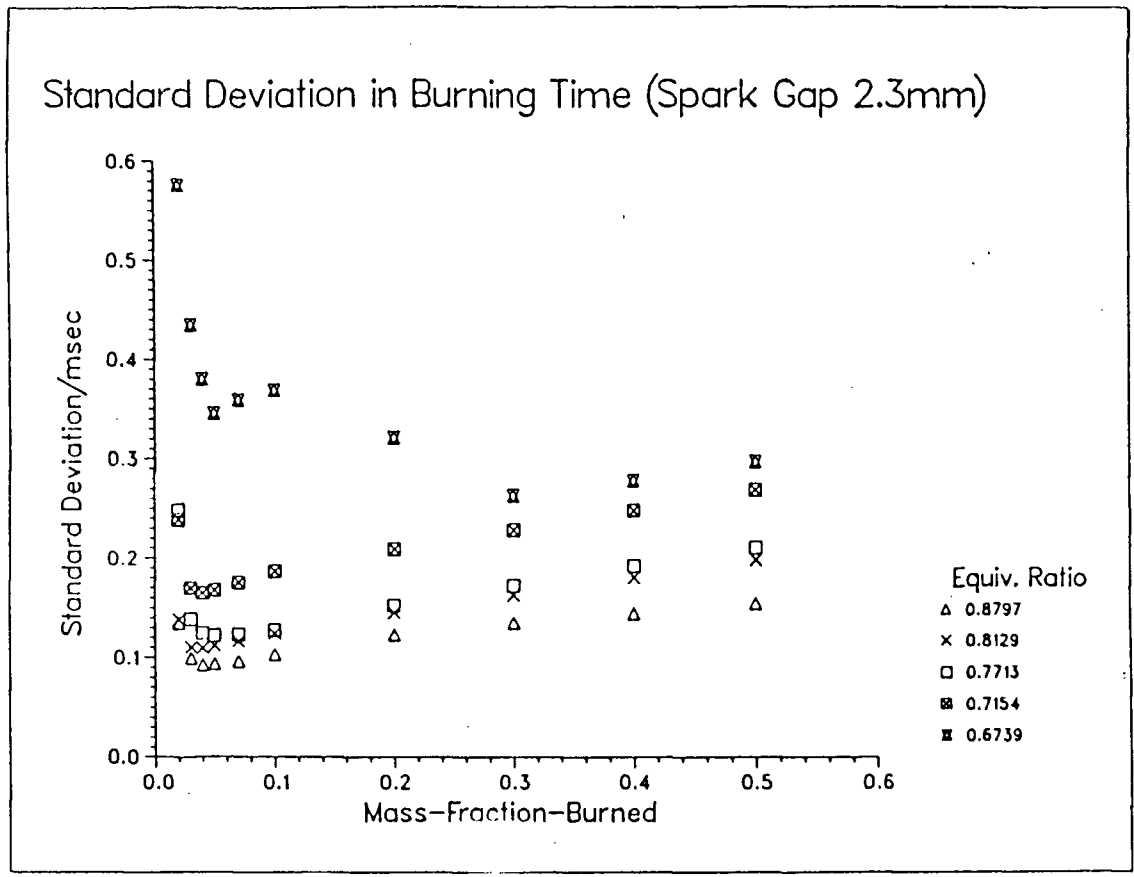


Fig 39. Standard Deviation in Burning Time. N = 3000 RPM.
 (Spark Plug Gap - 2.3 mm)

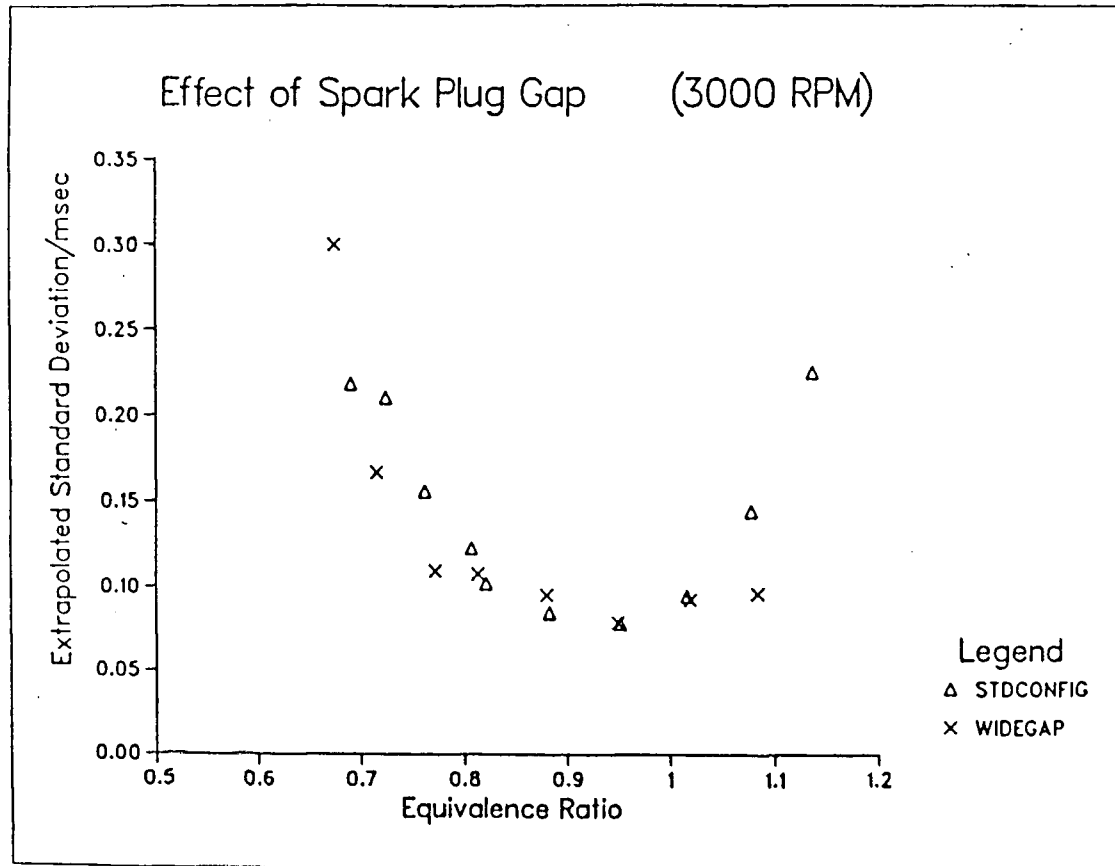


Fig 40. Extrapolated Standard Deviation in Early Burning Time.
 Different Spark Gaps N = 3000 RPM.

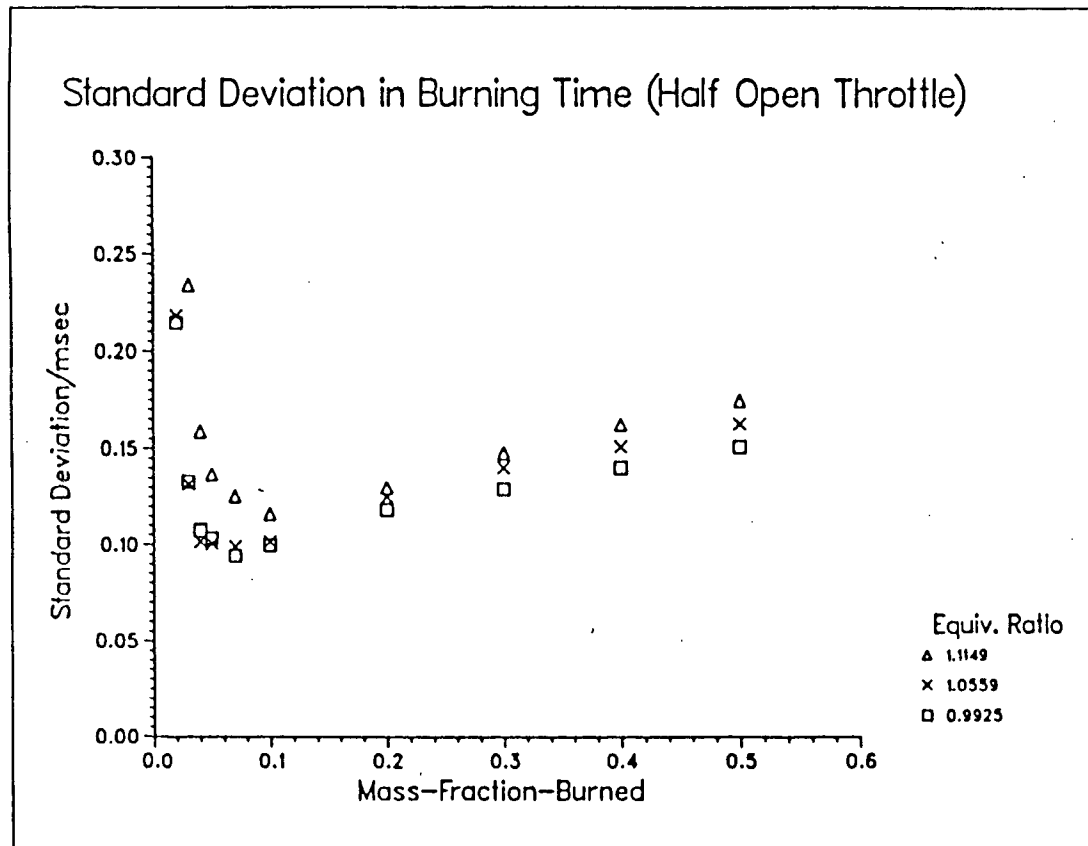


Fig 41. Standard Deviation in Burning Time. N - 3000 RPM.
(Half Open Throttle)

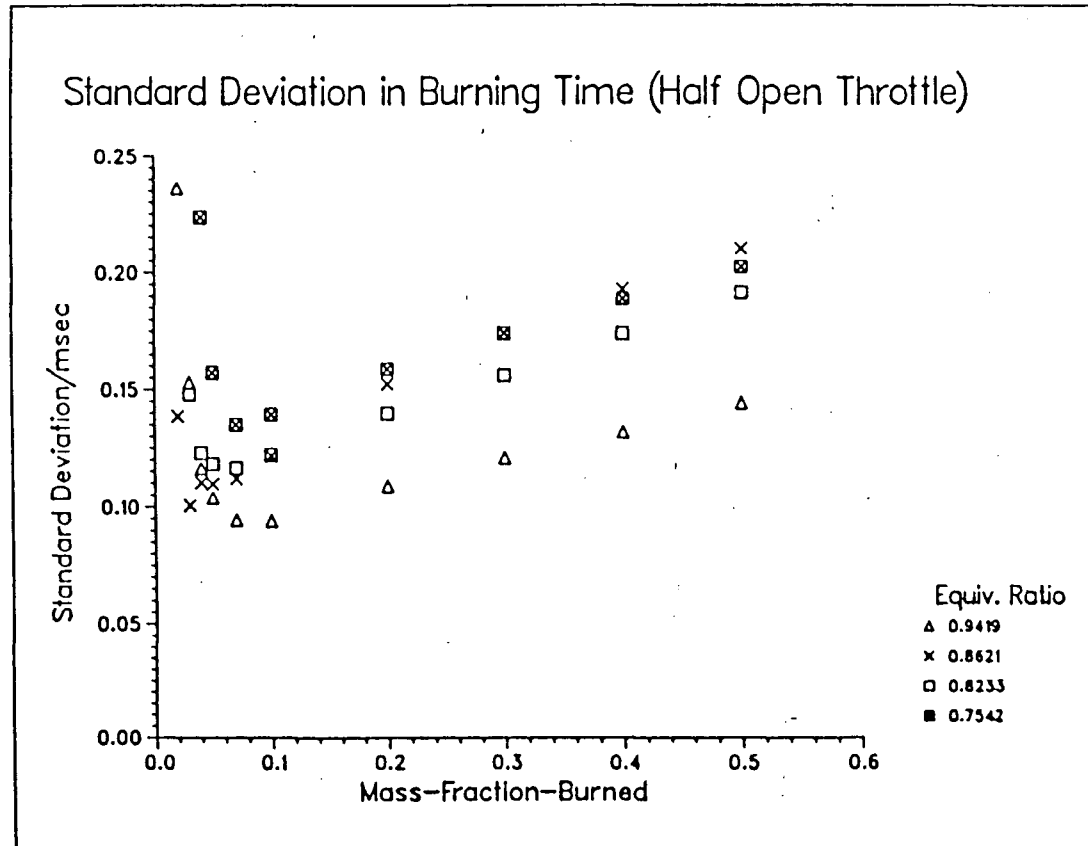


Fig 42. Standard Deviation in Burning Time. N - 3000 RPM.
(Half Open Throttle)

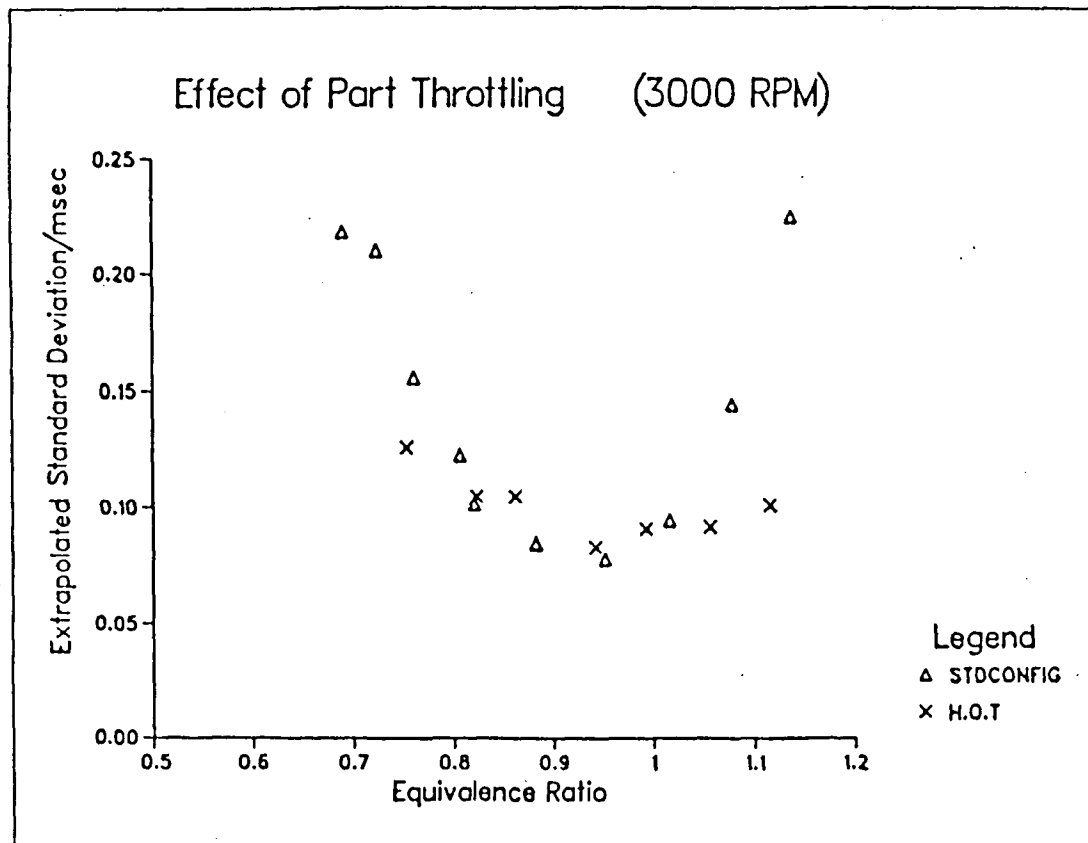


Fig 43. Extrapolated Standard Deviation in Early Burning Time.
 Different Throttle Settings N = 3000 RPM.

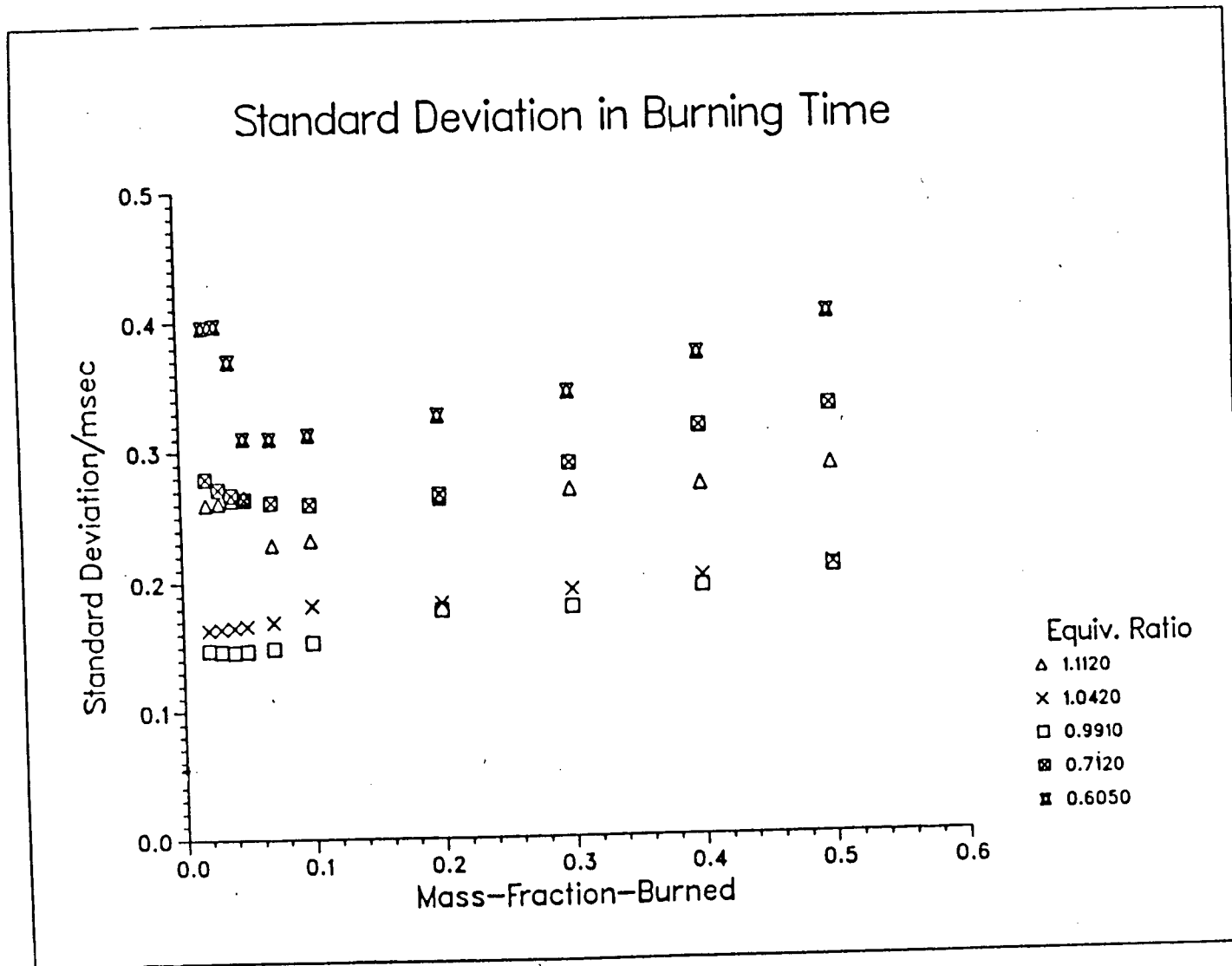


Fig 44. Standard Deviation in Burning Time. N = 2400 RPM. (Disc Chamber).

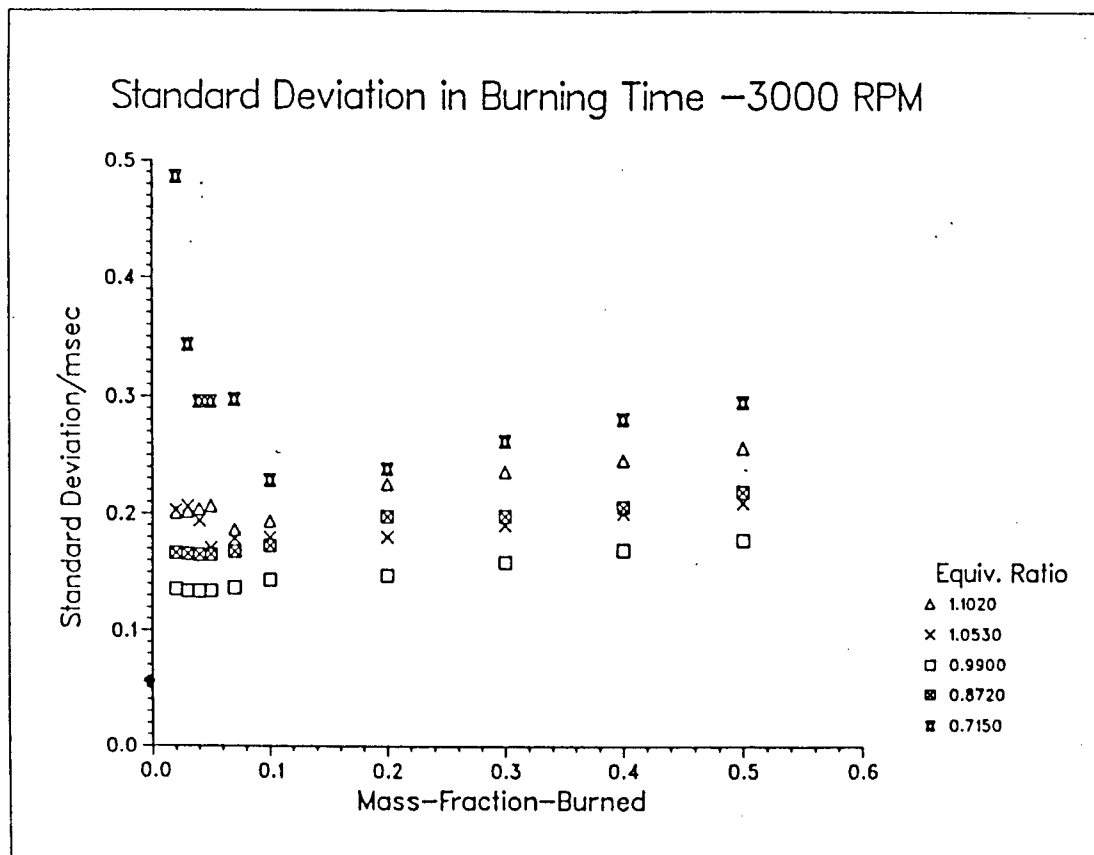


Fig 45. Standard Deviation in Burning Time. N - 3000 RPM. (Disc Chamber).

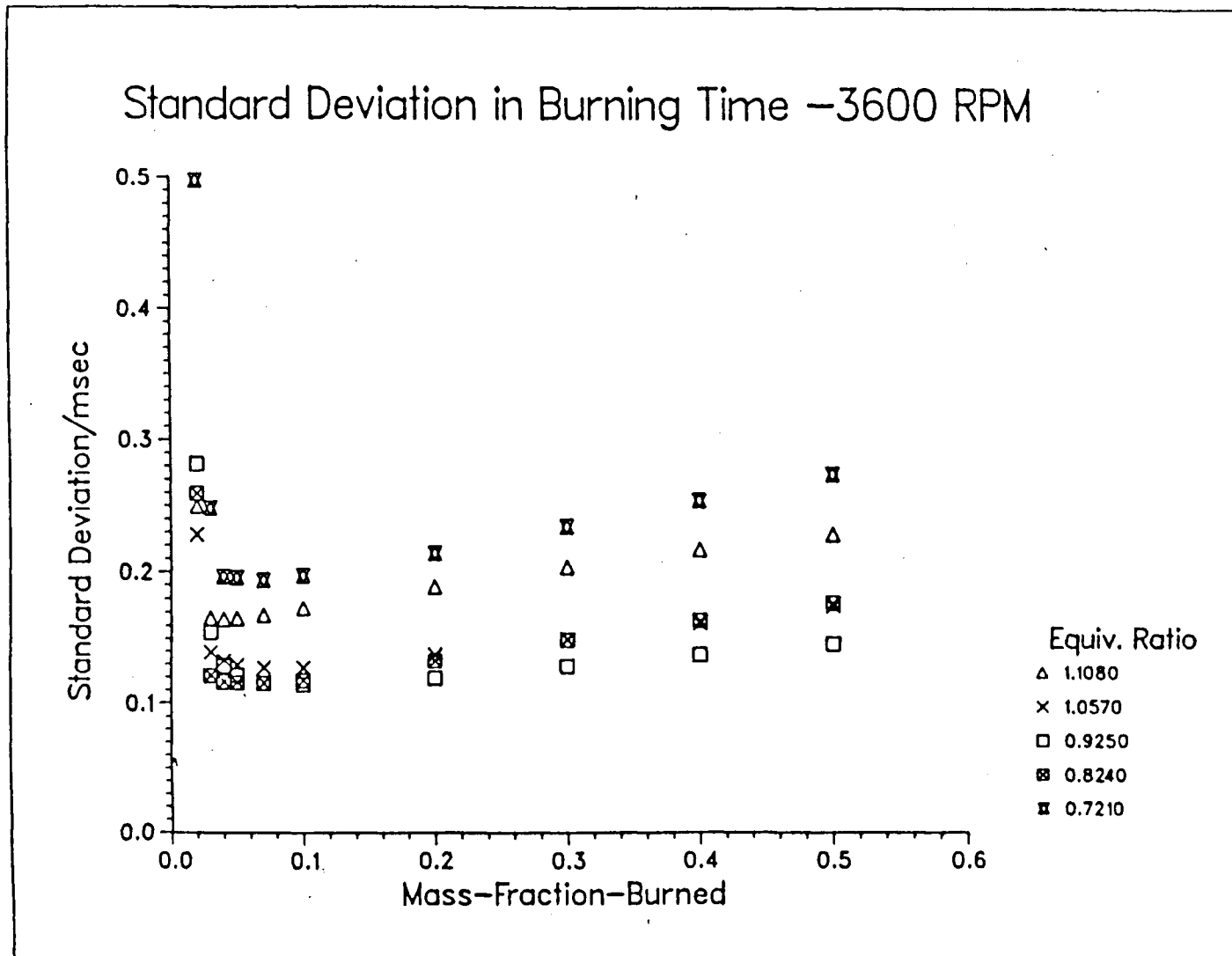


Fig 46. Standard Deviation in Burning Time. N = 3600 RPM. (Disc Chamber).

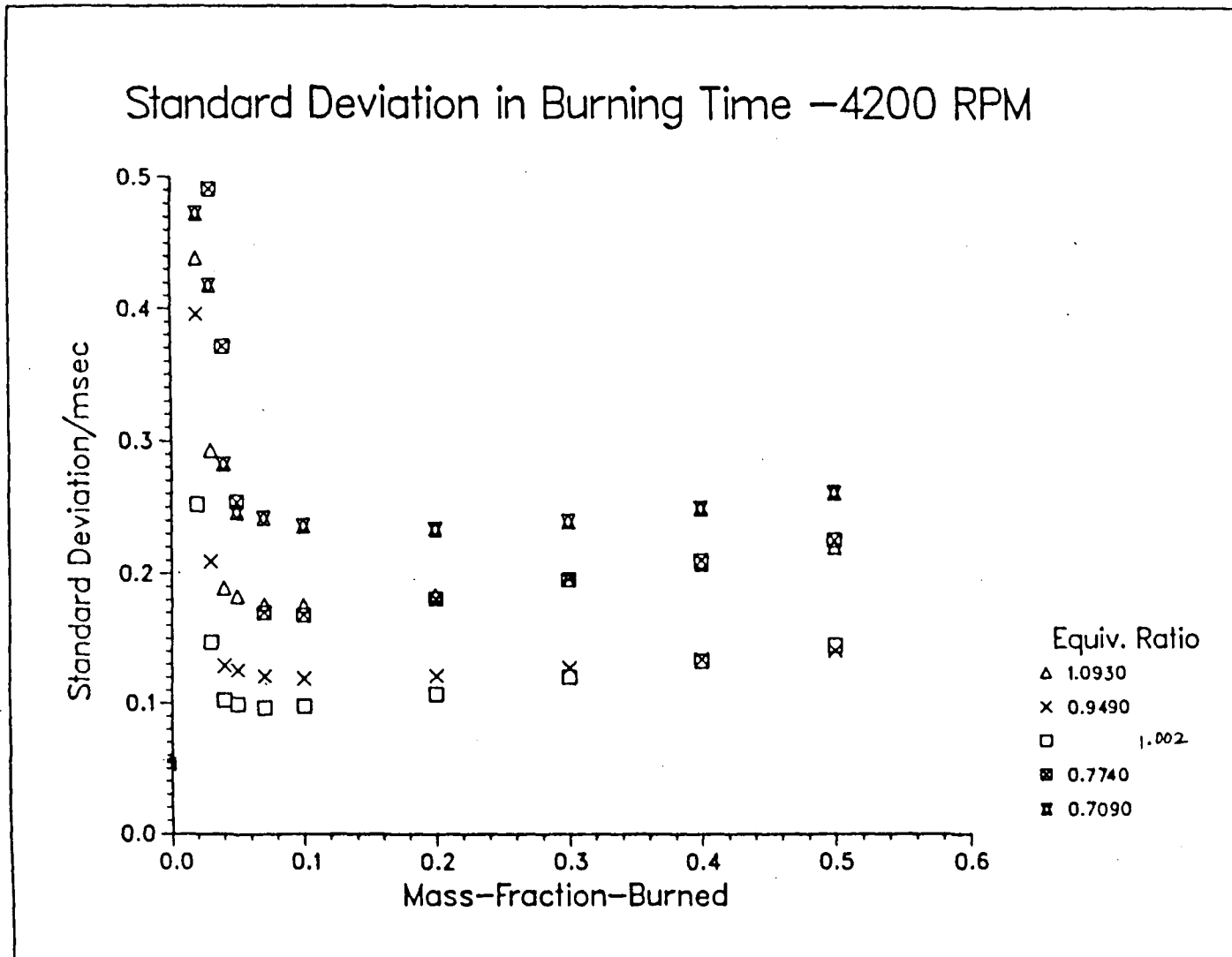


Fig 47. Standard Deviation in Burning Time. N = 4200 RPM. (Disc Chamber).

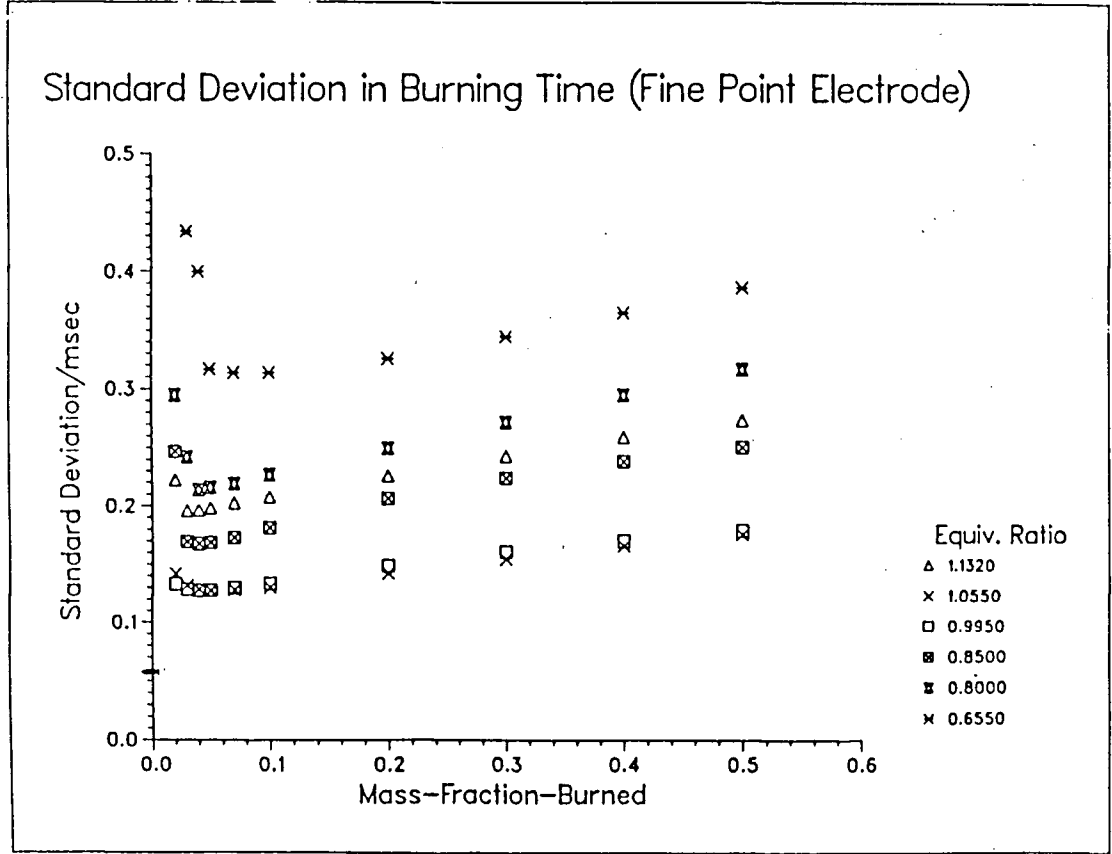


Fig 48. Standard Deviation in Burning Time. N = 3000 RPM. (Disc Chamber).
 (Fine Point Electrode Geometry).

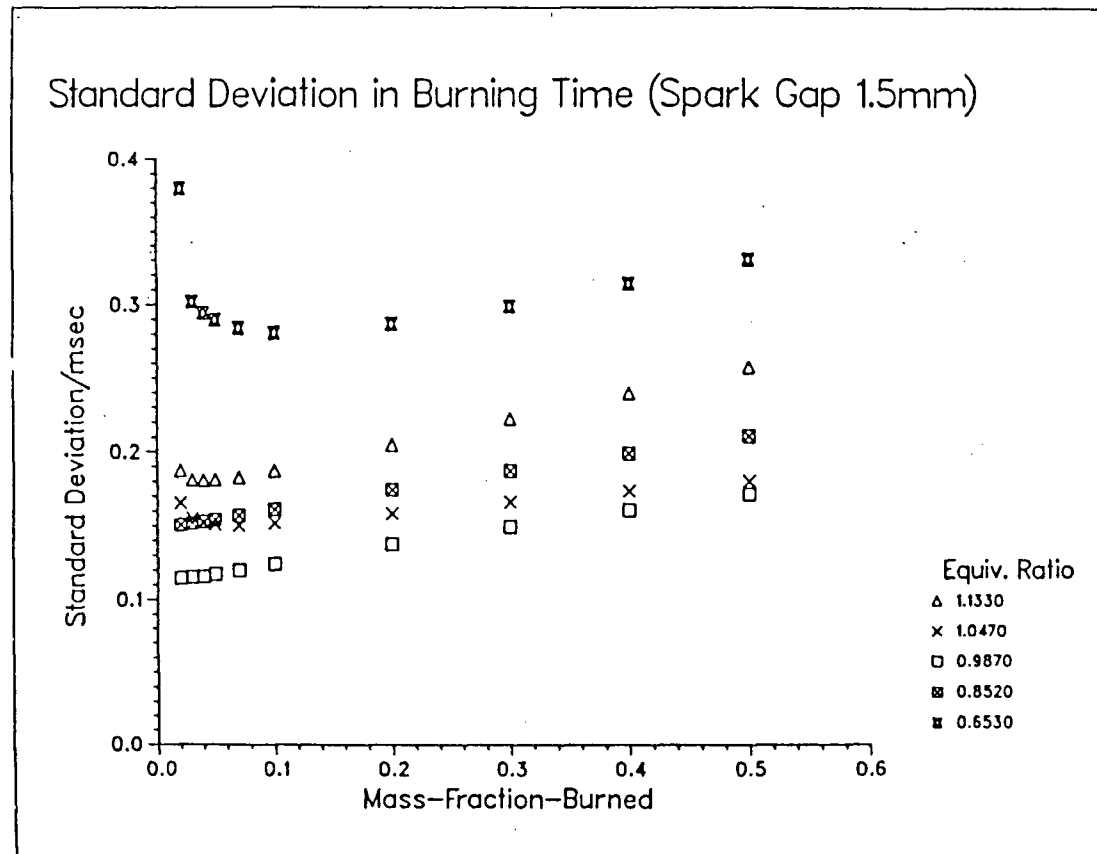


Fig 49. Standard Deviation in Burning Time. N - 3000 RPM. (Disc Chamber).
(Spark Plug Gap - 1.5 mm)

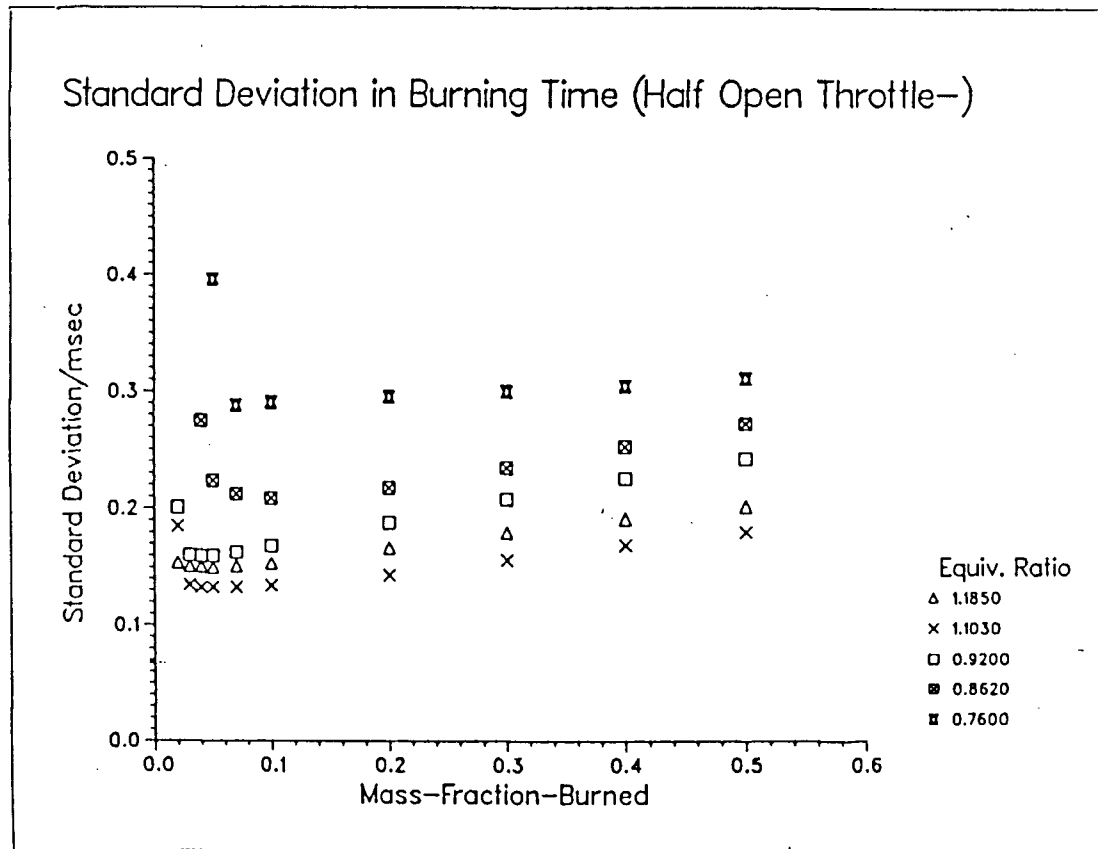


Fig 50. Standard Deviation in Burning Time. N = 3000 RPM. (Disc Chamber)
(Half Open Throttle)

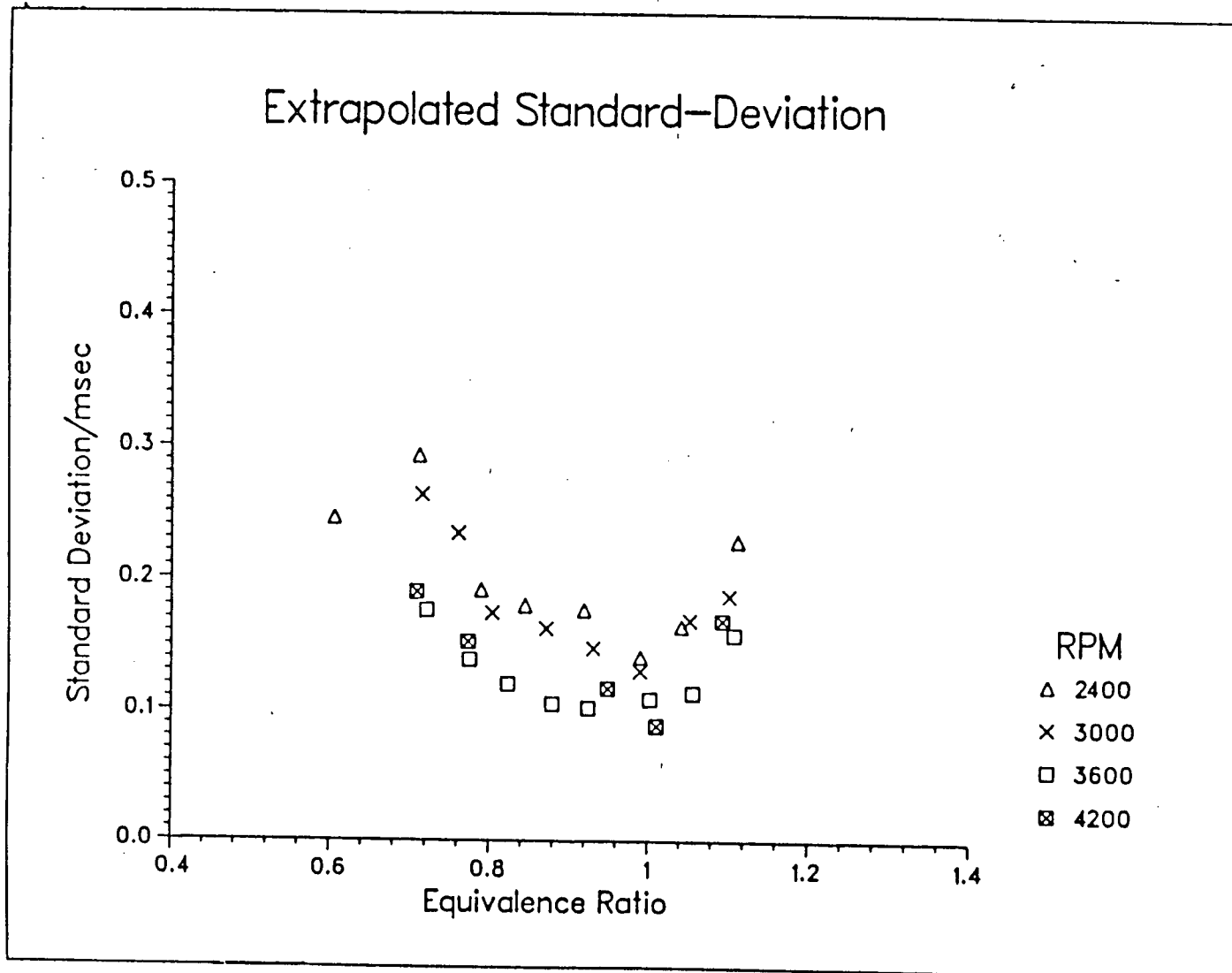


Fig 51. Extrapolated Standard Deviation in Early Burning Time. (Disk Chamber)

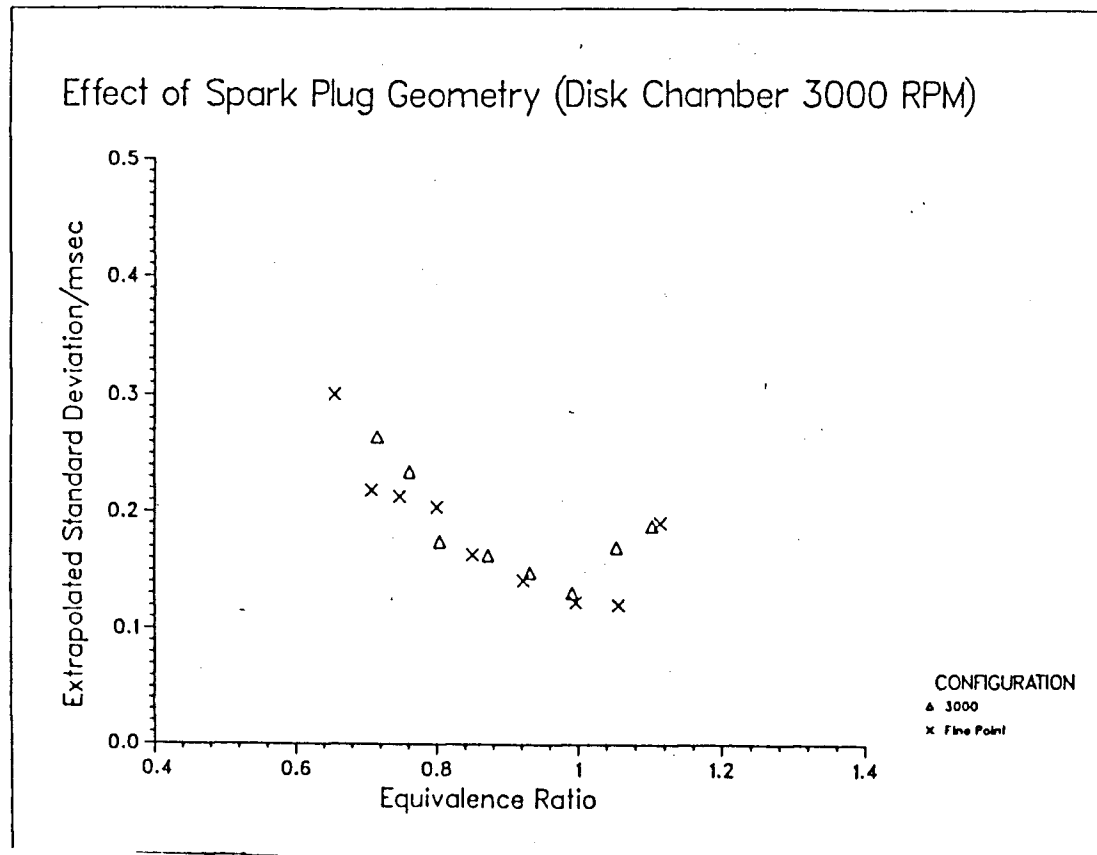


Fig 52. Extrapolated Standard Deviation in Early Burning Time. (Disk Chamber)
 Different Electrode Geometries N = 3000 RPM.

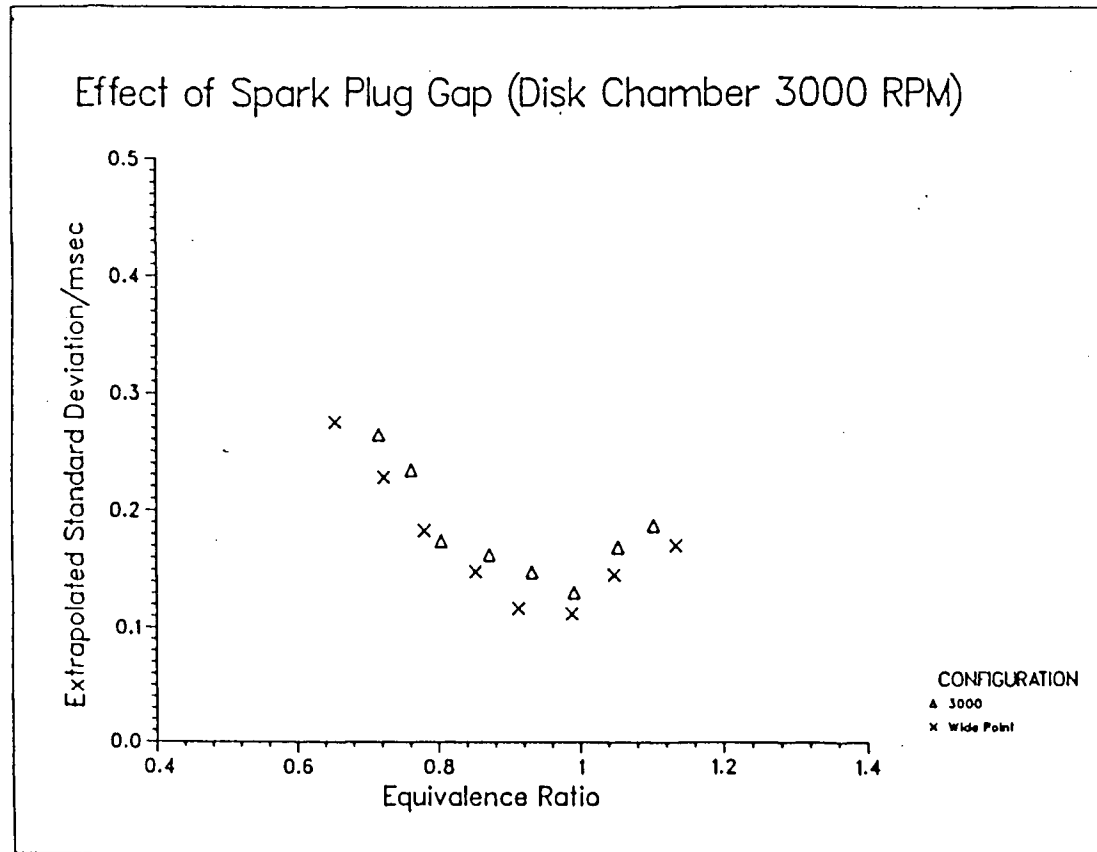


Fig 53. Extrapolated Standard Deviation in Early Burning Time. (Disk Chamber) Different Spark Gaps N = 3000 RPM.

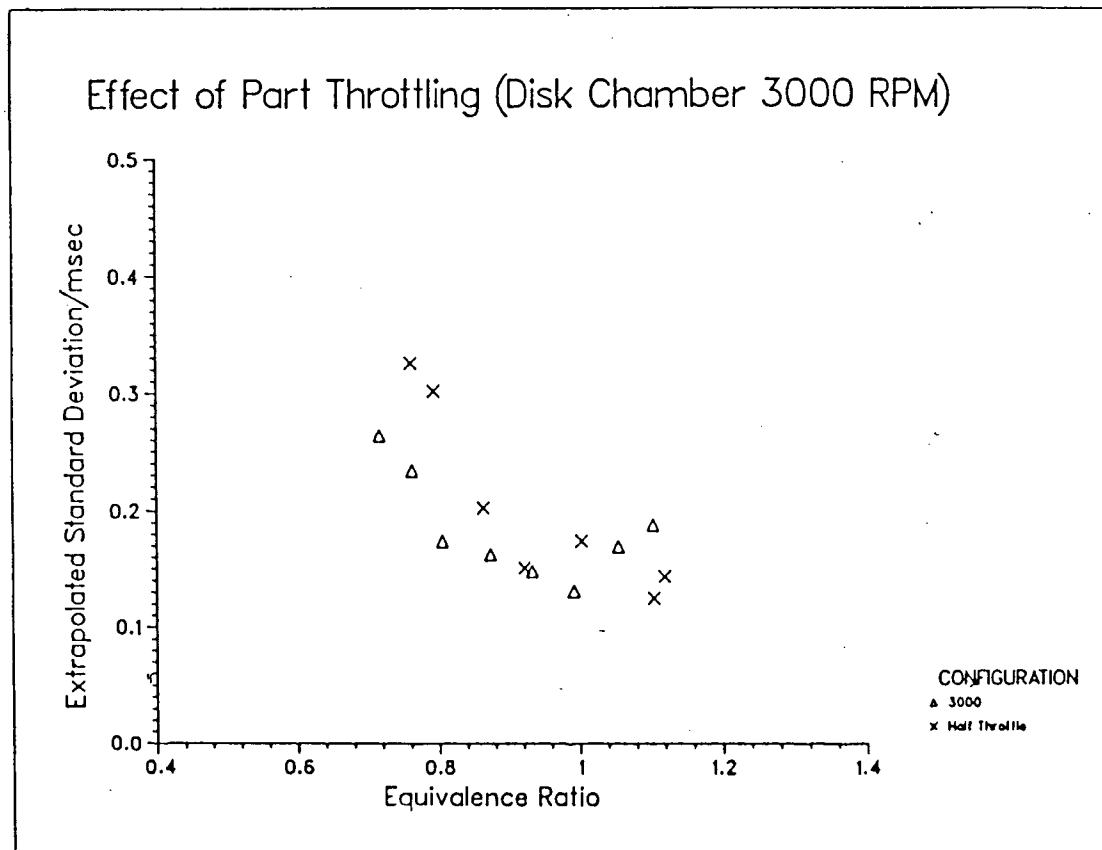


Fig 54. Extrapolated Standard Deviation in Early Burning Time.(Disk Chamber)
 Different Throttle Settings N = 3000 RPM.

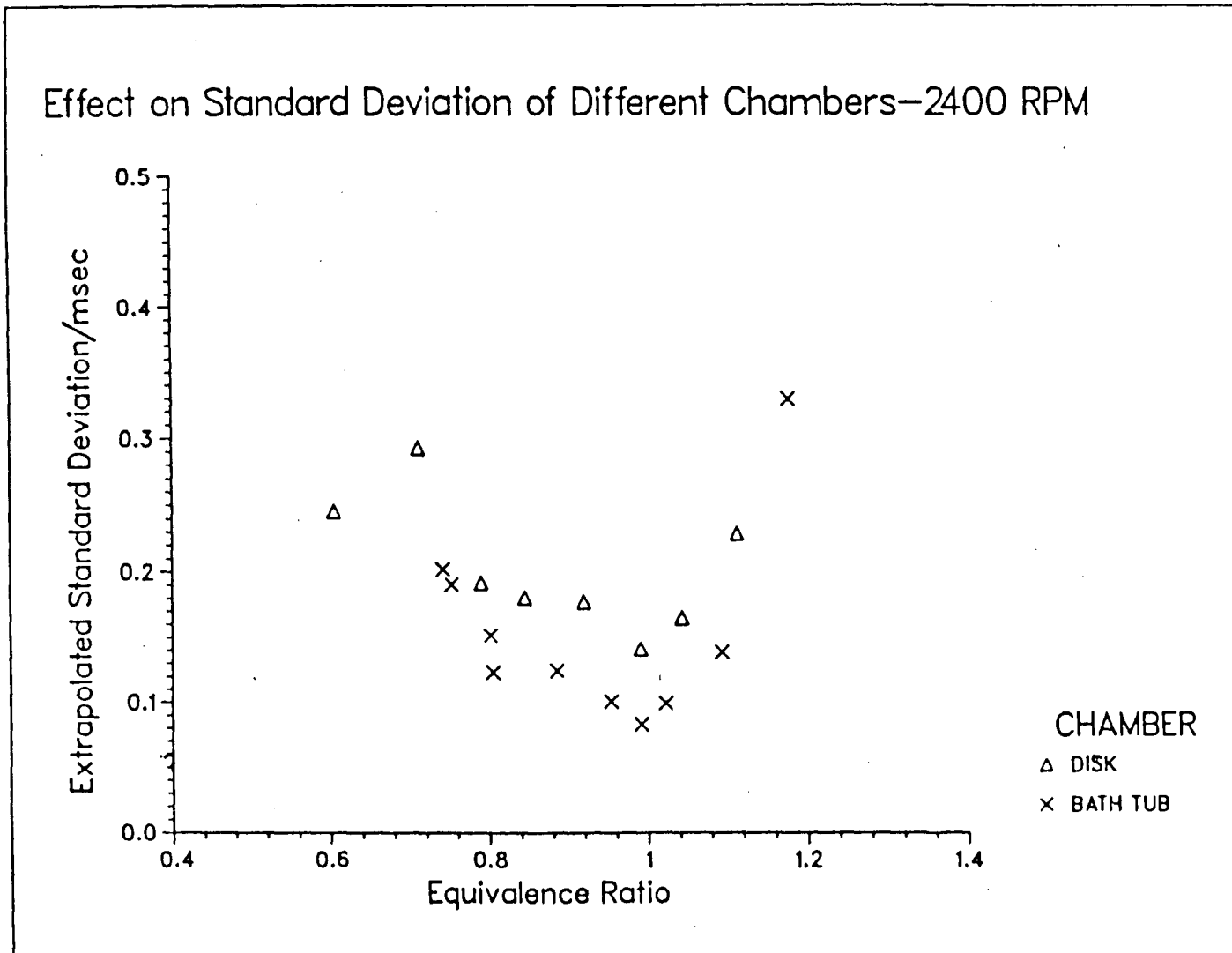


Fig 55. Effect of Different Combustion Chambers on Standard Deviation-2400 RPM

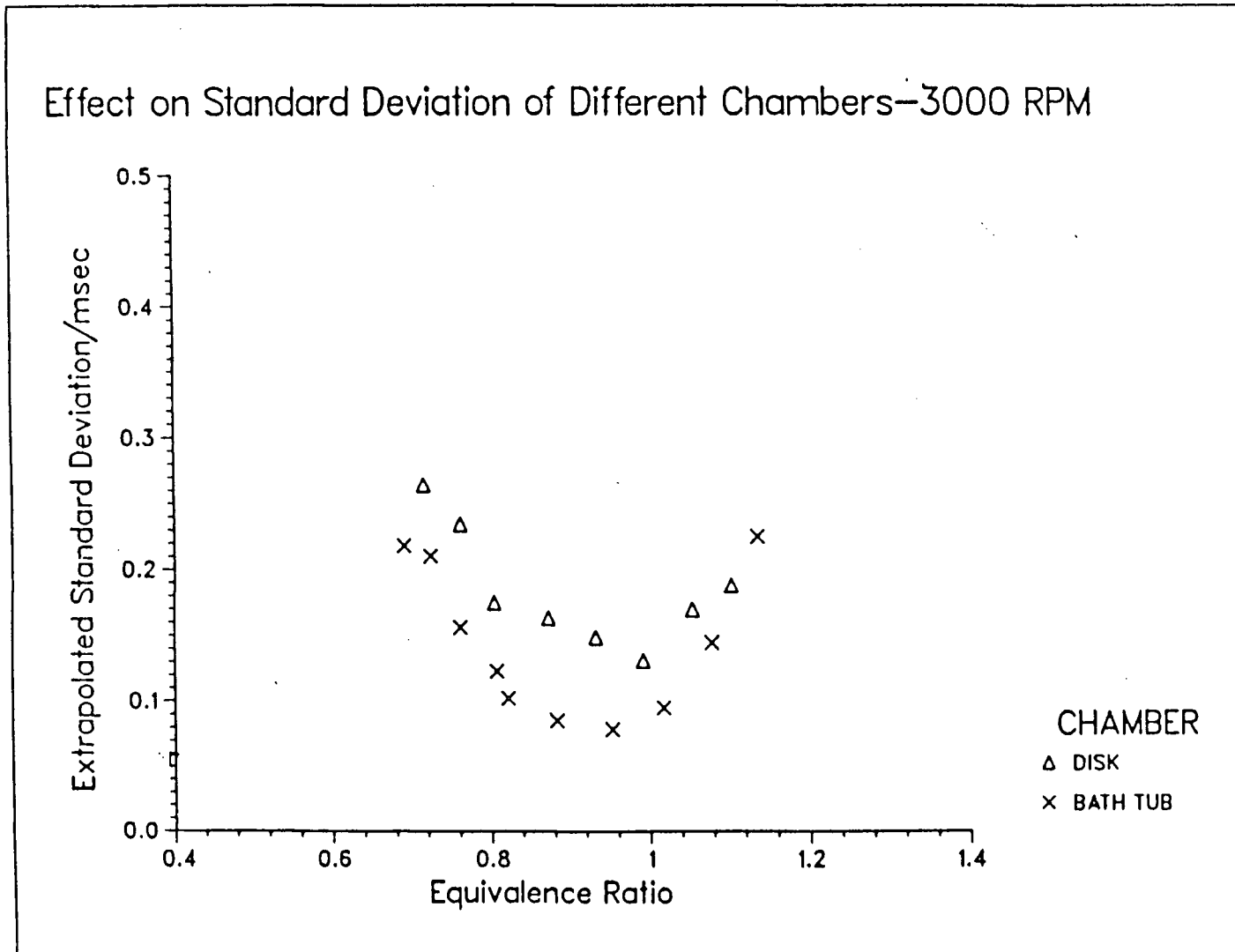


Fig 56. Effect of Different Combustion Chambers on Standard Deviation-3000 RPM

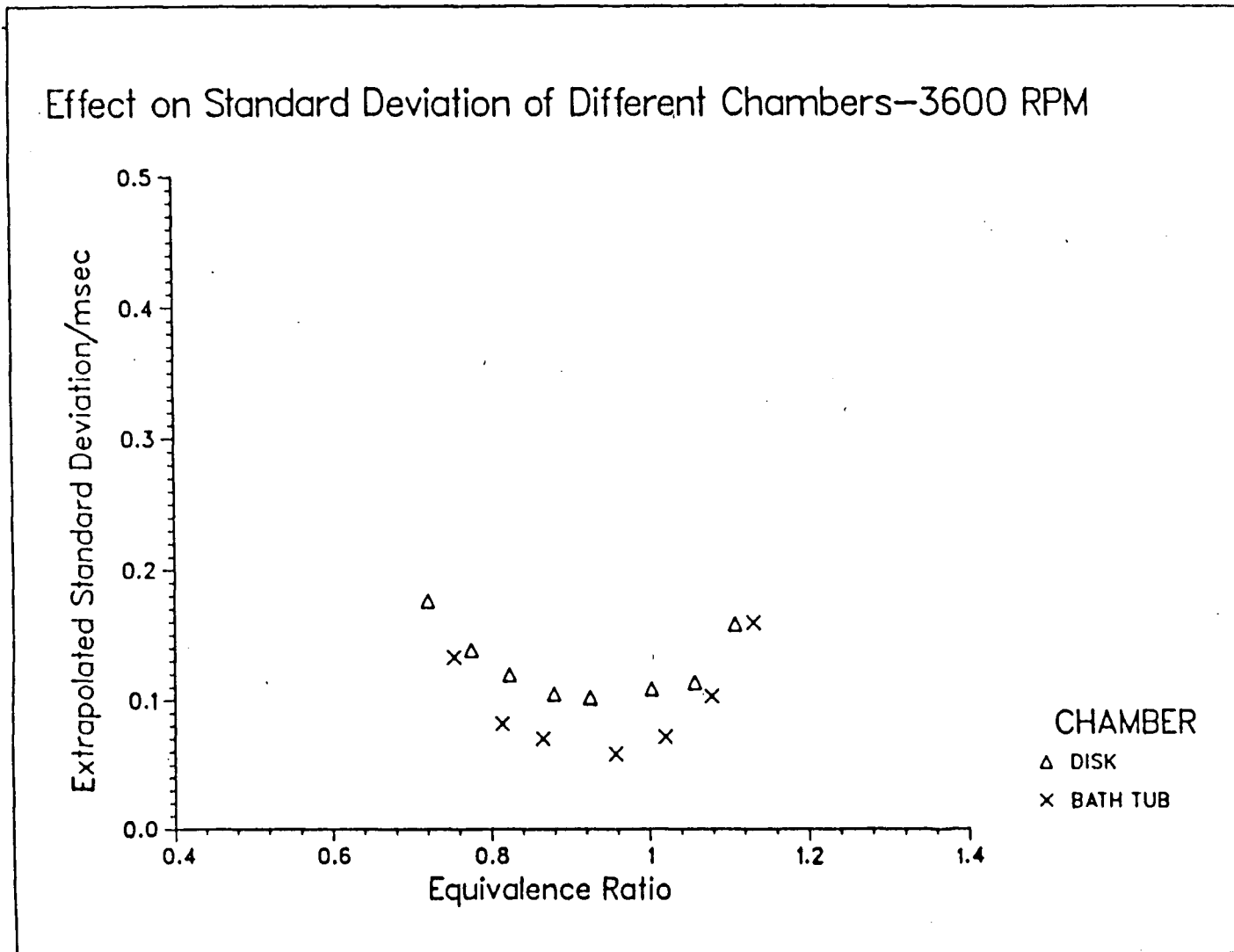


Fig 57. Effect of Different Combustion Chambers on Standard Deviation-3600 RPM.

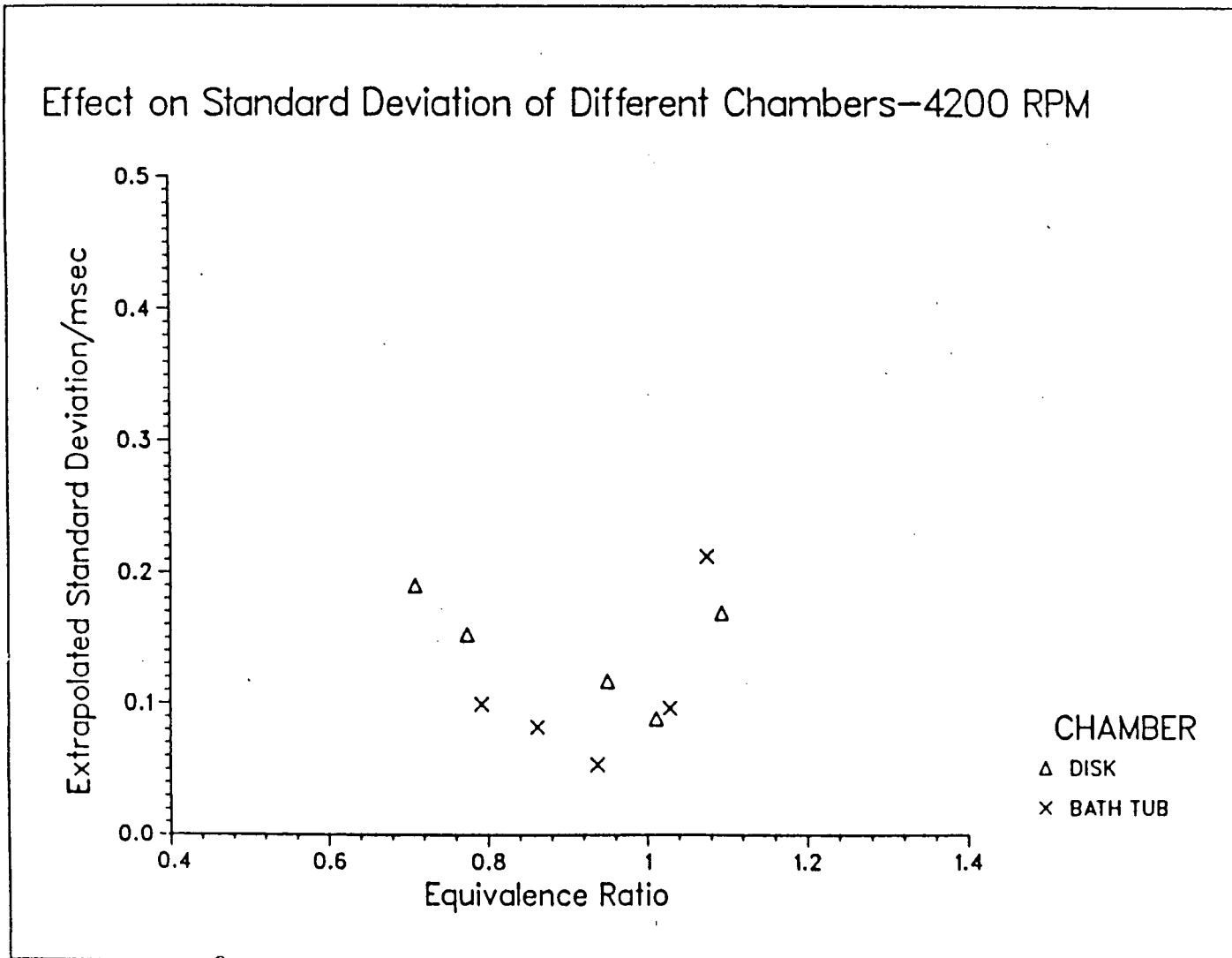


Fig 58. Effect of Different Combustion Chambers on Standard Deviation-4200 RPM

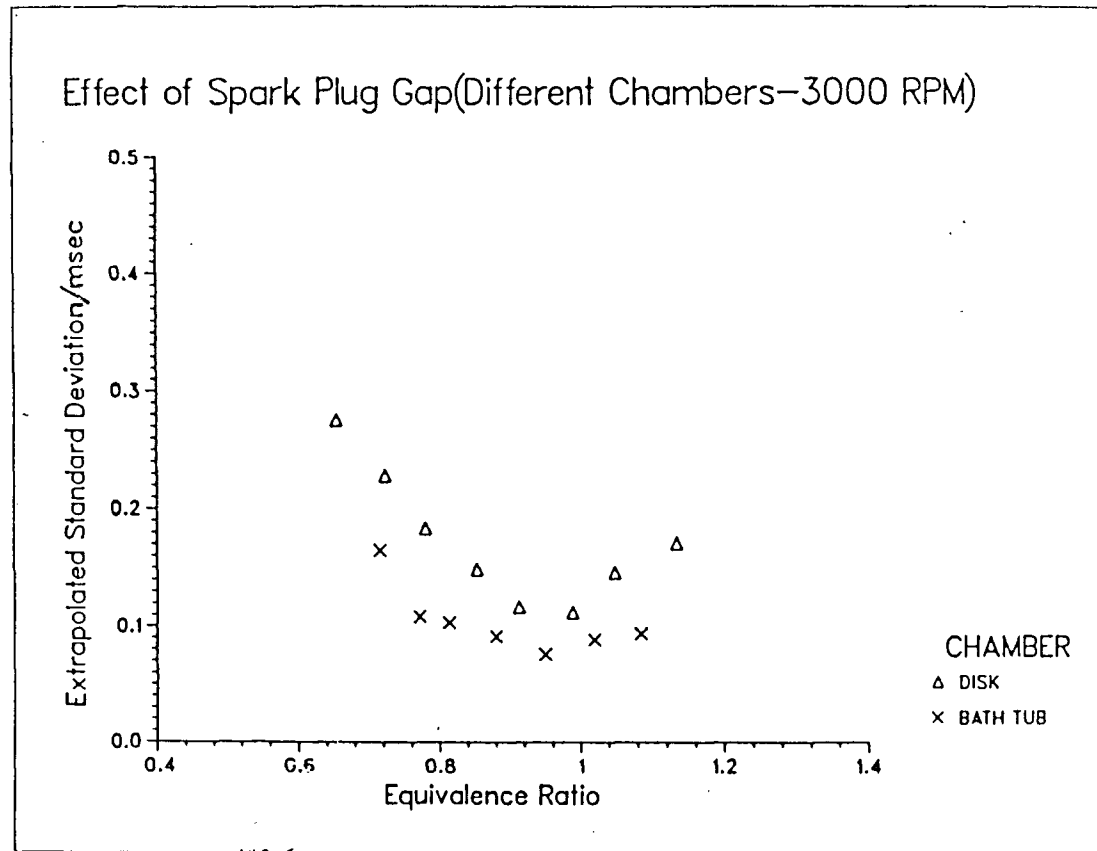


Fig 59. Effect of Different Combustion Chambers on Standard Deviation
 Different Spark Gaps.

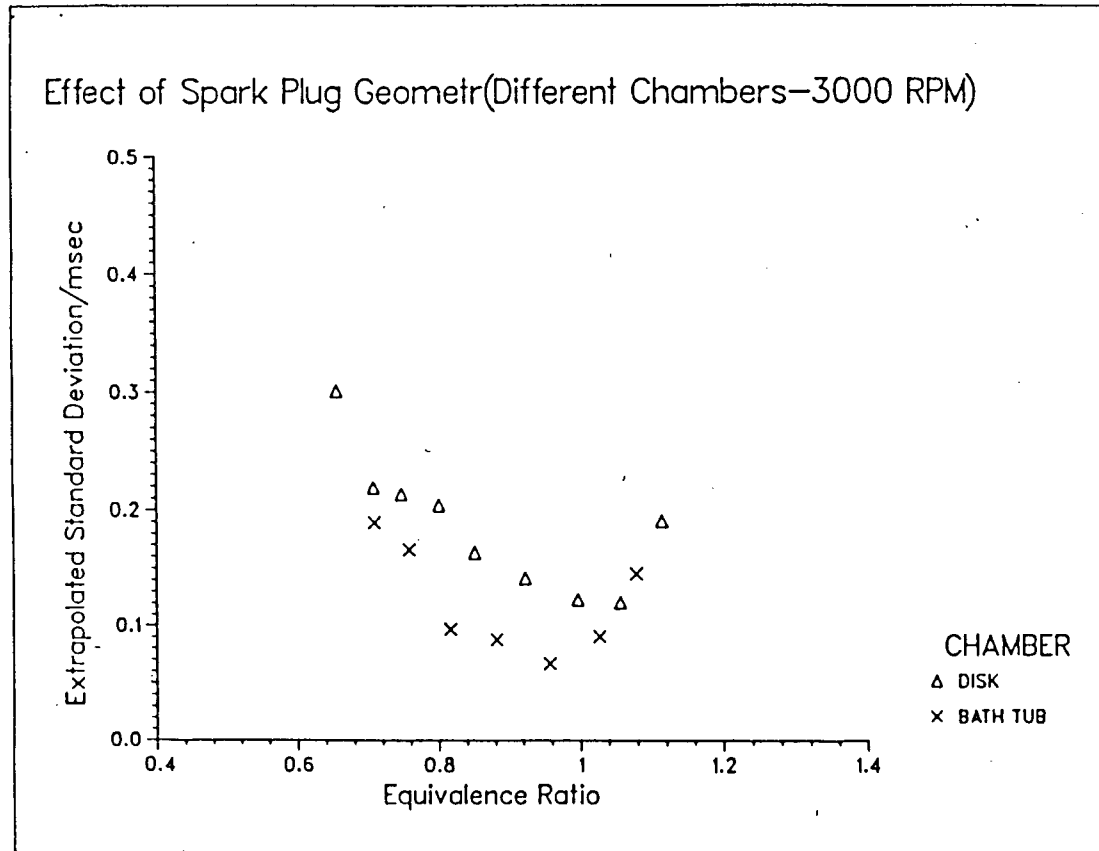


Fig 60. Effect of Different Combustion Chambers on Standard Deviation
 Fine Point Electrodes.

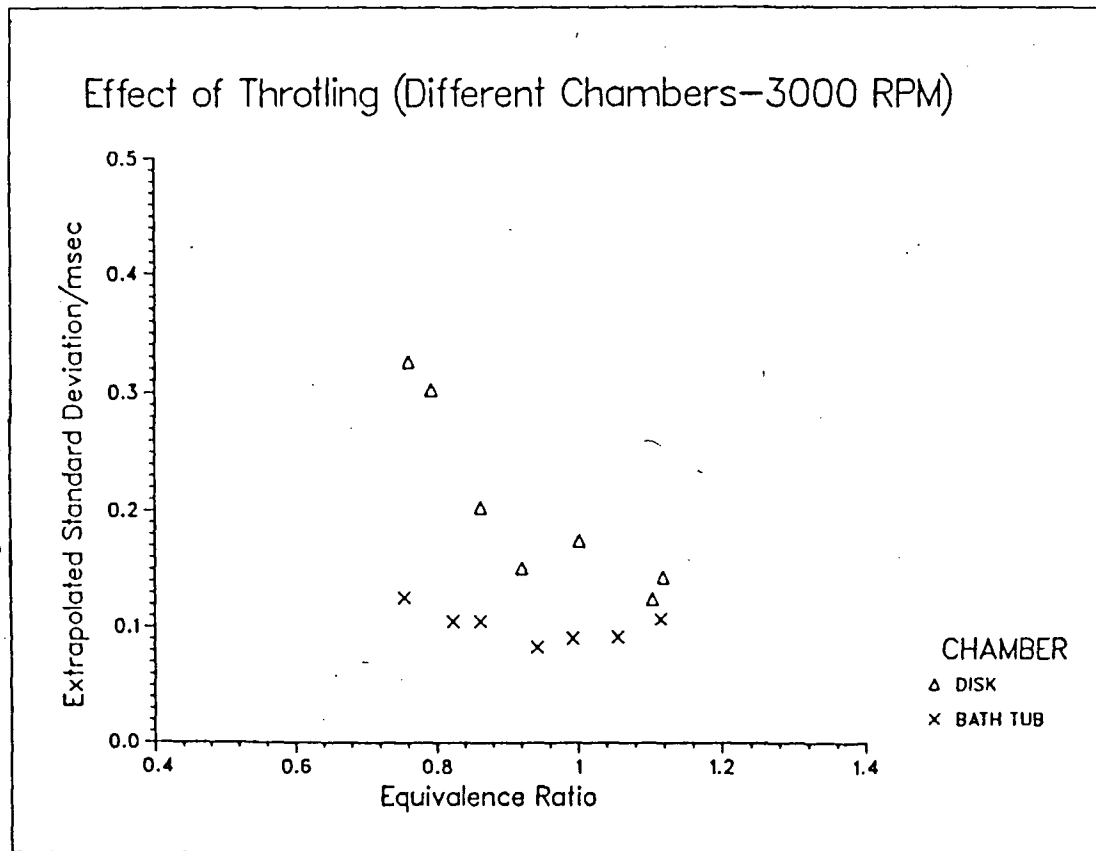


Fig 61. Effect of Different Combustion Chambers on Standard Deviation Partly Opened Throttle.

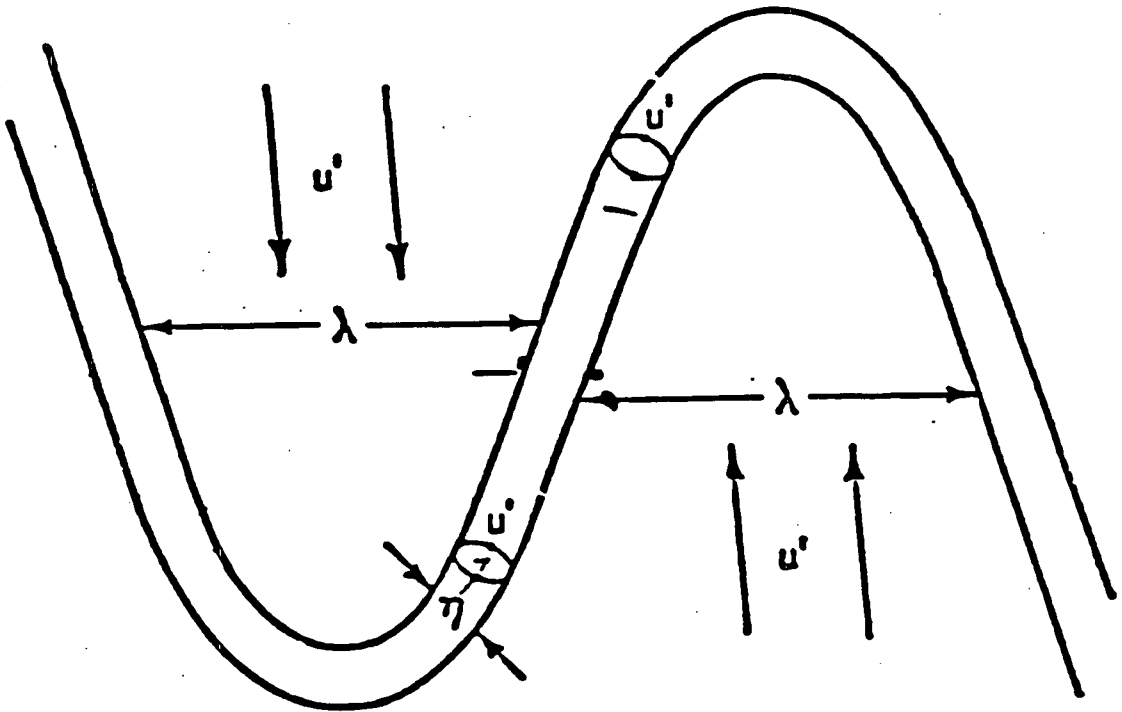


Fig 62. Model of Concentrated Vorticity Region as Proposed by Tennekes

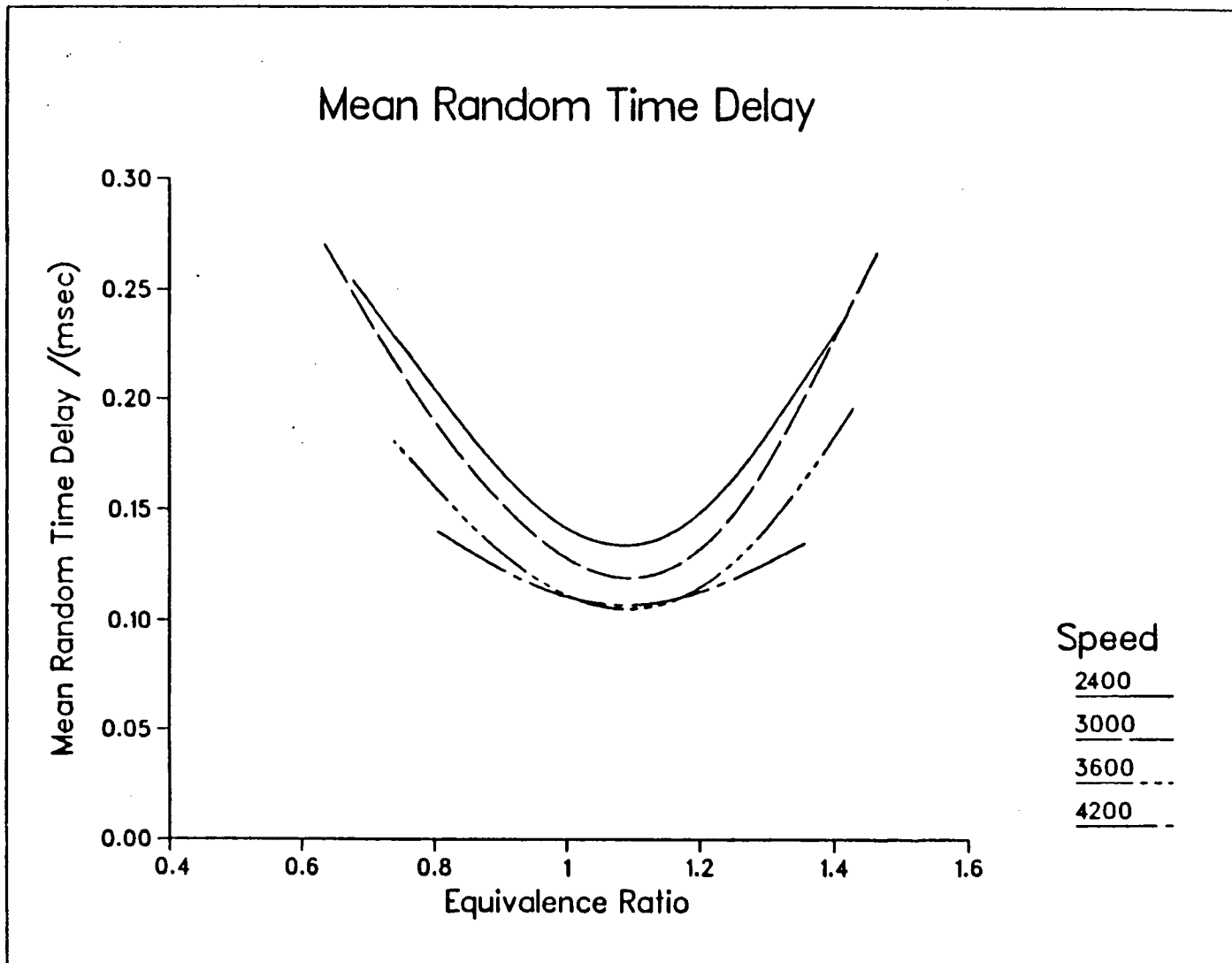


Fig 63. Effect of Equivalence Ratio on Mean Random Time Delay.

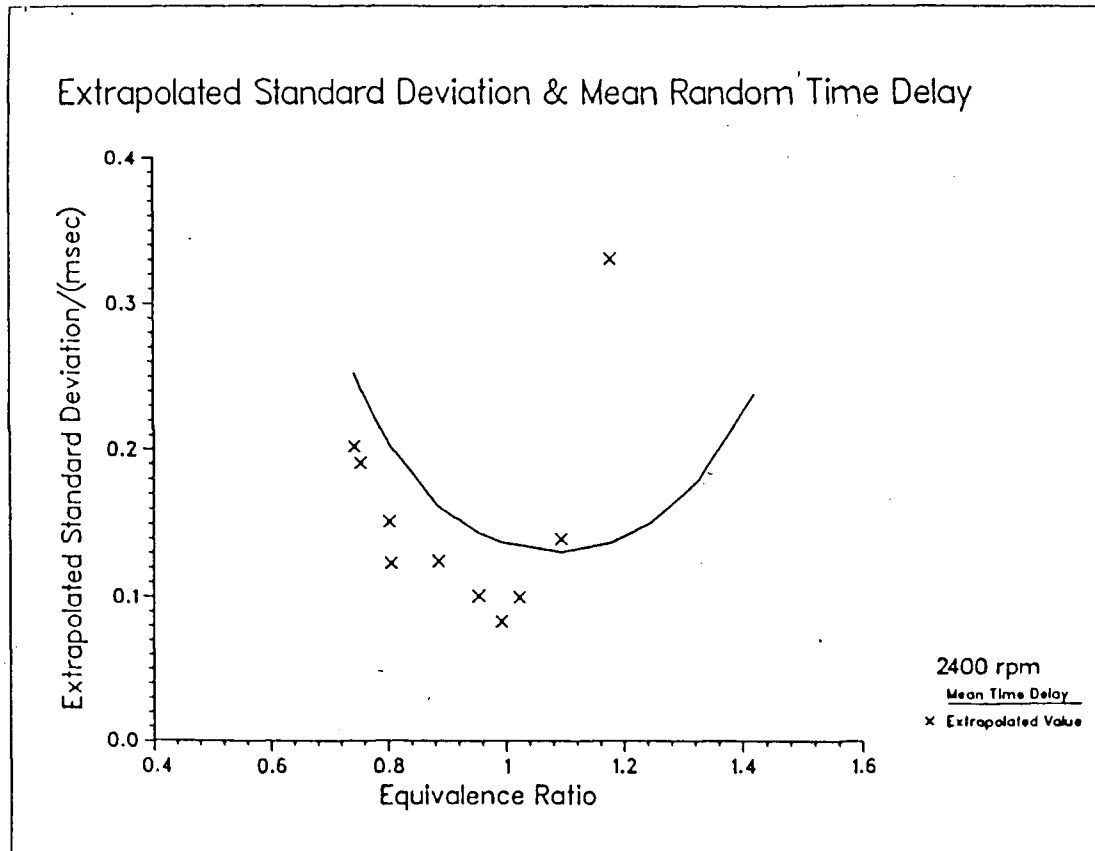


Fig 64. Comparison of Extrapolated Standard Deviation and Mean Random Time Delay with Equivalence Ratio. - 2400 RPM. (Bath-Tub Chamber)

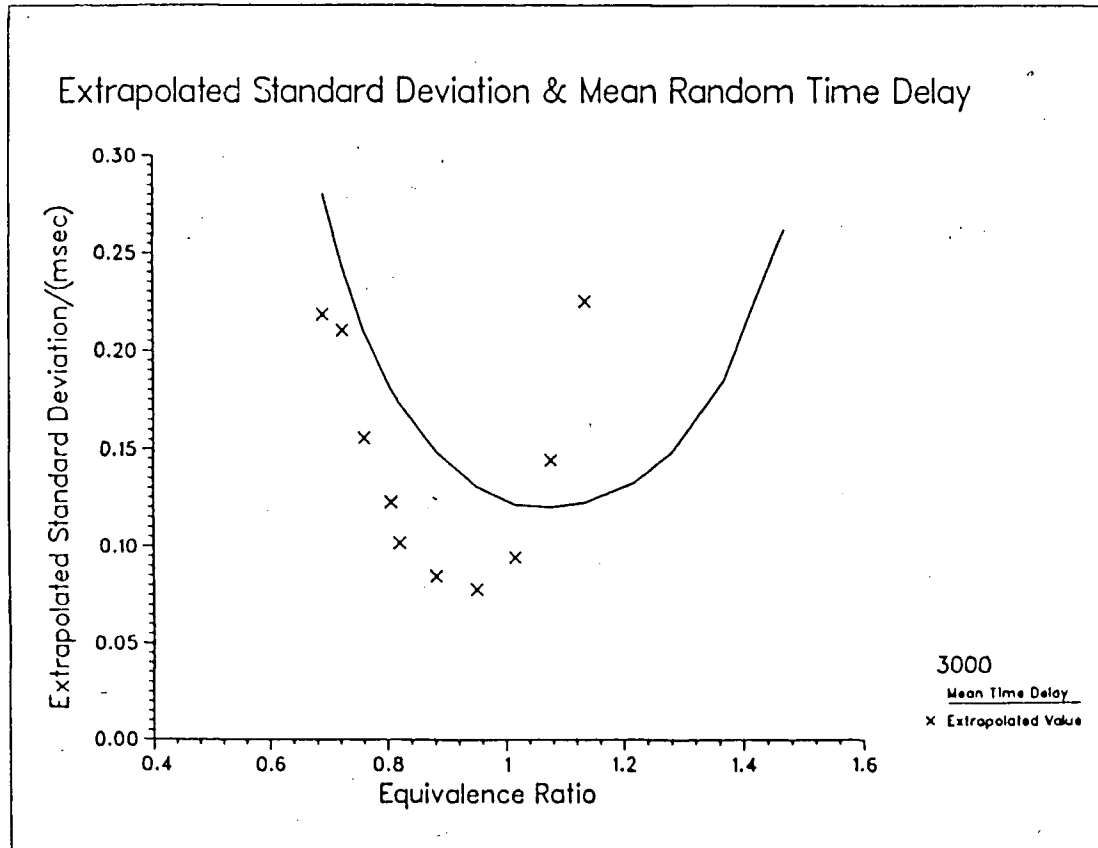


Fig 65. Comparison of Extrapolated Standard Deviation and Mean Random Time Delay with Equivalence Ratio. - 3000 RPM. (Bath-Tub Chamber)

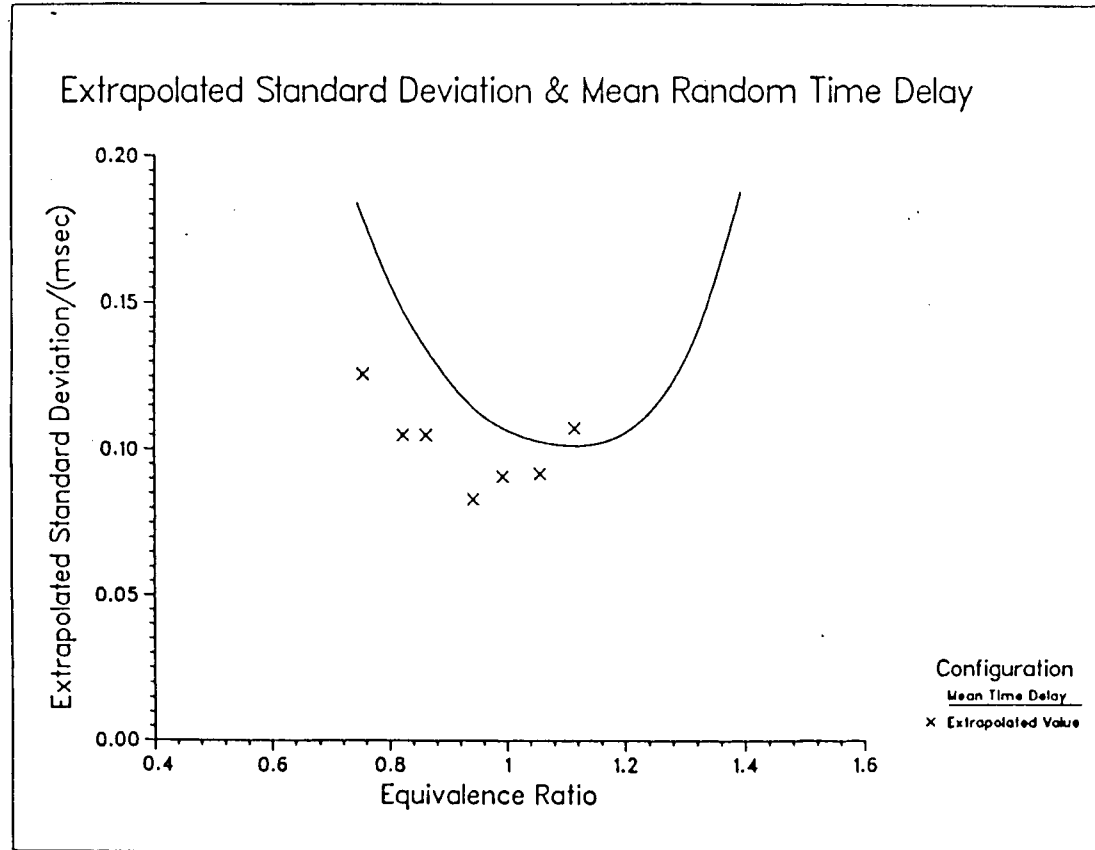


Fig 66. Comparison of Extrapolated Standard Deviation and Mean Random Time Delay with Equivalence Ratio. - 3600 RPM. (Bath-Tub Chamber)

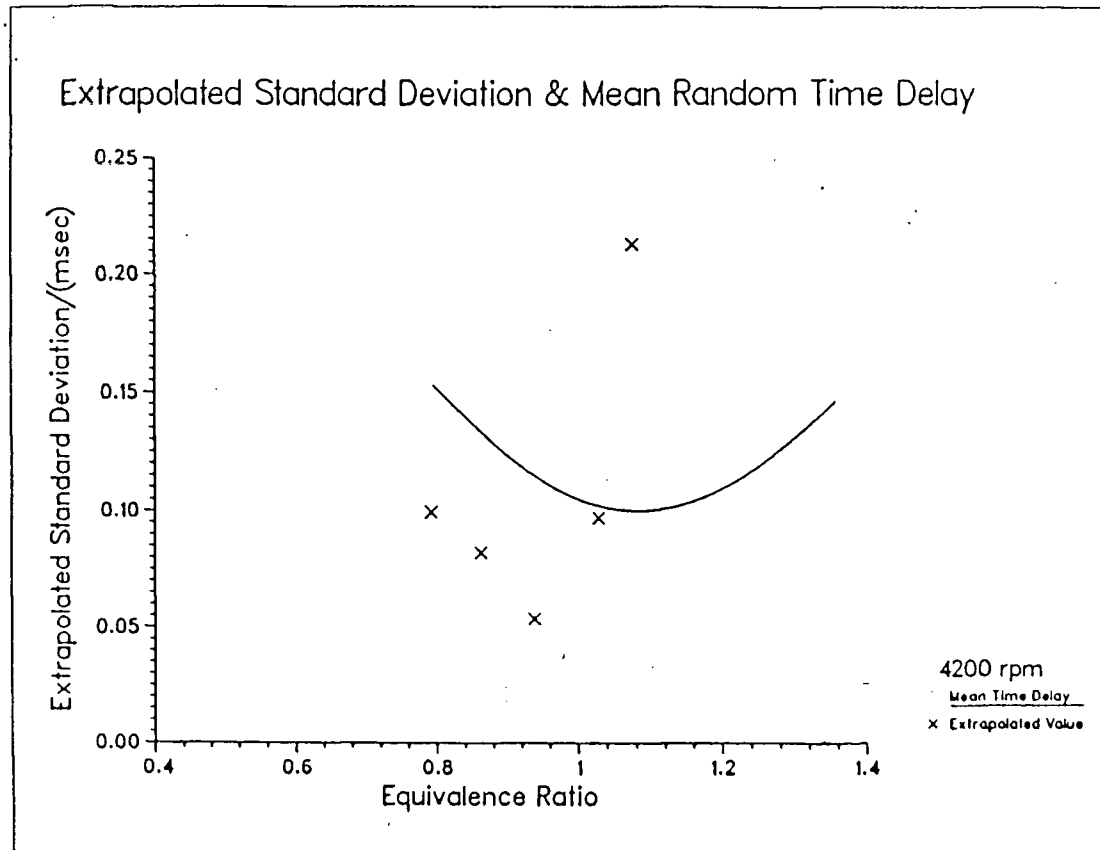


Fig 67. Comparison of Extrapolated Standard Deviation and Mean Random Time Delay with Equivalence Ratio. - 4200 RPM. (Bath-Tub Chamber)

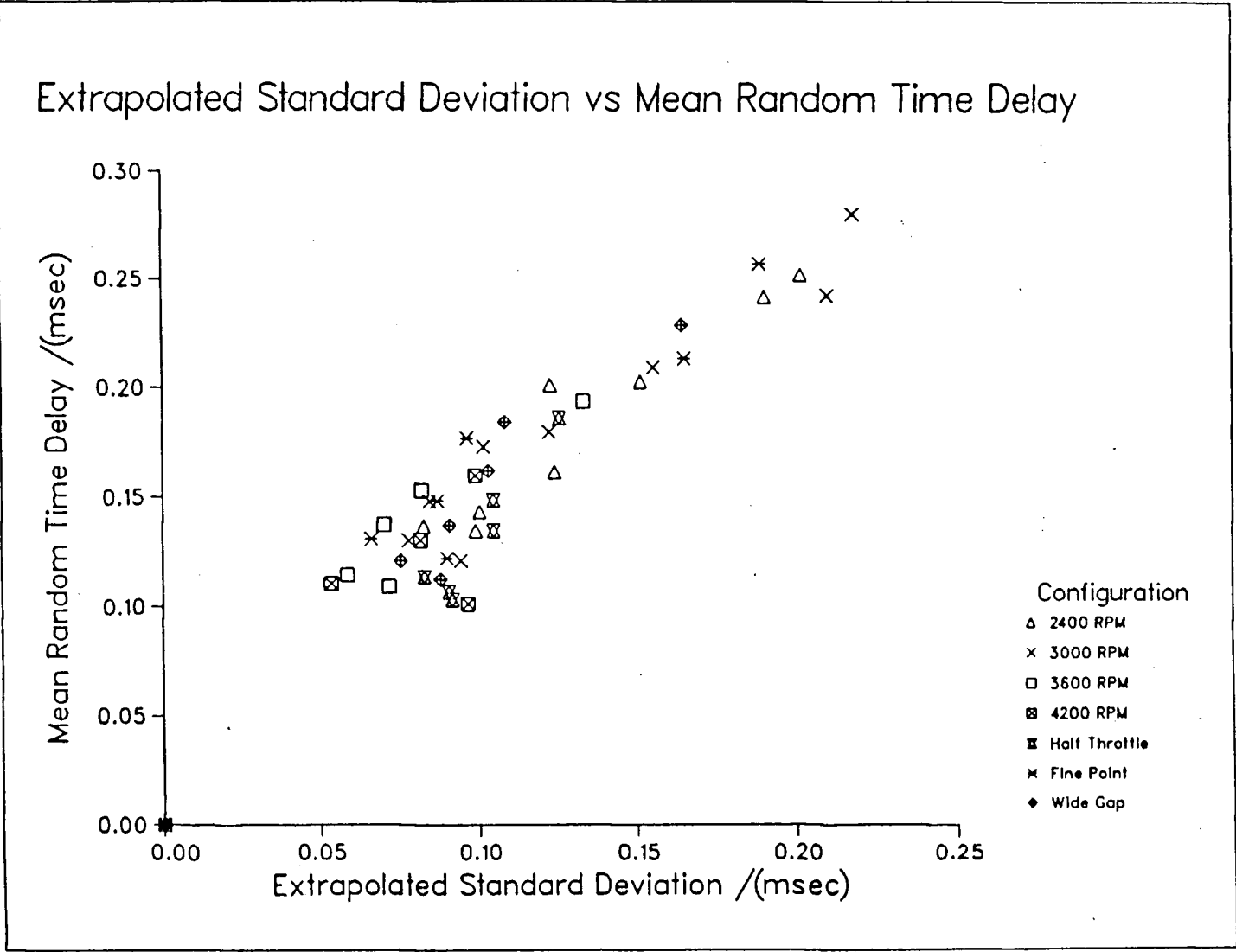


Fig 68. Relationship Between Mean Random Time Delay and Extrapolated Standard Deviation in Burning Time within a Bath-Tub Chamber.

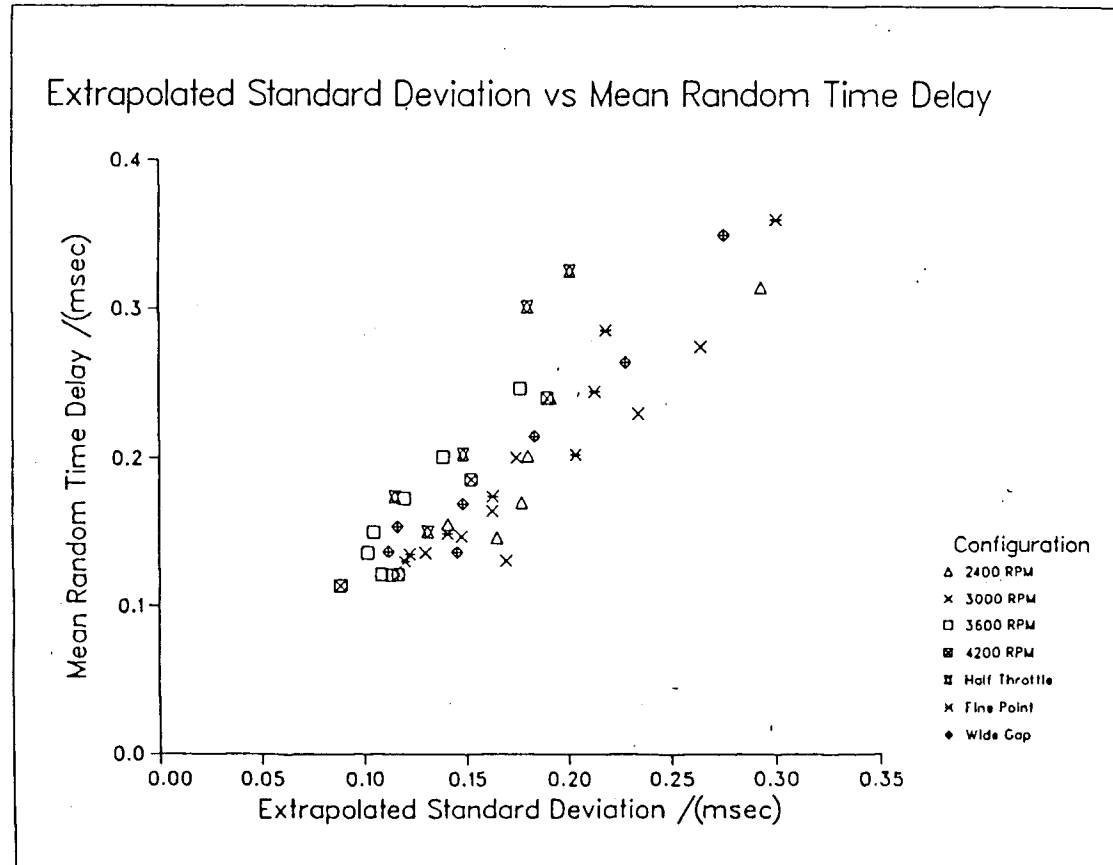


Fig 69. Relationship Between Mean Random Time Delay and Extrapolated Standard Deviation in Burning Time within a Disc Chamber.

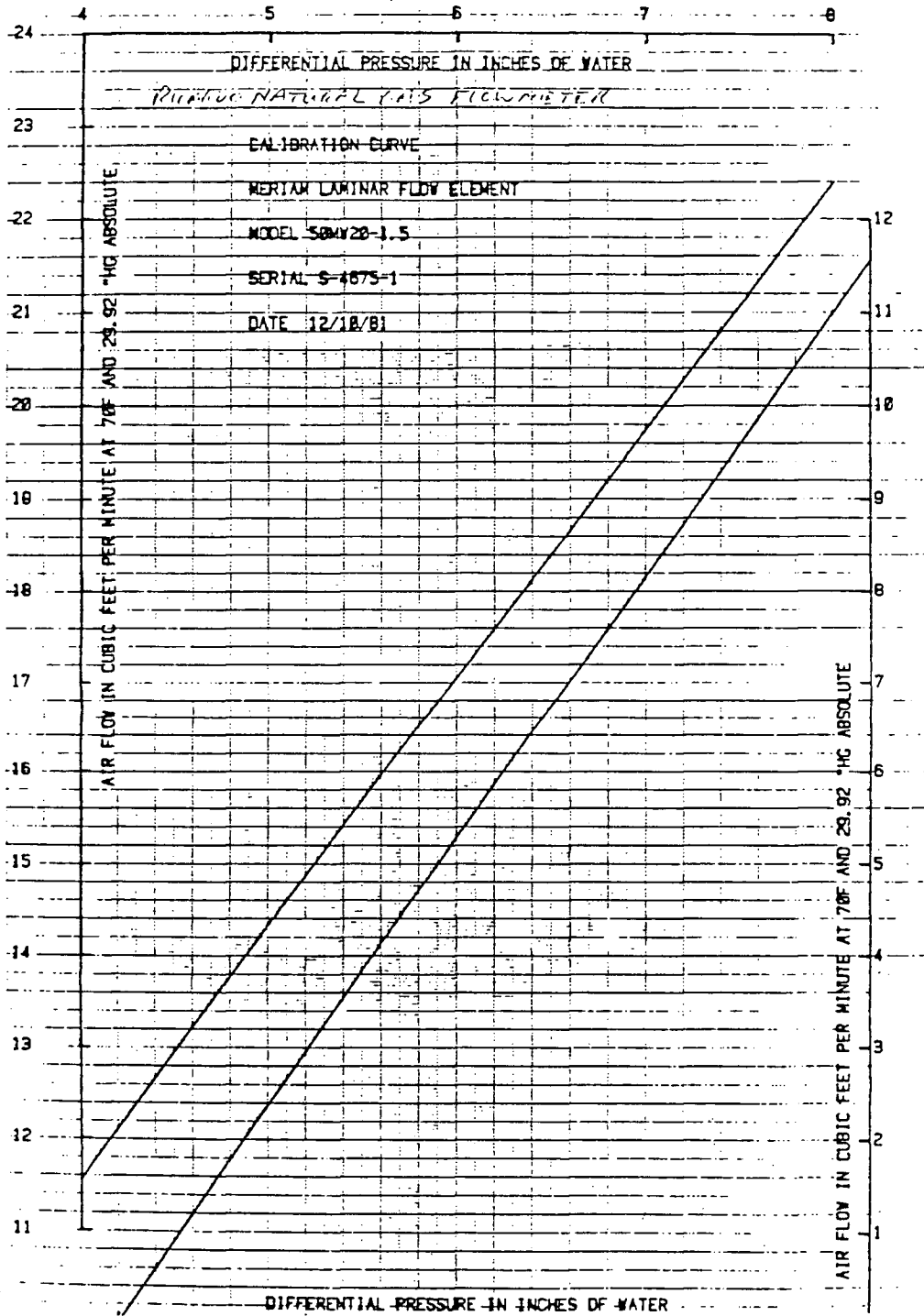


Fig 70. Calibration Curve For Laminar Flow Element (Natural Gas)

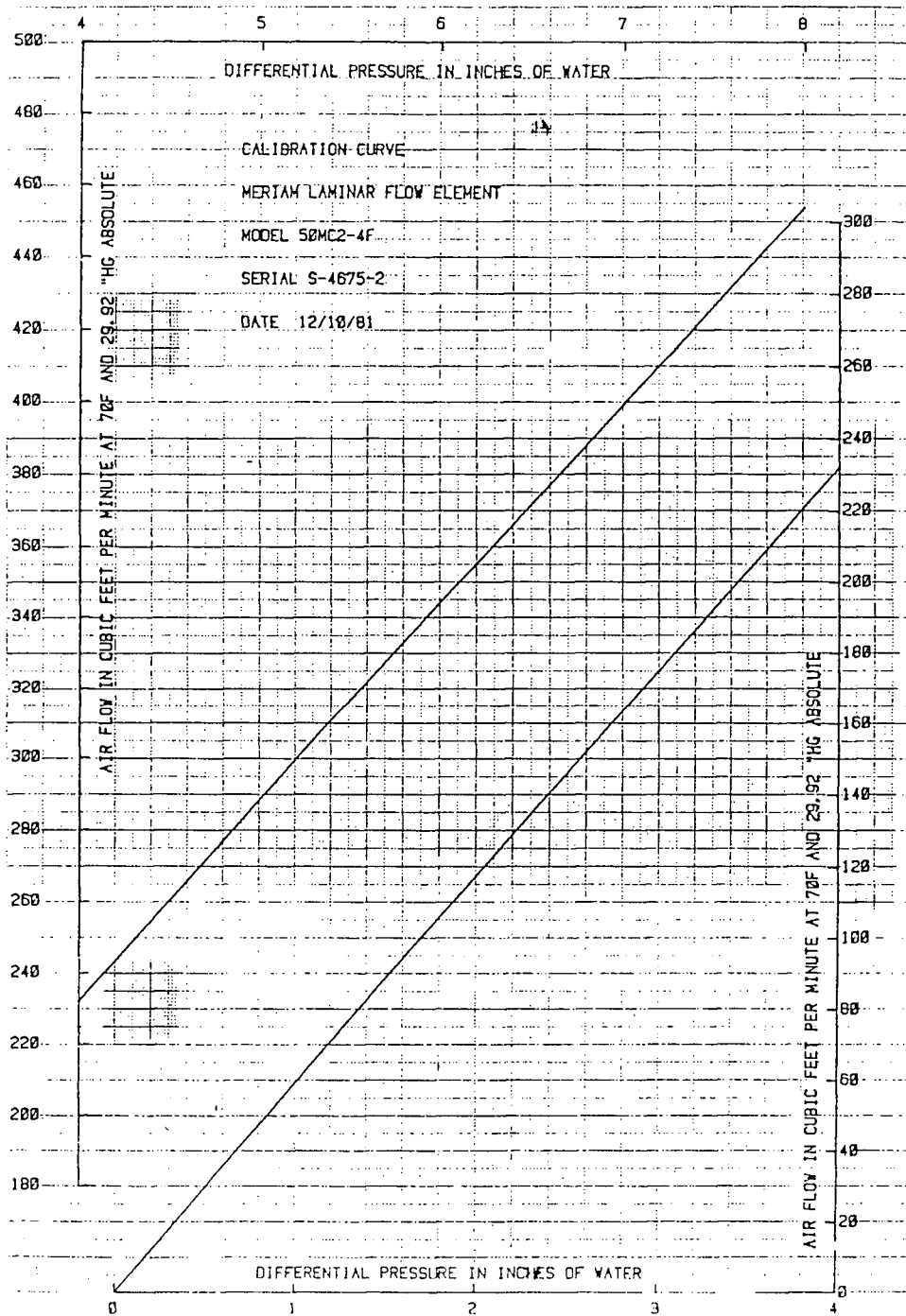


Fig 71. Calibration Curve For Laminar Flow Element (Air)

feuille d'étalonnage
Calibration sheet

Piezo-Instrumentation

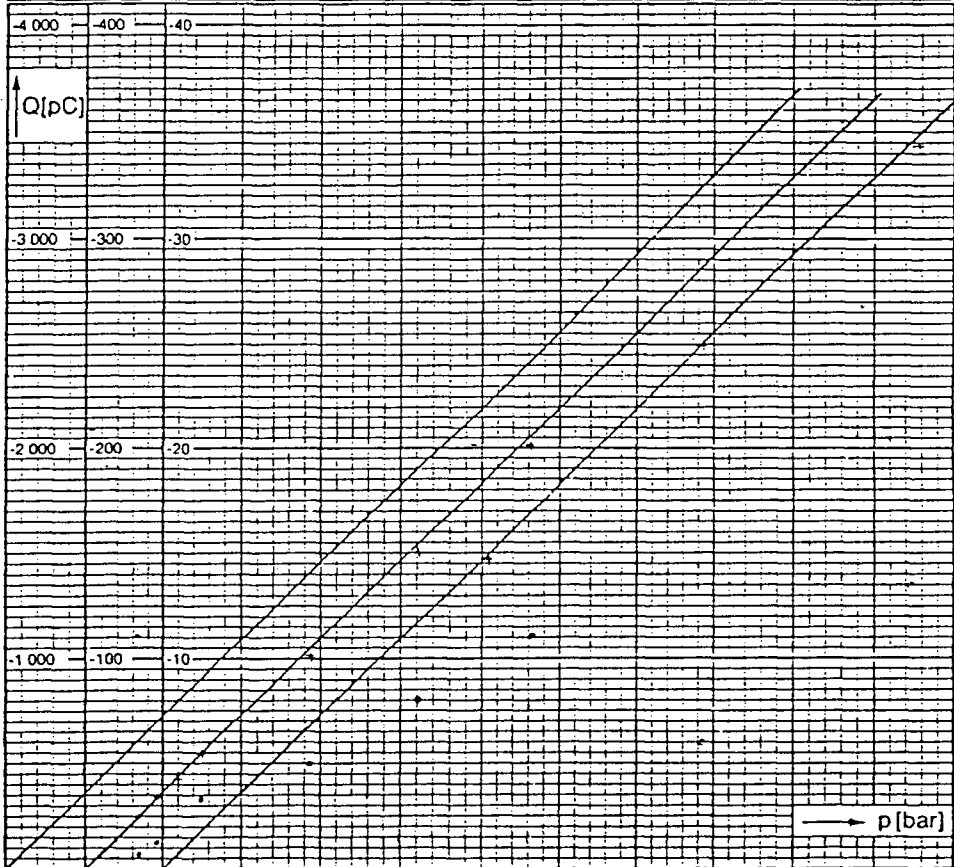
KISTLER

Druckaufnehmer
Capteur de pression
Pressure transducer

Type 6121 SN 282737

Kalibrierter Bereich Gamme étalonnée Calibrated range	[bar]	0...250	0...25	0...2,5	Betriebstemperaturbereich Gamme de temp. d'utilisation [°C] -80...350 Operating temperature range	
Empfindlichkeit Sensibilité Sensitivity	[pC/bar]	-14,7	-14,6	-14,6		Kalibriert bei Étalonné à Calibrated at 20 °C
Linearität Linéarité Linearity	< ± % FSO	0,3	0,3	0,3		by Sh Date 15.12.86

1bar = 10⁵ N·m⁻² = 1,019...at = 14,50...psi
 1at = 1kp·cm⁻² = 1kgf·cm⁻² = 0,980665 bar
 1psi = 0,06894...bar



0	25	50	75	100	125	150	175	200	225	250		
	0	2,5	5	7,5	10	12,5	15	17,5	20	22,5	25	
		0	0,25	0,5	0,75	1	1,25	1,5	1,75	2	2,25	2,5

Abhängigkeit der Empfindlichkeit
von der Temperatur

Sensibilité en fonction
de la température

Sensitivity versus temperature

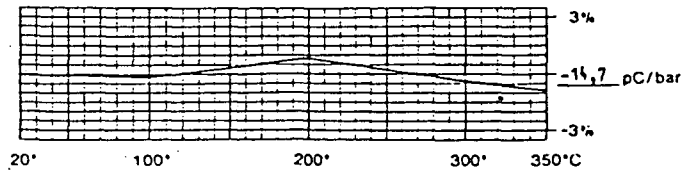


Fig 72. Calibration Curve For Kistler Pressure Transducer

PLOTTING POSITION

FROM RECORD

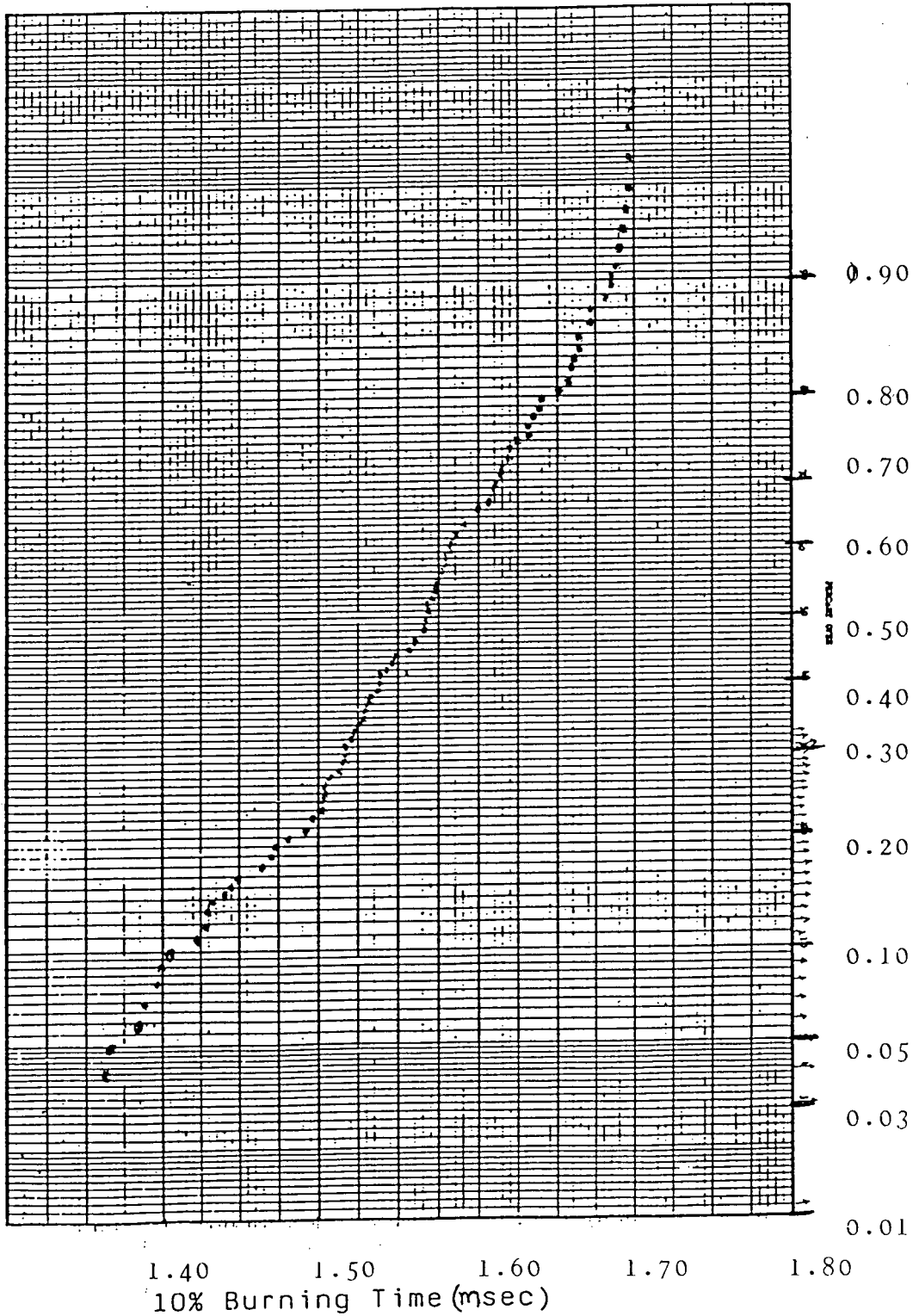


Fig 73 Combustion Time at 10% Mass-Fraction-Burned on Probability Paper.

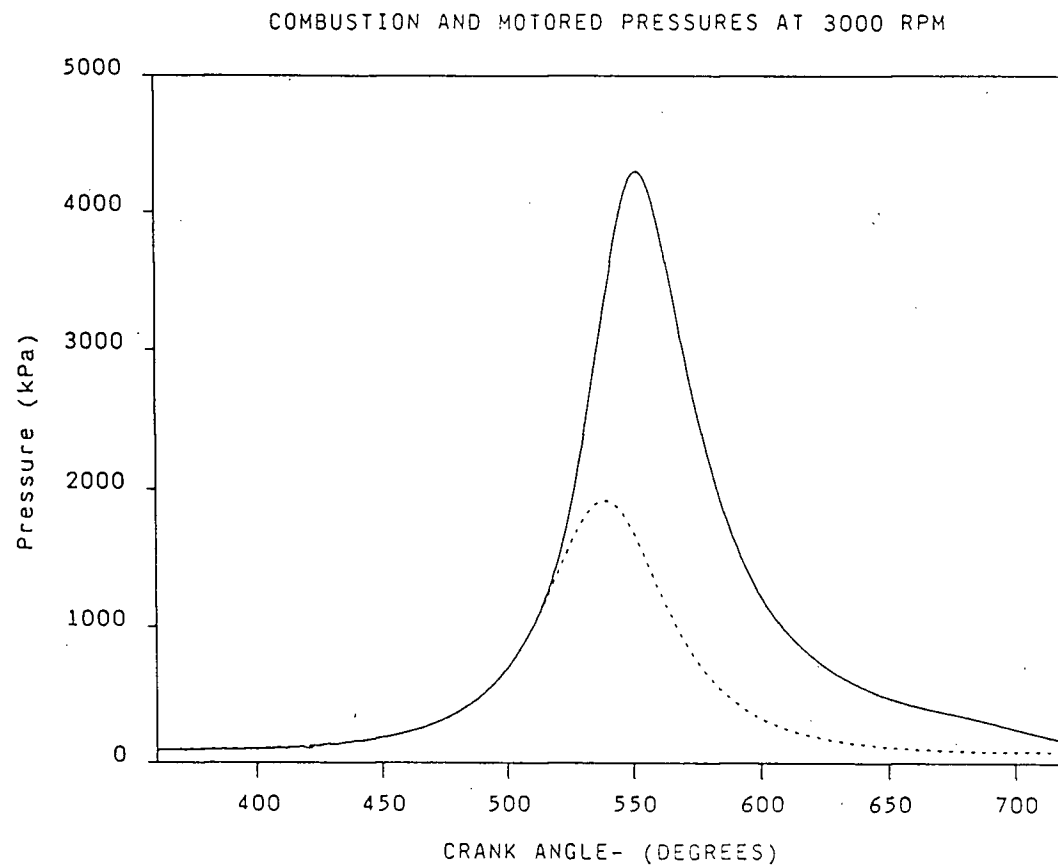


Fig 74. Combustion And Motored Pressure At Different Crank Angle Intervals - 3000 RPM. (For Sensitivity Analysis).....

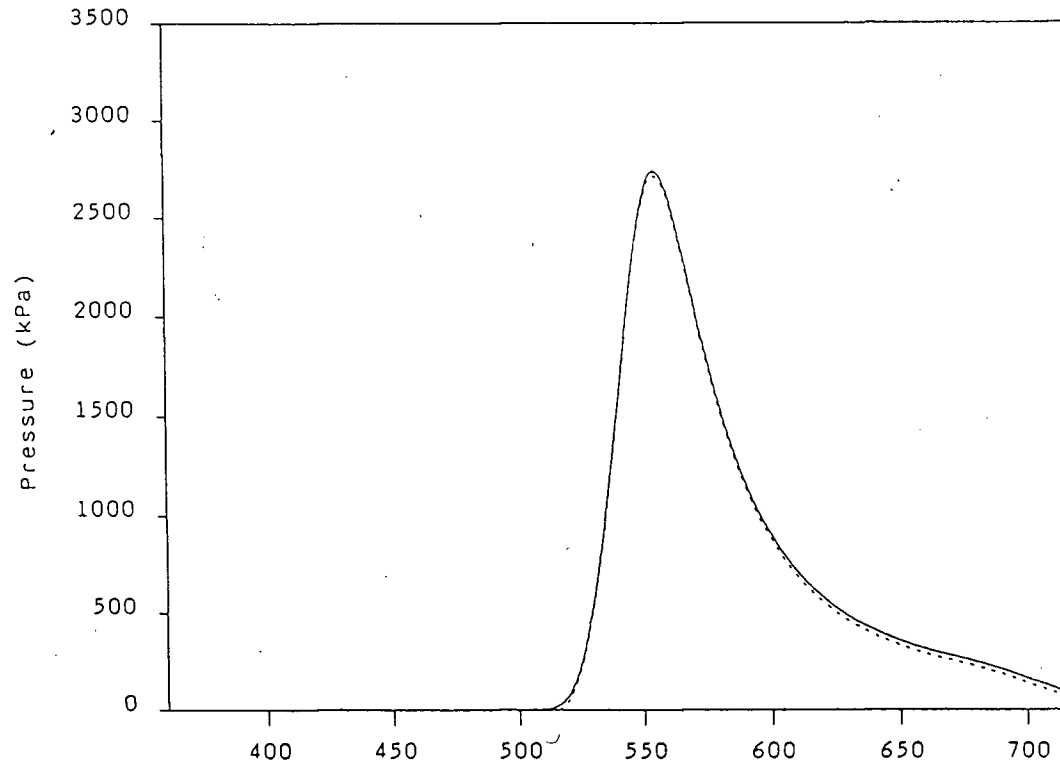


Fig 75. Combustion Pressure Less Motored Pressure at Different Crank Angle Intervals- 3000 RPM (Sensitivity Analysis)

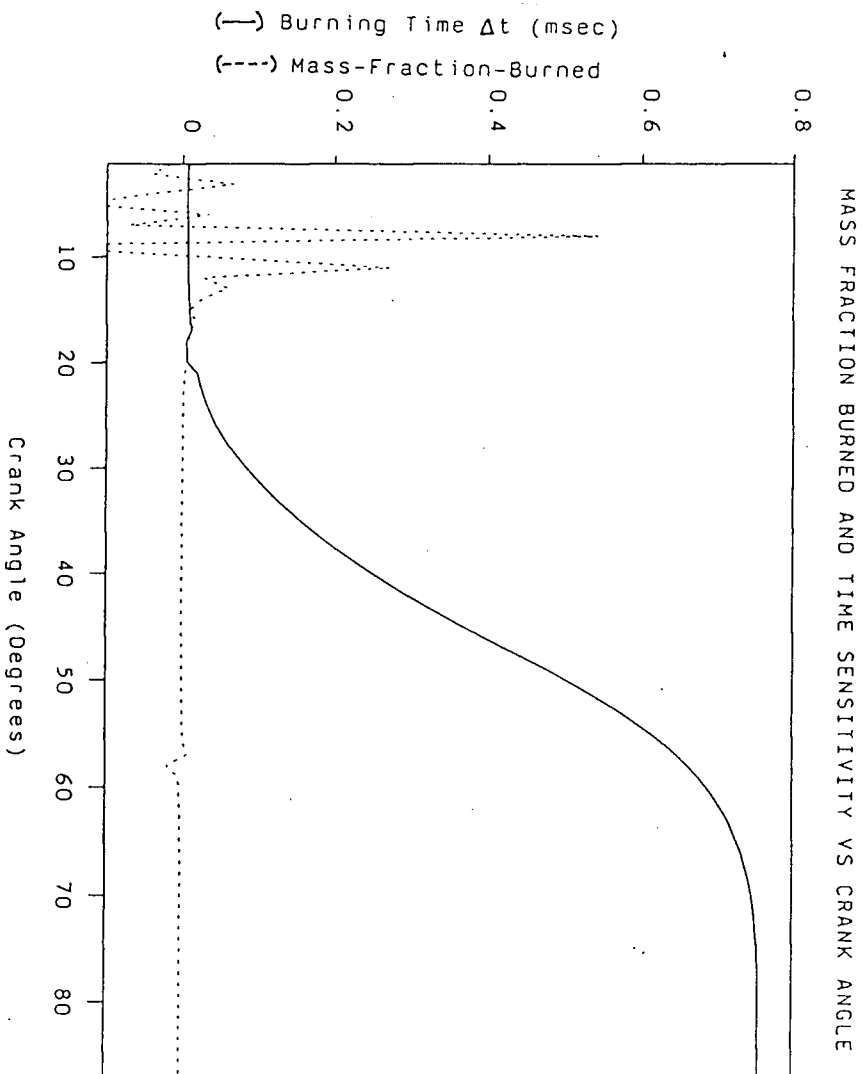


Fig 76. Mass-Fraction-Burned and Time Sensitivity at Different Crank Angles (Sensitivity Analysis)